Radiation induced brain necrosis after proton therapy for head and neck cancer

Grete May Engeseth

Thesis for the degree of Philosophiae Doctor (PhD)
University of Bergen, Norway
2022

UNIVERSITY OF BERGEN

Radiation induced brain necrosis after proton therapy for head and neck cancer

Grete May Engeseth

Thesis for the degree of Philosophiae Doctor (PhD)
at the University of Bergen

Date of defense: 09.12.2022

Scientific environment

The work in this thesis has been carried out at the Department of Oncology and Medical Physics, Haukeland University Hospital, Bergen, Norway in collaboration with clinicians and researcher at the Department of Radiation Oncology and the Department of Radiation Physics at the University of Texas, MD Anderson Cancer Center (MDA) in Houston, USA.

The candidate has been affiliated with the PhD educational program at the University of Bergen, Norway, within the Department of Clinical Science at the Faculty of Medicine.

The project was initiated by principal investigator Dr. Gary Brandon Gunn, Professor in the Department of Radiation Oncology and the Center Medical Director of the Proton Therapy Center at MDA. Fifteen months of the project period was spent at MDA as a member of the research group of Dr. Clifton Dave Fuller.

The project was funded by Trond Mohn Foundation and the Department of Oncology and Medical Physics at Haukeland University Hospital. It is part of the research effort "Establishing a framework for interdisciplinary clinical particle therapy research at Haukeland University Hospital", led by Liv Bolstad Hysing.

Acknowledgements

Abbreviations

BP	Bragg Peak
AIC	Akaike Information Criteria
AUC	Area Under the Curve
CT	Computer Tomography
CTCAE	Common Terminology Criteria for Adverse Events
CTV	Clinical Target Volume
DICOM	Digital Imaging and Communications in Medicine
DNA	Deoxyribonucleic acid
DSB	Double Strand Breaks
DVH	Dose Volume Histogram
FDC	Fast Dose Calculator
FDC	The Fast Dose Calculator
FLAIR	Fluid Attenuated Inversion Recovery
gEUD	Generelized Equivalent Uniform Dose
HNC	Head and Neck Cancer
IAEA	International Atomic Energy Agency
ICRU	International Commision on Radiation Units and measurements
IMPT	Intensity Modulated Proton Therapy
IMRT	Intensity Modulated Radiation Therapy

IQR	Interquartile Range
LET	Linear Energy Transfer
LKB	Lyman-Kutcher-Burman
LLH	Log-likelihood
LQ	Linear Quadratic
MDA	MD Anderson Cancer Center
MLE	Maximum Likelihood Estimation
MRI	Magnetic Resonance Imaging
NPC	Nasopharyngeal Carcinoma
NTCP	Normal Tissue Complication Probability
OAR	Organs at Risk
PBS	Pencil Beam Scanning
PET	Position Emission Tomography
PSPT	Passive Scattering Proton Therapy
PT	Proton Therapy
QUANTEC	Quantitative Analysis of Normal Tissue Effects in the Clinic
RAIC	Radiation Associated Image Change
RBE	Relative Biological Effectiveness
RIS	Radiology Information System
ROC	Reciever Operating Charateristic

ROS   Reactive Oxygen Species

RPA   Recursive Partitioning Analysis

RT   Radiation Therapy

RWD   RBE weighted dose

SD   Standard Deviations

SOBP   Spread Out Bragg Peak

SPECT   Single Photon Emission Computed Tomography

SSB   Single Strand Breaks

TD   Tolerance Dose

TLIC   Temporal Lobe Image Change

TLN   Temporal Lobe Necrosis

TRIPOD   Transparent Reproting of a multivariable prediction model for
             Individual Prognosis Or Diagnosis

VMAT   Volumetric Modulated Arc Therapy

Abstract

With proton therapy, reduction in normal tissue doses is achievable with equal or better target dose conformity due to the Bragg Peak effect. The main rationale for proton therapy today is based on an assumption that this will translate into a more favorable treatment outcome, specifically in terms of lower normal tissue complication rates. However, proton therapy is accompanied with an inherent uncertainty in the actual biological dose delivered. It is well recognized that the constant Relative Biological Effectiveness (RBE) currently applied in clinical proton beams is a simplification of the reality; rather than being a fixed factor, RBE varies depending on several physical, biological and treatment related factors. A wide range of models derived from in-vitro data have been proposed to describe the variable RBE based on the Linear Energy Transfer (LET), dose and α/β. Clinically, the relationship between biological effect and variable RBE is not well understood, however there are strong in-vitro evidence for an increase in RBE as a function of LET.

During radiotherapy for head and neck cancer (HNC) at the skull base region, patients may receive high radiation doses to parts of the brain and will therefore have a lifelong risk of developing radiation-induced brain necrosis. Patients are most commonly diagnosed on the basis of characteristic changes on Magnetic Resonance Images (MRI), including contrast enhanced lesions on T1-weighted sequences or hyperintensities on T2-weighted sequences. There are numerous publications addressing these radiation associate image changes (RAIC) after intensity modulated radiotherapy (IMRT) for HNC, however, there are limited number of studies in patients treated with proton therapy.

Previous research in pediatric and adult patient cohorts treated for both intracranial and extracranial skull base tumors suggest that RAIC occur more frequently after proton therapy. It has been hypothesized that this may be explained by an increase in the LET at the distal part of the proton beam.

The aim of this PhD work was to explore RAIC in patients treated with proton therapy for HNC at the skull base region. The patient material included a wide range of HNCs

treated with intensity modulated proton therapy (IMPT) and/ or passive scattering proton therapy (PSPT) at MD Anderson Cancer Center between 2010 and 2018.

In paper I, the incidence and patterns of RAIC were investigated, and practical brain dose constraints (RBE = 1.1) associated with RAIC were derived. The incidence of RAIC corresponded reasonably well with observed rates previously reported after proton therapy. During a median latency time of 24 months, RAIC were found on follow-up MRIs in 22 out of 127 patients (17%). The majority of the patients with RAIC were treated for nasopharyngeal or sinonasal cancers (77%). Lesions were found in the temporal lobes, frontal lobes and the cerebellum, typically outside or slightly overlapping with the CTV. All lesions were asymptomatic. On the last available follow-up MRI, 18% of the lesions were in progression, whereas 27% had resolved. RAIC was significantly associated with dosimetric variables only. Brain $V_{67\ Gy\ (RBE)} < 0.2cc$ was identified as the most important dose volume threshold in order to limit risk of developing RAIC.

In paper II, the aim was to investigate the influence of RBE variations on the assessment of risk of developing temporal lobe necrosis. The patient material included 45 patients treated with IMPT and who had a follow-up time of 24 months or longer. Image changes diagnosed radiation necrosis was observed in sixteen temporal lobes. Monte Carlo simulations were used to calculate RWD_{Var} based on two previously published RBE models. The RWD_{Var} was significantly increased compared to RWD_{Fix}. We further found indications that the risk of developing temporal lobe necrosis could be underestimated when evaluating dose constraints according to RWD_{Fix}. Dose-volume predictors with near-maximum doses were less influenced by RBE variations than the maximum dose. The result from this study suggests that including RWD_{Var} as part of IMPT treatment plan evaluation may provide valuable clinical information in terms of temporal lobe protection.

In paper III we looked for correlations between regions of radiation necrosis, dose and dose-averaged LET (LET_d). Fifteen patients with RAIC who had been treated with IMPT were included in the analysis. Accurate dose- and LET_d distributions were

calculated using Monte Carlo simulations and extracted voxel-by-voxel from the patients' treatment plans using an in-house developed MATLAB-script. Mixed effect logistic regression methodology were used for analysis. The analysis revealed substantial interpatient variations, however an overall significant correlation between increasing LET_d and regions with RAIC. Our results suggested that the LET_d effect could be of clinical significance for some patients and that LET_d assessment in clinical treatment plans should therefore be taken into consideration.

Overall, this work has provided increased knowledge on risk factors for development of radiation effects in the brain after proton therapy. Incidence rates of RAIC in HNC at the skull base are comparable to other proton series. Our findings suggest that variable RBE related uncertainties and potential LET_d effects are essential to consider in clinical treatment plan evaluation. Although often considered implicitly in the mind of the clinician for proton therapy, continued evidence such as the current work may lead to changes in clinical practice, namely the implementation of computerized calculation and planning tools based on specifically LET_d data along with physical dose.

Norsk sammendrag

Protonterapi gir reduksjon i normalvevsdoser sammenlignet med strålebehandling med fotoner, og det er antatt at dette vil resultere i en lavere forekomst av stråleinduserte seinskader. For å kompensere for en økt biologisk effektivitet av protoner benyttes en konstant verdi for den relative biologiske effektiviteten (RBE) som er satt til 1.1. Det er imidlertid kjent at RBE varierer blant annet med lineær energioverføring (LET), dose og strålesensitivitetsparameteren α/β. Et stort antall RBE-modeller basert på disse variablene har blitt utviklet for bedre å beskrive proton RBE. Klinisk er det manglende kunnskap om effekten av en variabel proton RBE, men det er sterke in vitro-bevis for en økning i RBE som en funksjon av LET.

For kreft lokalisert i skallebasisregion kan strålebehandling medføre at deler av hjernen får høye stråledoser. Disse pasientene har derfor en livslang risiko for å utvikle stråleindusert hjernenekrose. Denne diagnosen stilles som oftest på grunnlag av MR-radiologi, typisk ser en kontrastoppladede lesjoner på T1-vektede sekvenser og økt intensitet på T2 sekvenser. I litteraturen er insidensen av disse bildeendringene (RAIC) godt beskrevet etter intensitetsmodulert strålebehandling (IMRT) for HNC, men det er begrenset antall studier på pasienter behandlet med protonterapi. Nylig har det kommet forskning som indikerer at RAIC forekommer hyppigere etter protonterapi. Det har blitt stilt en hypotese om at dette er relatert til økning i RBE på grunn av forhøyet LET i distale delen av protonstrålen.

Målet med dette doktorgradsarbeidet var derfor å utforske risikofaktorer for utvikling av RAIC hos pasienter behandlet med protonterapi for hode-halskreft lokalisert i skallebaseregionen. Pasientene i studien hadde blitt behandlet med intensitetsmodulert protonterapi (IMPT) og/eller passiv teknikk (PSPT) ved MD Anderson Cancer Center mellom 2010 og 2018. I første artikkel ble insidens av RAIC undersøkt og dose grenser for å redusere risiko ble identifisert. Insidens av RAIC var 17% noe som samsvarte godt med det som har blitt funnet i andre studier etter protonterapi. Flertallet av disse ble behandlet for nasopharynx eller sinonasal kreft (77%). Det ble funnet lesjoner i temporallappene, frontallappen og i cerebellum, de fleste i kant eller så vidt

overlappende med CTV. Ingen av pasientene hadde symptomer assosiert med hjernenekrose. Lesjoner var i progresjon hos 18% av pasientene. $V_{67 \text{ Gy(RBE)}} < 0.2$cc til hjerne be identifisert som den viktigste dose-variabelen for å begrense risikoen for å utvikle RAIC.

I artikkel II var målet å undersøke hvordan RBE-variasjoner kan påvirke estimert risiko for å utvikle stråleindusert temporallappsnekrose. Monte Carlo-simuleringer ble brukt til å beregne variabel RBE-vektede doser (RWD_{Var}) ved hjelp av to publiserte RBE-modeller. Vi fant at RWD_{Var} var signifikant høyere enn doser kalkulert med RBE = 1.1 (RWD_{Fix}). Vi fant videre indikasjoner for at risikoen for å utvikle temporallappsnekrose kan bli undervurdert hvis dosegrenser vurderes basert på RWD_{Fix}. Maksimal dose til temporallappen var svært influert av variabel RBE, noe som resulterte i store usikkerheter og økning i estimert risiko, mens de andre undersøkte dosevariablene var mindre påvirket av variabel RBE. Resultatet fra denne studien viser at å inkludere RWD_{Var} som en del av IMPT behandlingsplanevaluering kan gi verdifull klinisk informasjon når det gjelder beskyttelse av temporallappen.

I artikkel III så vi etter korrelasjoner mellom områder med strålingsnekrose, dose og dose-gjennomsnittlig LET (LET_d). Femten pasienter diagnostisert med RAIC som hadde blitt behandlet med IMPT ble inkludert i analysen. Nøyaktige dose- og LET_d-fordelinger ble beregnet ved hjelp av Monte Carlo-simuleringer og ekstrahert på voxelnivå fra pasientenes behandlingsplaner. En logistisk regresjonsmodell som estimerer tilfeldige og faste effekter ble brukt i analysen. Analysen avdekket betydelige interpasient variasjoner, men allikevel en signifikant korrelasjon mellom økende LET_d og regioner med RAIC. Resultatene våre antydet at LET_d-effekten kan være av klinisk betydning for noen pasienter, og at LET_d-vurdering i kliniske behandlingsplaner derfor bør tas i betraktning.

Samlet sett har dette arbeidet gitt økt kunnskap om risiko for utvikling av stråleeffekter i hjernen etter protonterapi. Forekomsten av RAIC for hode-hals kreft i skallebasisregionen er sammenlignbar med det en har sett i andre protonserier. Våre funn tyder på at variabel RBE-relaterte usikkerheter og potensielle LET_d-effekter kan

være avgjørende og bør inngå som del av klinisk behandlingsplanevaluering. Selv om dette ofte vurderes implisitt ved protonterapi, bør av beregnings- og planleggingsverktøy basert på spesifikke LET_d-data sammen med fysisk dose implementeres i klinisk praksis.

List of Papers

I. **Engeseth GM**, Stieb S, Mohamed ASR, He R, Stokkevåg CH, Brydøy M, et al. "*Outcomes and patterns of radiation associated brain image changes after proton therapy for head and neck skull base cancers*". Radiother Oncol. 2020;151:119-25.

II. **Engeseth GM,** Hysing LB, Yepes P, Pettersen HES, Mohan R, Fuller CD, et al. "*Impact of RBE variations on risk estimates of temporal lobe necrosis in patients treated with intensity-modulated proton therapy for head and neck cancer*". Acta Oncologica, 2022; 61:2, 215-222

III. **Engeseth GM,** He R, Mirkovic D, Yepes P, Mohamed ASR, Stieb S. et al. "*Mixed effect modelling of dose and Linear Energy Transfer correlations with brain image changes after intensity modulated proton therapy for skull base head and neck cancer.*" Int J Radiat Oncol Biol Phys. 2021 Nov 1;111(3):684-692

Contents

1. General introduction

With nearly 10 million people dying of cancer in 2020, it ranks as one of the leading causes of premature death worldwide. Globally, approximately 19 million new cancer cases were reported in 2020, a number which is expected to increase by 47% in 2040 (1). For close to 50% of all patients with cancer, radiotherapy is considered a key modality for successful treatment, disease control and symptom palliation, either as a stand-alone treatment or in combination with surgery and chemotherapy (2).

Already shortly after William Conrad Roentgen announced the discovery of x-rays in 1895 (3), they were used for the first time in a single-fraction treatment of a patient with breast cancer (4). Since then, the field of radiotherapy has evolved tremendously through several groundbreaking technological innovations, and a continuously growing insight and understanding of biological response to ionizing irradiation. As radiation side effects were observed both in patients and staff from the very beginning (5), it soon was acknowledged that the accompanying healthy tissue irradiation limited utilization of the full potential of radiotherapy. This motivated research efforts to better understand the underlying mechanisms of the radiation action. In 1934, Coutard et al. reported long term cure rates and toxicity outcomes, emphasizing the marginal boundary between curation of cancer and the induction of harmful side effects and the importance of a fractionated treatment approach to increase the so-called therapeutic window (6). The introduction of three dimensional conformal radiotherapy (3DCRT), and not least the implementation of intensity-modulated radiotherapy (IMRT), have been important milestones when it comes to reducing normal tissue doses and increasing target volume dose conformity. Still, the potentially harmful effects of radiation place restrictions on the dose considered safe in terms of normal tissue complication probability (NTCP), which in turn can affect the probability of cure.

In the 125-year history of radiation therapy, most of the patients have been treated with high energy photons, but the last decades there has been a growing belief that a gain in the therapeutic ratio can be achieved when using proton therapy, also compared to state-of-art IMRT. Proton beams traverse tissue with minimal dose deposition until the end

of their range, where energy deposition peaks within a few millimeters. This is known as the Bragg Peak (7). Dose deposition beyond the Bragg Peak falls off rapidly. Thus, in contrast to photons, the exit dose from a proton beam will be almost zero. Furthermore, the input dose is greatly reduced. Overall, the decrease in integral dose of protons will be approximately 60% (8). This enables a reduction of delivered normal tissue doses and a potential clinical benefit over photon radiotherapy in terms of a lower risk of radiation induced side effects. First and foremost, it is widely assumed that this will be of benefit for children, but also for adults with tumors in proximity to critical organs at risk (OAR), such as brain tumors, and cancers at the skull-based region (9).

However, proton therapy is accompanied with an inherent uncertainty in the actual biological dose delivered. It is well recognized that the constant Relative Biological Effectiveness (RBE) currently applied in clinical proton beams is a simplification of the reality; rather than being a fixed factor, the RBE varies depending on several physical, biological and treatment related factors. The biologically effective dose distributions calculated by the treatment planning system using a fixed RBE value of 1.1 may very well differ significantly from what is actually delivered to the patients, which in turn to could result in suboptimal treatments and unforeseen normal tissue complications. Recent years, retrospective analysis of pediatric and adult patient cohorts have indicated a clinical effect of variable RBE in normal tissue (10-15). Thus, the uncertainties stemming from the variable RBE is of concern in clinical proton therapy, and there is a great demand for more research and publications investigating the impact of variable RBE on the probability of toxicity incident (16).

1.1 Proton therapy physics and technology

The potential use of protons in cancer treatment was first outlined in a paper by Robert R Wilson (17) where both the biological and physical foundation as well as technical and fundamental aspects of beam delivery were described. Less than 10 years later the first patient was treated at Lawrence Berkeley University (18). In the following decades there was a slow increase in patients, as well as an expansion of the disease sites considered for treatment with proton therapy (19). During the 1990s the first hospital-based treatment facility started operating (20), and in 2001 commercial proton therapy systems became available. From here on the number of facilities have rapidly increased, and by the end of 2020 approximately 250 000 patients have been treated with proton therapy worldwide (21).

1.1.1 Interaction mechanisms

The most prevalent proton interaction mechanisms are Stopping, Scattering and Nuclear reactions, of which Stopping is the most important in terms of energy deposition in the tissue. Stopping involves inelastic collisions between the incoming proton and an electron, whereupon the electron is either excited or released from the atom (ionization). In this process the proton loses energy while continuing on its original path (Figure 1.1a). The released electron may carry sufficient energy to cause further ionizations at some distance from the proton's trajectory (so-called delta rays). The proton energy loss per unit path length is called Stopping Power and can be calculated using the Bethe Bloch formula (22). When the incoming proton interacts with the electromagnetic field of the nucleus (Scattering), it is deflected laterally from its initial trajectory (Figure 1.1b). More rarely, the proton directly interacts with the nucleus releasing secondary particles which, like the delta rays, may have high energy and ionizing capacity (Figure 1.1c) (19).
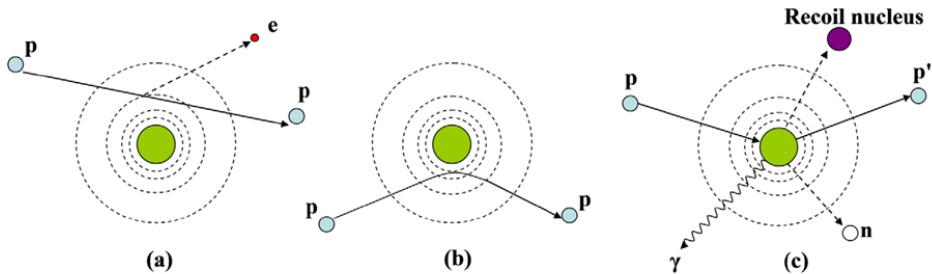
Figure 1.1: a) Stopping: Ionization occur as a result of proton interaction with the atomic electron. The proton loses a small amount of velocity (i.e kinetic energy), but continues in a straight line. Secondary electrons (delta rays) are released carrying energy away from the beam b) Coloumb scattering: proton is deflected from its original trajectory through elastic interaction with the nuclei, c) Nuclear collisions: in-elastic collition between the proton and the nuclei result in the release of high energetic nuclear fragments. (Figure from Newhauser et al (19), reused with permission).

1.1.2 Depth dose distribution of protons

When high energy protons enter the patient, the dose are mostly deposited through a very large number of ionization (and excitation) events where the proton successively loses a small amount of energy and thus velocity. The probability of such an ionization event, and the amount of energy lost in the process, is roughly inversely proportional to the square of the incoming proton's velocity. When the proton energy is high, the ionization density is therefore relatively sparse and dose deposition low, however, as the protons slow down, the probability of interactions with the electrons increases. Thus, there is a prompt increase in ionization density just as the proton are about to stop; the majority of dose is hence deposited within millimeters in the so-called Bragg Peak (Figure 1.2). Behind this depth, the dose deposition is nearly negligible (23).
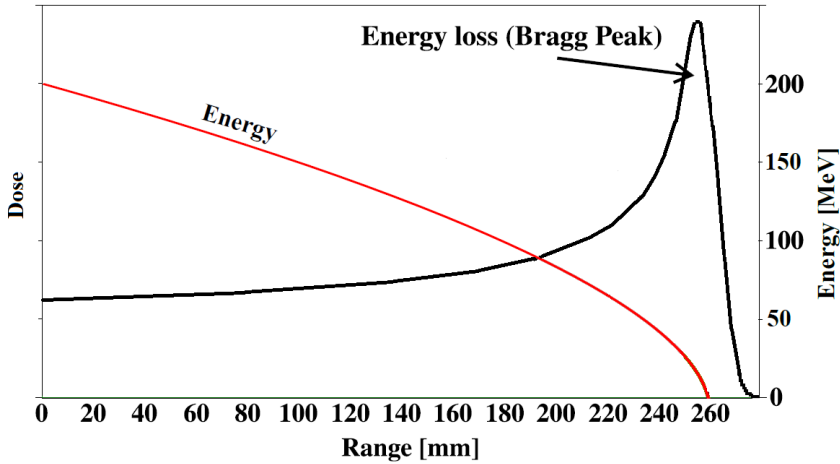
Figure 1.2: Depth dose distribution of a mono energetic proton beam showing the energy loss as protons traverses matter. The majority of energy deposition occurs in the Bragg Peak when the proton energy is approaching zero. The depth of where this occur is dependent on the initial proton kinetic energy (Figure: Courtesy of Helge Egil Seime Pedersen).

1.1.3 The Linear Energy Transfer

The interaction mechanisms causing a particle to lose energy, occur randomly along its track; the frequency and spatial distribution of these energy deposition events are decisive for radiation quality and hence the biological effect. Radiation quality is therefore commonly specified by the term Linear Energy Transfer (LET), which is a measure used to quantify the energy deposition density of ionizing irradiation (24). It is defined as the mean energy (*dE*) transferred to the tissue per unit travelled length (*dl*) along the track of an ionizing particle. It has the unit keV/μm and is expressed as

$$LET = \frac{dE}{dl} \tag{1.0}$$

The LET is lowest in the entrance region and reaches its maximum downstream of the Bragg Peak.

Both the LET spectrum of protons and average values can be accurately calculated using Monte Carlo codes (e.g Geant4, FLUKA and TOPAS) (25). When calculating the LET,

one can apply an energy threshold (Δ), where the energy transported by delta rays exceeding Δ are excluded from the calculations. Hence, the LET is termed *restricted* and *dE* will only correspond to mean energy transferred locally, i.e energy deposited through ionization and excitations in close vicinity of the proton track. When no energy cutoff is applied and all delta rays are included in the calculation of the LET, the LET is referred to as *unrestricted* and is equal to the proton's linear electronic stopping power (26).

As previously pointed out, individual protons interact randomly, consequently the energy transfer per unit path length vary between the protons in a beam. Therefore, in each point in a clinical proton beam there will be several protons of different LET values (LET fluence spectrum). Reporting average values of LET rather than the LET spectrum may be more applicable in clinical research. In principle, two different methods are applied for LET averaging. The dose average LET (LET_d) is the most commonly used when studying clinical outcomes as it takes into account both the dose and the LET. When calculating the LET_d, dose deposited within each voxel j in position (x,y,z) is used as a weighting factor. The LET_d is calculated by:

$$LET_d(x, y, z) = \frac{\sum_j \varphi_E(x,y,z,E_j) SP^2(E_j) \Delta E_j}{\sum_j \varphi_E(x,y,z,E_j) SP(Ej) \Delta E_j} \tag{1.1}$$

Here, $\varphi_E(x,y,z,E_j)$ is the proton energy spectrum with an energy of E_j, whereas $SP(E_j)$ corresponds to the unrestricted stopping power of the protons with an energy of E_j (25). In the track average LET (LET_t), the fluence spectrum of the LET is taken into account, the LET_t is therefore weighted according to the arithmetic mean of the LET fluence spectrum distribution within a voxel j (25):

$$LET_t(x, y, z) = \frac{\sum_j \varphi_E(x,y,z,E_j) SP(E_j) \Delta E_j}{\sum_j \varphi_E(x,y,z,E_j) \Delta E_j} \tag{1.2}$$

The LET and absorbed dose

The absorbed physical dose D is defined as the mean energy *dE* imparted by ionizing radiation to matter of mass *dm* (26):

$$D = \frac{dE}{dm} \qquad (1.3)$$

The unit for absorbed dose is Gy where 1 Gy corresponds to 1 Joule of energy absorbed per kg matter (J/kg) (24). At a point of interest in tissue, the absorbed dose is determined by the proton fluence (number of proton particles) and their capability to lose energy (i.e LET). The absorbed dose delivered by protons with a given LET may be found by calculating the proton fluence with the corresponding unrestricted LET (27).

$$D = \frac{\Phi}{\rho} LET \qquad (1.4)$$

Here Φ corresponds to the proton fluence and ρ to the tissue density. Thus, the same dose in a given point could be a result of fewer protons of high LET or more protons of lower LET.

1.1.4 Proton treatment planning and delivery

Protons are accelerated in cyclotrons or synchrotrons before being transported to the treatment room and delivered to the patients either using passive scattering proton therapy (PSPT) or pencil beam scanning (PBS). As protons are emitted from the accelerators as a narrow and nearly monoenergetic beam (so-called pencil beam), both range modulation (i.e. energy modulation) and beam shaping are required in order to achieve clinical applicable 3D-dose distributions. There are distinct technical differences between PSPT and PBS in how dose distributions are generated and delivered in order to cover the target volume laterally and in depth (beam spread out laterally and longitudinally), as well as differences in the flexibility and possibility of tailoring the dose distribution to the target volume during the treatment planning process. In principle, range modulation is performed by superposition of several pristine Bragg Peaks of varying energy and weights, resulting in a depth dose distribution with

a high-dose region wide enough to cover the target volume (the so-called Spread Out Bragg Peak) (Figure 1.3). The range modulation is achieved either by varying the beam energy output from the accelerator or by using energy degraders in the beam (28) .
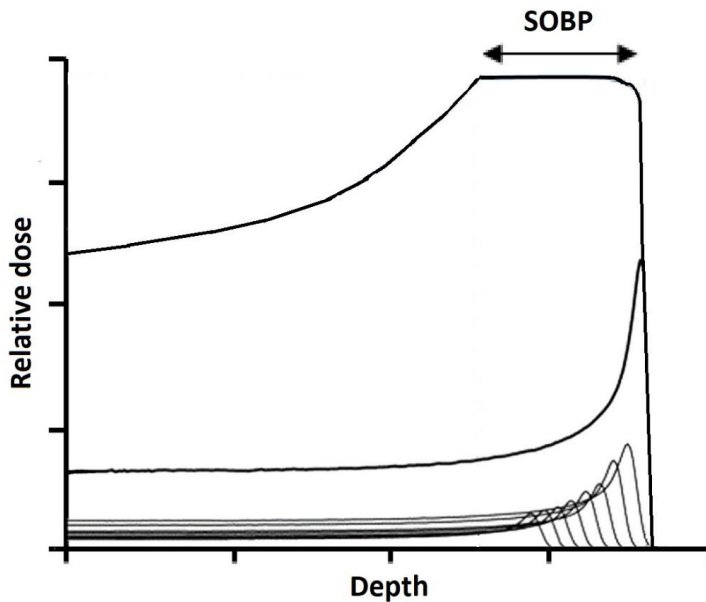
Figure 1.3: Illustration of the generation of the Spread Out Bragg Peak (SOBP). Multiple BPs of different energies and weights superimposed to produce a flat high dose plateau wide enough to cover the target volume (Figure: Courtesy of Nora May Engeseth).

Passive scattering proton therapy (PSPT)

In PSPT the high-dose plateau in the SOBP is flat and uniform. It is generated using a rotating modulating wheel or a ridge filter with steps of varying thickness, each corresponding to a pristine peak in the Spread Out Bragg Peak (SOBP). Additional range shifters are normally applied in order to shift the SOBP to the desired depth in order to

cover the target volume from the most distal to the most proximal part. A uniform lateral spreading of the beam is obtain by introducing scattering foils into the beam path providing lateral coverage of the target. Aperture blocks (collimators) and range compensators are used for further lateral and distal shaping of the beam to the target volume (29). This enables conforming of the dose lateral and distal to the target, however no conforming of the dose proximal to the target volume is possible (Figure 1.4a).
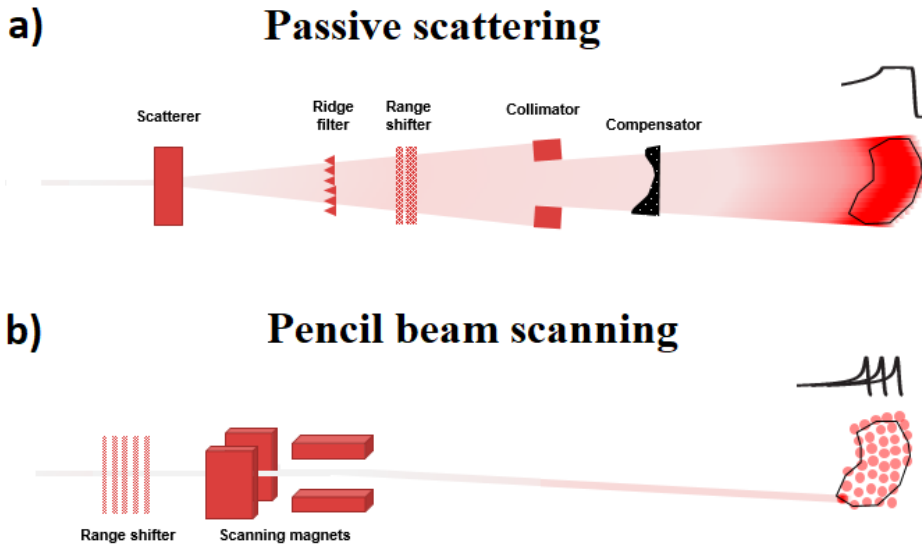
Figure 1.4: Principles of PSPT (a) where physical beam devices are used to shape the beam to the target volume delivering a uniform dose distribution, and PBS where the proton beam is steered by magnets placing pristine BP throughout the target volume (b). (Figure: Courtesy of Jon Espen Dale)

Pencil Beam Scanning (PBS)

In PBS, magnets are used to steer a number of range modulated pencil beams throughout the target volume. The target volume is irradiated by iso-energy layers, whereupon each energy layer is successively scanned in the x and y direction starting at the deepest layer (i.e. the layer that requires the highest energy). The Bragg Peaks are delivered voxel wise either in discrete spots (so-called spot scanning) in which the beam is turned off between each voxel location, or continuously where delivered dose is determined by either beam intensity or the beam time at each of the voxel locations (Figure 1.4b) (30).

There are primarily two approaches to obtain a uniform dose coverage in PBS where both of these optimization techniques allow an additional shaping of the beam, and hence dose sparing, proximal to the target volume compared to PSPT. In single field optimization (SFO), the spots are optimized so that each field covers the target with a uniform dose. In Intensity Modulated Proton Therapy (IMPT), an inhomogeneous dose distributions within each field are allowed and a homogeneous target dose coverage is obtained through simultaneously optimizing all fields (multifield optimization) (31).

1.2 Biological effect of irradiation

Ionizing irradiation set in motion a cascade of physical, chemical and biological reactions in the tissue exposed. The phase of physical and chemical reactions are finalized within seconds, whereas the biological phase span from seconds to years after exposure (32). Curative intended radiotherapy is delivered to the patient with the aim of killing cancer cells and heal the patient, while at the same time sparing surrounding healthy tissue. If treatment is successful and patient is cured (or become a long-time survivor), there is still a concern of potential late normal tissue complications induced by radiotherapy. Both the killing of cancer cells and the induction of side effects are initially caused by energy deposition events leaving the cellular atoms in ionized or excited states. In principal these interaction events may harm all molecules in the cell. However, the DNA is considered the critical radiobiological target as it controls all cellular activity. Therefore, any damage to the DNA immediately activates a chain of complex and correlated response pathways, which are decisive of the cell's faith. Most commonly a complete DNA repair is achieved, but if damage is irreparable, cell death or (malignant) DNA transformations will occur (33)

The DNA is damaged either through direct ionizations of the DNA molecule or indirectly by highly reactive radicals released as a result of radiation interacting with the surrounding water (34). A variety of different types of base damages and strand breaks of the DNA are induced by these interactions of which biological implications differs. The pattern and the consequential severity of the DNA damages are largely driven by the radiation track structure (i.e. energy deposition distribution). In low-LET irradiation, base damages and single strand breaks (SSB) occur far more frequent than double strand breaks (DSB), but have only minor biological impact as they are quickly repaired. In contrast to SSB, which make use of the opposite DNA strand as template during repair, DSB are more complex and therefore more difficult to repair. Furthermore, when the energy deposition events along the proton track are concentrated in space, two or more closely spaced DNA damages may occur. This is referred to as clustered damages (35). The amount of clustering and the biological consequence of the DNA damages are dependent on radiation quality; as LET increases, both the likelihood of clustered

damages as well as the complexity of the DSB will increase (36). Furthermore, higher ionization density is believed to increase the release of reactive oxygen species (ROS) (37).

Following radiation exposure, most cells die when attempting cell division (mitotic death), however in some cells, apoptotic death is dominant. It is believed that type of cell deaths affect radiosensitivity and it is considered to be a correlation between apoptosis and radiosensitivity. Cells in which death mechanisms are dominated by apoptosis are in general radiosensitive, cells where apoptosis is absent, and are in general radioresistent (34).

1.2.1 The linear quadratic model for modelling cell survival

The linear quadratic (LQ) model describes the radiobiological effects of cell killing and sub lethal repair, and is widely used for quantifying and predicting radiation responses both experimentally and clinically. It describes the relationship between cell survival and radiation dose, and is expressed by

$$S = e^{-\alpha D - \beta D^2} \tag{1.5}$$

where S is the probability of cell survival after being exposed to a radiation dose D, and where the radiosensitivity of the cell is described by the two parameters α and β. The model has two components. It is considered that cell death caused by a single particle track is describe by αD (Gy^{-1}) and thus reflects lethal DNA damage whereas the βD^2 (Gy^{-2}) describe the amount of cell death induced by multiple radiation tracks, and thus reflects sub lethal DNA damage (38). In a LQ curve for cell survival, the low dose region are dominated by the linear α term of the equation, whereas the quadratic β term, dominate the higher dose regions, i.e. in the shouldered part of the curve. The curvature of the LQ curve is described by the α/β ratio (Gy), which corresponds to the dose where the linear and quadratic component contribute to equal amount of cell kill (i.e. $\alpha D = \beta D^2$) (Figure 1.5a) (39).

Survival curves for cell lines with a low α/β ratio will have a pronounced curvature, reflecting increased cell killings per unit dose at higher dose levels. They are considered to have lower sensitivity to irradiation and display a strong fractionation effect, as sub-lethal damages are repaired between fractions. For cell populations with high α/β ratio, the curvature are much less pronounced with nearly constant cell killing across the dose range (Figure 1.5b). Thus, for high α/β ratio dose fractionation effect is low (39).
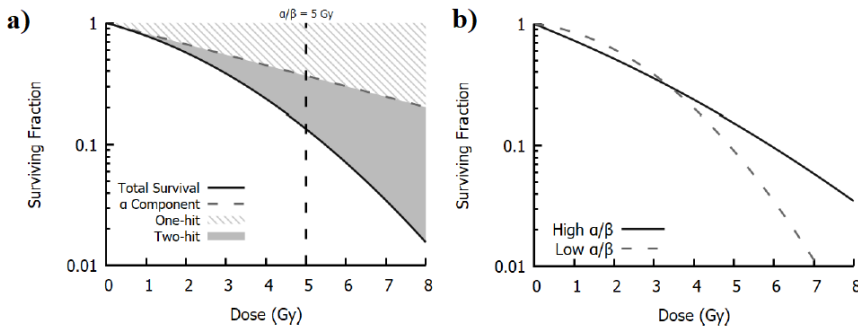
Figure 1.5: a) Illustration of the linear and quadratic term in the LQ model, which represent cell kill induced by a single and multiple tracks, respectively. The α/β ratio corresponds to the dose where the two components contribute equal to the amount of cell kill   b) Cell lines with high α/β exhibit an almost straight survival curve indicating a roughly constant cell killing regardless of dose level, whereas cell survival curves for low α/β are shouldered showing higher rates of cell killing with increasing dose. (Figure from McMahon et al. (39) Reused with permission).

Early and late responding tissue

The α/β ratio describes cells and tissues sensitivity to radiation. As a general rule, high α/β ratios are associated with tissues characterized by high proliferative activity such as most tumour tissues, skin epidermis, hematopoietic tissues, and the epithelium of the gastrointestinal system. In these biological systems, radiation effects manifest early. In contrast, tissues with slow turnover such as brain tissue respond late to irradiation and are typically characterized by low α/β ratio (37).

There is a distinct difference in pathogenies and clinical expression between early and late responding tissue. The predominant response to radiation in turnover tissues is a rapid reduction in the proliferative activity. Normal cell loss rate, however, persists, thus hypoplasia and ultimately complete loss in functional cells occur. This is commonly accompanied by vascular and inflammatory responses, which are either induced by the radiation exposure itself, or secondary to the progressive cell depletion. The acute effects are usually completely healed through proliferation of the surviving cells or by migration of stem cells outside the exposed region (40).

Late effects may display in all organs and are latent for months to years before becoming apparent. They are considered irreparable, and typically progresses over time. It is recognized that any radiation treatment may carry a lifelong risk of late radiation effects (41). It is a complex orchestrated response where inactivation of parenchymal cells (slowly progression of parenchymal hypoplasia), radiation induced fibrosis formation in the connective tissue compartment, and vascular tissue injuries such as loss in capillaries and telangiectasia eventually lead to loss in organ function. It is further believed that the immune system plays an important contributing role (42). As a general rule, there is no interaction between acute and late effects. The exception is for so-called consequential late effects (CLE). CLE is defined as late effects, of which the severity are correlated with the grade or duration of prior acute reactions in the same organ or tissue (43). Clinical studies have demonstrated this association primarily in organs where the acute responding tissues function as a barrier against mechanical and chemical stress; any damages resulting in break down in the protective function will therefore add to the direct effect of irradiations, thus increasing the risk and severity of the late effect (43).

1.3 Predictive modelling of normal tissue effects

1.3.1 Normal tissue complication probability

Normal Tissue Complication Probability (NTCP) models estimate the probability of radiation-induced complications based on planned dose distributions, some models may also include variables related to patient (e.g. sex and age), disease (e.g. T-stage), and treatment (e.g. chemotherapy) as well as baseline data (44). A variety of NTCP models exist, and most commonly these predict binary outcomes, i.e. the absent or occurrence of a complication (45-51), NTCP models can be used, among other things, for biological treatment plan optimization (52), for comparing the risk of complications between photon and proton treatment plans in a model based patient selection approach (53-55), or for identifying patients eligible for randomized trials that compare treatment effects from photon- and proton therapy (56).

Validation is key aspect of predictive modelling (57). Internal model validation is applied to avoid overfitting of the data by correcting the model for optimism, either through bootstrapping or cross validation (58, 59). In external validation, generalizability of the model is tested by applying the model in a new population and evaluate whether a model adjustment is required to achieve appropriate performance (60). Performance is typically assessed in terms of the ability of the model to discriminate between events and non-events (discrimination), and by evaluate the agreement between predicted probability and observed outcome (calibration) (59).

1.3.2 The logistic regression model

Logistic regression is appropriate for modelling binary response and are commonly used for NTCP modelling. In contrast to linear regression, which estimates absolute response values, the logistic regression estimates the probability that an event will occur. The relationship between the outcome, and one or more explanatory or predictor variables is expressed by the logistic function:

$$P = \frac{1}{1+exp^{(-X\beta)}}$$
(1.6)

In this function the P is the probability of an event. The $X\beta$ stands for $\beta_0 + \beta_1 x_1 + \ldots + \beta_k x_k$ where the x's are the model predictor(s) and the β's the estimated coefficients, respectively (61). The logistic function restrict the P to range between 0 and 1, whereas as X has unlimited range as illustrated in Figure 1.6.
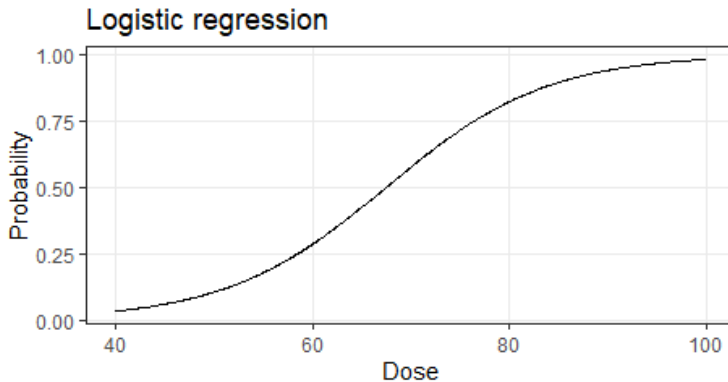
Figure 1.6: The logistic regression curve for model with dose as the only predictor.

The odds is defined as the probability of an event of interest occurs (P) divided by the probability that the event does not occur ($1 - P$). The logistic regression function can be transformed into:

$$ln\left(\frac{p}{1-p}\right) = X\beta$$
(1.7)

The left side of the formula is the logarithm of the odds and is called the logit (or log-odds). The relationship between the logit and $X\beta$ is assumed to be linear, therefore, for a model with a single predictor x_1, a one unit change in the x_1 will correspond to a β_1 change in the logit (62). The same is true for a multivariate model if there is no interaction between x_1 and any of the other predictors, and if all other model predictors are held constant. The β_0 is the intercept (constant) of the model. If all x's in a model is 0, then the logit is equal to β_0.

1.3.3 Mixed effect logistic regression

In logistic regression all observations in the data set are handled as if they were independent and at the same hierarchical level. In this model, the estimated predictor effects are fixed, meaning that they are constant across individuals. However, in many scenarios data are nested by some characteristic such as for longitudinal data where measurements are repeated on the same individual several times, or in case of clustered multilevel data such as observations on patients within a department, departments within a hospital and hospitals within a region. For these situations it is likely that observations from the same cluster are correlated. Mixed effect logistic regression is an extension of logistic regression which incorporates the clustering structure of the data and allows estimating both the fixed and random effects in the data (63, 64) . In mixed effect model with only a random intercept, the intercept (i.e. group mean) will vary between the subjects, however the predictor slope will be similar for all subject. The random intercept model is illustrated in Figure 1.7a). A model with both random intercepts and slopes, are illustrated in Figure 1.7b). In addition to varying group means the effect of the model predictor also varies between the subjects.
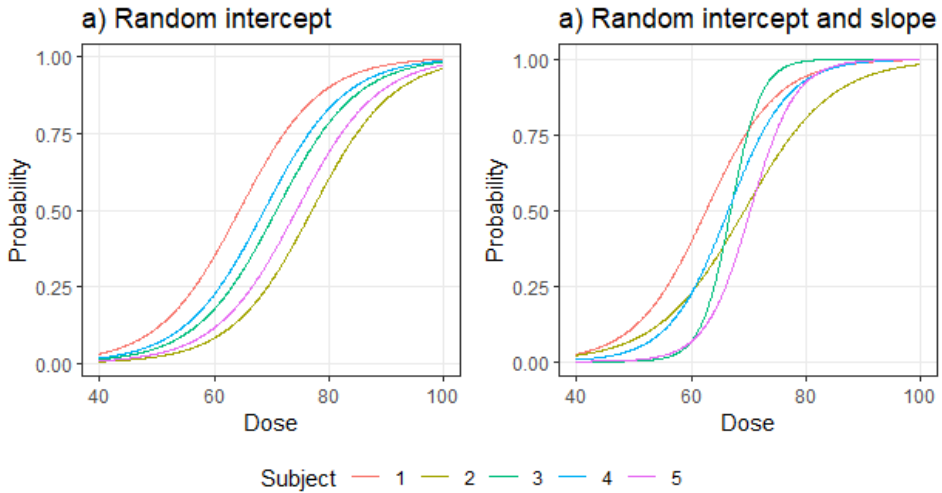
Figure 1.7: Illustration of a univariate mixed effect model for a) a model with a random intercept, but a constant slope for dose, b) model with random intercept and random slope.

1.3.4 Recursive partitioning analysis

The recursive partitioning algorithm works by performing binary splits of the variables in the data set in order to create a decision tree for either regression or correct classification of observations. It is a step-by-step analysis which divides the data into sub-groups of similar observations. The so-called root node is the starting point of the analysis and consist of the entire data set. The splitting variable is the variable most associated with the response, and a splitting criterion determines the optimal cutoff point of the variable. According to this decision, the data are divided into two so-called daughter nodes, one of which consists of observations with variable values above the cut-off point, and the other with variable values below and equal to the cut-off point. The procedure is then repeated independently on each node until a stopping criteria is met (Figure 1.8) (65).

The goal of each split is to create daughter nodes that are as pure (homogeneous) as possible. Splitting are performed on all available variables, and by measuring the resulting impurity (heterogeneity) of all possible splits, the split with the lowest impurity

are selected. Impurity can be measured by The Gini Index, which calculates the probability of misclassification of randomly selected variable and is defined as:

$$Gini\ index = 1 - \sum_i p_i^2 \qquad (1.8)$$

with p_i being the probability of belonging to class *i*. A full-grown tree is likely to overfitting the data. This can be avoided through pre-and post-pruning of the tree. Pre-pruning involves setting various restrictions before running the analysis, such as constraining the tree-depth or put a minimum number of observations in a node before splitting is allowed. By post-pruning, nodes will be removed that do not increase prediction accuracy through e.g. cross-validation.
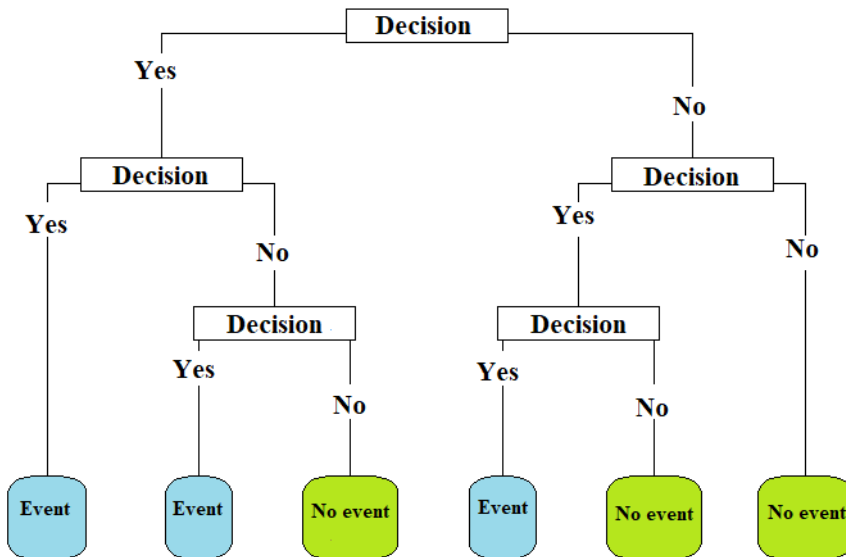
Figure 1.8: Illustration of a decision tree. The data is recursively partitioned in order to create groups of similar observations. The first binary splitting is performed on the root node, and observations are grouped according to this decision into daughter nodes. The binary splitting is then performed separately on each daughter-node and repeated until, ideally, the observations belong to the same class, or until a stopping criteria is met.

1.4 The relative biological effectiveness of protons

Currently, dose prescription and normal tissue dose constraints used in proton therapy relies on extensive clinical experience from radiotherapy with photons. Compared to photons, protons are considered to be slightly more effective in inducing biological damage. Quantitatively, the difference in radiobiological efficiency is described by the concept Relative Biological Effectiveness (RBE). For a given endpoint, and equal biological effect measured under identical conditions, the RBE is defined as

$$\text{RBE} = \frac{D_{reference}}{D_{proton}} \tag{1.9}$$

where $D_{reference}$ and D_{proton} is absorbed dose from the reference irradiation, typically photons (6 MV x-rays or ^{60}cobolt γ-rays), and protons, respectively (66, 67). To calculate RBE weighted doses (RWD) the physical dose is multiplied with the RBE.

The RBE of protons is a complex variable known to be influence by several physical, biological and treatment related factors. However, despite decades of research, we still fail to fully explain the mechanisms behind the proton RBE. Clinical data are almost lacking, and there is a limited amount of in-vivo experimental data on proton RBE (68). Most commonly clonogenic cell survival have been studied for different in-vitro cell lines with emphasis on assessing potential variations/dependencies in the proton RBE with LET, dose and α/β (69-71).

1.4.1 Proton RBE variability as a function of LET, dose and α/β

As previously described in chapter, energy deposition become denser with decreasing proton energy, leading to clustered and more complex DNA damages, in particular at the end of the proton range. In-vitro experiments show a consistent trend, where the increasing LET translates into an increase in RBE as illustrated in Figure 1.9. In a comprehensive review of previous publications, available experimental data were summarized and analyzed (70). For example, for 2 Gy dose, an averaged RBE of 1.15 was found for LET values ranging from 1 keV/µm to 3 keV/µm. For LET values ranging

from 6 keV/µm to 9 keV/µm, the average RBE was 1.35 which increased to 1.72 for even higher LET (9-12 keV/µm). The increase in RBE as a function of LET could extend biological range with up to 0.4 cm (72).
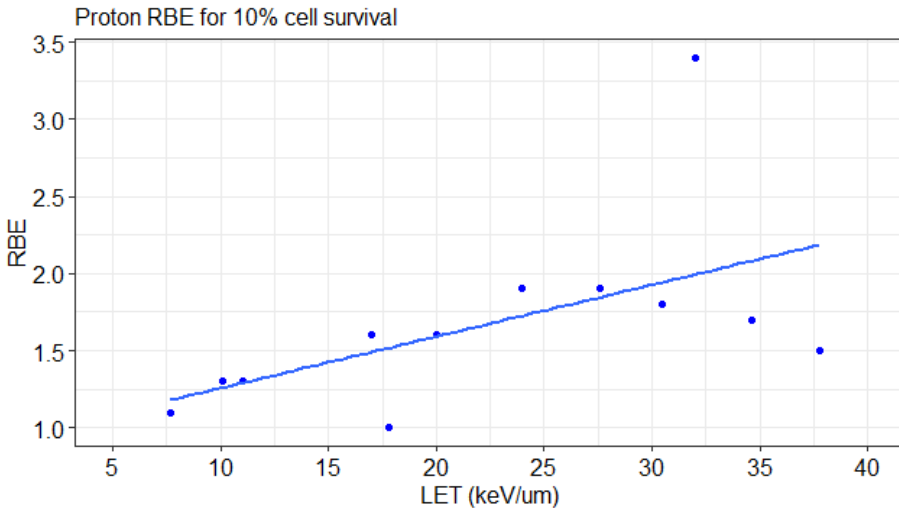
Figure 1.9: Linear fit of proton RBE as a function of LET for 10 % cell survival for V79 hamster cell lines. The plot is created based on data published in Sørensen et al. (73)

The RBE dependency on dose is less evidenced. There is a limited number of experiments assessing the RBE-dose relationship at clinical relevant dose levels, and existing experimental data have few data points below 2 Gy (74). In general, data suggest an increase in RBE with decreasing dose, an effect which seems to be more prominent at high LET. Furthermore, the increase in RBE with decreasing dose is expected to be more rapid for low α/β (i.e. late responding tissues) compared to high α/β (i.e. early responding tissues) (70).

Theoretically, an increase of RBE is expected with decreasing α/β (72), and early experimental data found a significant increase of RBE for α/β, but only for α/β values below 5 Gy (75). In a later analysis of available published in-vitro cell survival data, the exact relationship between RBE and α/β could not be demonstrated (70). There were

however indications for a slight increase in RBE with decreasing α/β for clinical relevant LET values (< 15 keV/μm).

To summarize, it is generally assumed that the proton RBE will increase with increasing LET as well as with decreasing dose and α/β. Translated in to a clinical setting one would expect the highest RBE to occur in late responding tissue (e.g. low α/β) located in regions with high LET (e.g. at the end of the proton range) and for lower dose (e.g. outside the target volume).

1.4.2 Modelling proton RBE

The development of models for accurate prediction of the proton RBE has been an area under active investigation/research for many years. Several variable RBE models have been developed and these can roughly be categorized into two groups. Mechanistic models estimate cellular damage (DSB) and to some extent also DNA repair, and relate these to cell survival (74). Phenomenological RBE models are fitted using in- and output data from experiments on clonogenic cell survival for various cell lines (76). Most commonly they are mathematically expressed within the LQ formula using the physical proton dose (D_p) and the radiosensitivity parameters of the reference irradiation (α_x and β_x), and the proton irradiation (α and β), respectively (69):

$$RBE\left(D_p, \alpha, \beta, \left(\frac{\alpha}{\beta}\right)_x\right) = \frac{1}{2D_p}\sqrt{\left(\frac{\alpha}{\beta}\right)_x^2 + 4D_p\left(\frac{\alpha}{\beta}\right)_x\frac{\alpha}{\alpha_x} + 4D_p^2\frac{\beta_p}{\beta_x}} - \left(\frac{\alpha}{\beta}\right)_x \qquad (2.0)$$

The RBE reaches its maximum (RBE_{max}) and minimum (RBE_{min}) for doses towards zero and infinity, respectively (77) and is expressed as:

$$RBE_{max} = \frac{\alpha}{\alpha_x} \qquad (2.1)$$

$$RBE_{min} = \sqrt{\frac{\beta}{\beta_x}} \qquad (2.2)$$

Rewriting the equation 2.0 as a function of RBE$_{max}$ and RBE$_{min}$ gives

$$RBE\left(D_p, \left(\frac{\alpha}{\beta}\right)_x, RBE_{max}, RBE_{min}\right)$$

$$= \frac{1}{2D_p}\sqrt{\left(\frac{\alpha_x}{\beta_x}\right)^2 + 4D\left(\frac{\alpha_x}{\beta_x}\right)RBE_{max}D_p + 4D_p^2RBE^2_{min}} - \frac{\alpha_x}{\beta_x} \qquad (2.3)$$

Equation 2.1 applies to all LQ based phenomenological models, however the models differ in their definitions of the RBE$_{min}$ and RBE$_{max}$ (69, 76). RBE$_{max}$ is assumed to be dependent on LET by most of the models. This is also the case for RBE$_{min}$ in some models, whereas others assume no LET dependency for RBE$_{min}$.

1.4.3 The RBE in clinical proton therapy

Current clinical practice disregard the above mentioned uncertainties in the RBE and apply a constant RBE value of 1.1 (RBE$_{Fix}$) (23). Thus, for both tumor and normal tissues the delivered proton dose is equivalent to a 10% higher photon dose. The use of a RBE$_{Fix}$ is based on experiments conducted in the early era of proton therapy (1960s-1970s) (23). The value is primarily chosen to ensure tumor control when applying proton therapy based on experience from photon therapy. It is an average of several RBE values for multiple in vivo endpoints, measured at the center of the SOBP at 2 Gy(RBE) fraction doses using Co-60 as reference irradiation (71). The use of a constant RBE of 1.1 is undoubtedly a simplification of reality, thus in line with an increasing knowledge base, it has regularly been questioned whether this holds in a clinical setting. The validity of using RBE$_{Fix}$ in clinical practice has therefore been evaluated and discussed on several occasions by the proton therapy community. Both a change in the current value of 1.1, continued us of constant value that are different for OARs and tumors, as well as implementation of RBE models have been considered without finding sufficient evidence that could support a revise of current practice (70, 71, 74, 78). This is based, among other things, on major uncertainties in the experimental data material as well as

the lack of in-vivo data and limited amount of clinical outcome data confirming the effect of variable RBE.

Despite the current use of an RBE of 1.1, the variability of RBE is widely acknowledge and taken into considerations in clinical routine. In a recent published survey amongst 25 European proton therapy facilities, all centers had introduced precautionary measures to counteract uncertainties from variable RBE. Most commonly the so-called LET effect were considered, and beam arrangements were selected to avoid or reduce number of beams stopping in front or inside critical structures (16).

1.5 Proton therapy for head and neck at the skull base region.

Cancers at the skull base region are in close proximity to numerous critical and dose limiting organs at risk (OAR). For curative intent, doses from 66-74 Gy are prescribed in the definitive setting, and from 50-66 Gy in the post-operative setting (79), thus poses challenges in the trade-off between delivering adequate tumor dose and the risk of developing late complications. Considering the favorable dose distribution that can be achieved with proton therapy (Figure 1.10), it is therefore believed that a large proportion of these patients will benefit from proton therapy in terms of a reduction in normal tissue toxicity (80). However, this belief lacks supporting evidence from randomized controlled clinical trials; existing data on the potential benefit of proton therapy stems mostly from dosimetric comparisons (80-84), and retrospective or prospective outcome studies from single institutions reporting promising disease control, and moderate rates and severity of acute and late toxicity (82, 85-89).

Recently, Lee et al. (90) published a systematic review of proton therapy for nasopharyngeal cancers. After reviewing available literature, nine studies met the inclusion criteria of which eight were NPC only and one consisted of both NPC and sinonasal cancers. All studies were retrospective and four of them included comparisons with IMRT. Overall, disease outcomes were comparable to IMRT. Both acute and late effects seemed to be improved with proton therapy, however were only statistically significant for grade 2 mucositis and feeding tube rates.

Previously a systematic review and meta-analysis (41 publications) by Patel et al. compared particle therapy (mainly proton and carbon ions) to IMRT for sinonasal cancers. The authors reported overall improved disease outcome after particle therapy, and in a subgroup analysis comparing proton therapy to IMRT, an increased 5 year overall survival, and better locoregional tumor control (91). The toxicity outcomes were similar between particle therapy and IMRT with the exception of significantly higher neurological toxic effects after particle therapy. However, the authors highlighted a potential reporting bias, as a significantly higher proportion of the particle therapy studies included reports on toxicity compared to the IMRT studies.

Thus, the superiority of proton therapy over photon therapy for HNC at the skull is weakly evidenced. Currently, HNC and skull base tumors are treated at 88% and 92% of the European proton therapy centers (n = 19), respectively (92).
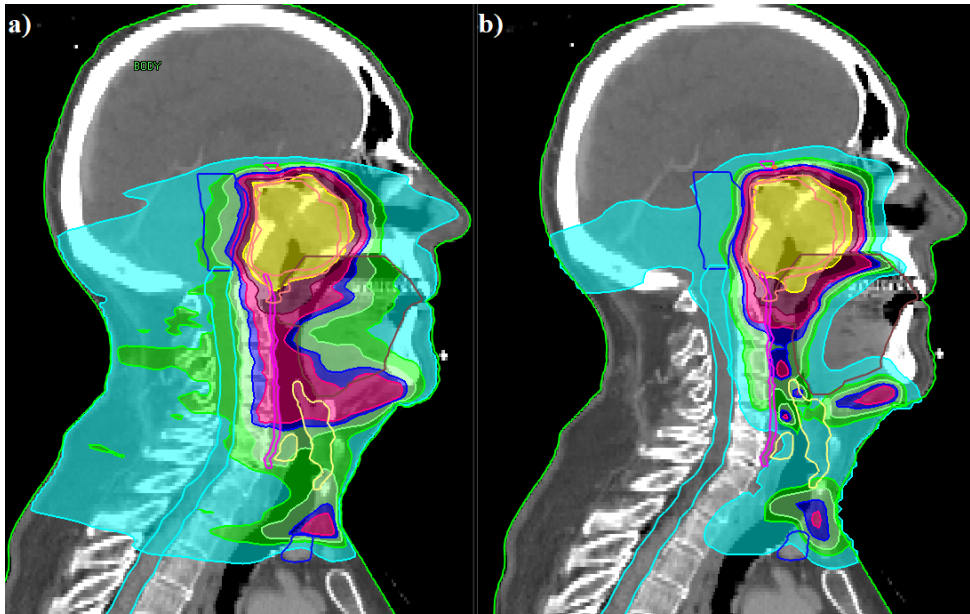
Figure 1.10: Visualization of dose distributions for state-of-art photon (a) and proton (b) therapy in a patient with nasopharyngeal cancer. Target dose conformity are approximately similar, however with better sparing of normal tissue for the proton treatment plan (courtesy of Camilla Grindeland Boer).

1.5.1 The risk of radiation induced brain necrosis

Brain necrosis is one of several potential late effects that is paid attention to during treatment planning of HNC at the skull base region. The first report of radiation induced brain necrosis dates back to the 1930s where the complication was thoroughly describe in a paper by Fischer and Holfelder (93). Although numerous case reports (94), experiments and pathological examinations have since contributed to a better understanding of the mechanisms behind radiation necrosis, the pathogenesis is still not fully explained (95). There is, however, a general understanding that it develops as a

result of radiation damages to the glial cells and the vascular endothelial cells. These damages trigger a series of multiple chemical and biochemical reactions, which ultimately result in a disruption of the blood-brain-barrier (BBB). Consequently, cerebral edema and micro bleeds, ischemia and small vessel occlusion may occur. Important contributing mechanisms include the up-regulation of vascular endothelial growth factor (VEGF) and angiogenesis, the demyelination of nerve fibers and inflammation induced by the release of reactive oxygen species (ROS) (94, 96). It is believed that these processes interact and lead to an increased overall effect (97). The histopathological findings include tissue necrosis and telangiectasia, microvascular dilatation, thickening and hyalinization of the vessel walls (98, 99).

Diagnosis

The diagnostic gold standard for radiation necrosis is based on pathological examination of the resected lesion. As being an invasive procedure this entails obvious drawbacks, non-invasive radiological procedures are therefore a commonly used alternative. Contrast enhancement and ring enhancing lesions on T1-weighted ($T1_w$) sequences and edema visualized on T2-weighted ($T2_w$) sequences are specific structural changes which can be observed on Magnetic Resonance Imaging (1.11) (95). These image features are however similar to tumor recurrence and supporting functional imaging like diffusion and perfusion imaging, MR spectroscopy and PET/SPECT are recommended guide in distinguishing between the two (100).
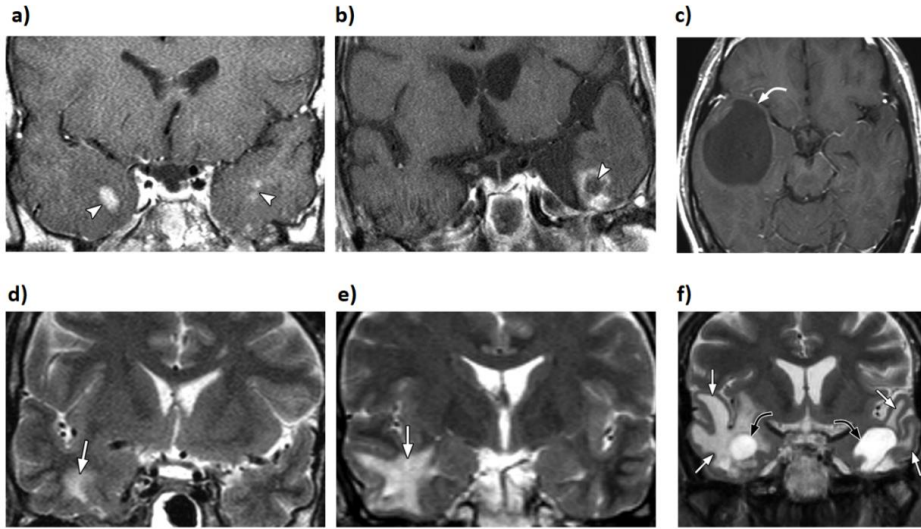
Figure 1.11: Manifestations of radiation necrosis on post contrast T1 weighted MRI sequences on the top row and T2 weighted sequences on the bottom row: a) bilateral contrast enhanced solid nodules, b) contrast enhanced nodule with central necrotic region, c) cyst with low signal intensity including slight rim enhancement, d) small white matter lesion, e) medium sized white matter lesion and f) white matter lesions (white arrows) and cysts (black arrows). Images from Wang et al. (101) (reused with permission).

Clinical symptoms and treatment

Clinically, radiation associated brain necrosis show a highly variable course of which the severity is believed to be mostly dependent on radiation dose and volume of brain irradiated. Some patients present with asymptomatic lesions solely expressed as radiological features on post-treatment surveillance images, whereas progressive necrotic lesions with pronounced symptoms on intracranial pressure, cognitive decline and focal deficits, represent one of the most severe radiation induced injury. Both the size and location of the necrotic region are decisive of the symptomatology (99). Brain necrosis are preferably graded using a standardized scoring system like the Common Criteria for Adverse Events (CTCAE) developed by the National Cancer Institute (102) (Table 1.1).

Table 1.1: Clinical grading of cerebral necrosis according to the Common Criteria for Adverse Events (CTCAE v4.03).

Grade 1	Grade 2	Grade 3	Grade 4	Grade 5
Asymptomatic; clinical or diagnostic observations only; intervention not indicated	Moderate symptoms; corticosteroids indicated	Severe symptoms; medical intervention indicated	Life-threatening consequences; urgent intervention indicated	Death

For small asymptomatic lesions, a wait and see strategy supported by more frequent imaging surveillance is recommended (103). Conventional treatment interventions for symptomatic and/or progressive lesions include treatment with corticosteroids, anticoagulants, hyperbaric oxygen and resection/surgery. Novel treatments include Bevacizumab, free radical scavengers, gangliosides and nerve growth factor of which Bevacizumab is considered to have the best supported evidence (104).

Dosimetric risk factors and recommended dose constraints

The main risk factor for the development for radiation necrosis are radiation dose, irradiated volume and fraction size (105). The majority of published dose constraints emphasizes the importance of focal high doses, although some authors also have pointed out a potential volume effect. Estimated dose constraints (i.e. D_x indices) are typically $\leq 2cc$, whereas volume thresholds (V_x indices) range from V_{20Gy} to V_{70Gy}. The exact dose response relationship is however unclear; for the same dosimetric indices the suggested thresholds for toxicity may vary by up to several Gy's or cc's (106-119). The international radiotherapy community has reached a consensus based on review of existing literature, and provided recommendations and guidelines on dose constraints for the brain (105, 120, 121). The Quantitative Analysis of Normal Tissue Effects in the Clinic (QUANTEC) (122-124) updated in 2010 the guidelines on normal tissue dose- and volume thresholds for toxicity initially published in 1991 by the Emami et al (125).

Radiation dose constraints for the brain (and substructures of the brain) in neuro oncology was published by The European Particle Network (EPTN) in 2018 (120). Most recently, the International Guideline on Dose Prioritization and Acceptance Criteria in Radiation Therapy Planning was published for Nasopharyngeal Carcinoma (121). The recommendations are listed in Table 1.2.

Table 1.2: International consensus guidelines for dose criteria to the brain and temporal lobes to minimize risk of developing radiation necrosis.

Reference	Dose constraints
Quantitative Analysis of Normal Tissue Effects in the Clinic (QUANTEC)*	$D_{Max} \leq 72.0$ Gy
The European Particle Therapy Network consensus (EPTN)*	$V_{60.0} \leq 3.0$ cc
International Guideline on Dose Prioritization and Acceptance Criteria in Radiation Therapy Planning for Nasopharyngeal Carcinoma**	$V_{65.0} \leq 0.03$ cc
	$V_{70.0} \leq 0.03$ cc***

* Brain, ** Temporal lobe, *** T3-T4 tumors

Clarification of concepts

In the literature there is no consistency in the definition of brain necrosis and the term is used for a spectrum of outcome measures. The most conservative definition accept only biopsy-proven necrosis, more often necrosis are defined as symptomatic image changes, in other cases the definition is solely based on characteristic MRI features and may include both symptomatic and asymptomatic image changes.

When reporting incidence rates the latter is the most common. Most commonly reported incidence rates of brain necrosis are radiographically diagnosed, and often include both symptomatic and asymptomatic lesions. The labels used to describe the effect are used

interchangeably and include image change, necrosis, contrast enhanced lesions, injury, reactions, toxicity and damage. In this PhD work we have used the terms image change, more specifically radiation associated image change (RAIC) and temporal lobe image change (TLIC), in addition to necrosis.

2. Aims of the project

The overall goal of this thesis was to explore radiation induced brain necrosis in patients treated with proton therapy for cancers in the upper head and neck and skull base region. This comprised of identification of proton specific prognostic factors and dose constraints, predictive modelling and analysis in terms of RBE variations, and investigating spatial dose- and LET correlations with MRI changes associated with brain necrosis. The specific aims were:

Paper I:

- Characterize the incidence and patterns of RAIC after PT for skull base HNCs
- Identify candidate clinical and dose–volume parameters associated with RAIC
- Propose practical dose constraints to minimize the risk of RAIC

Paper II

- To investigate the effect of RBE variations on NTCP estimates of temporal lobe necrosis in skull base HNC previously treated with IMPT
- To evaluate and compare the applicability of previously proposed dose constraints for limiting risk of temporal lobed necrosis according to fixed and variable RBE weighted doses.

Paper III

- To explore dose and LET correlations with RAIC in patients treated with IMPT for HNC and skull base cancer.

3. Material and Methods

3.1 Patient material

The patients in the present PhD project were participants in two Institutional Review Board-approved and ongoing prospective observational studies at the University of Texas MD Anderson Cancer Center, Houston, Texas, USA; "Data collection to assess acute and late normal tissue sequel in proton therapy for adults" and "Prospective Data Collection of Patients Treated With Proton Therapy for Head and Neck Malignancies". These studies aim to evaluate outcomes and treatment related side effects after proton therapy, to investigate correlation of normal tissue response to proton dose distribution and to derive and refine dose-response relationships for normal tissue toxicity after proton therapy. A variety of diagnosis and disease sites are included in these studies, therefore, to form a database of eligible patients for the current PhD project, the patient had to meet the following criteria to be included:

- Patients with HNC and anatomic disease location at the base of skull
- A maximum dose (D_{max}) to the brain (i.e. point dose) of at least 40 Gy($RBE_{1.1}$)
- One or more post-treatment MRIs acquired ≥ 6 months after completion of proton therapy

Patients with prior radiotherapy to the skull base region and/or photon based treatment as part of therapy were excluded. A semi-automatic approach where used to identify eligible patients. Three hundred and seven patients were selected after the initial review of the study database based on anatomic disease site. For these patients, the radiology reports from the Radiology Information System (RIS) where filtered for "MRI" and further screened using the key words/terms "necrosis", "radionecrosis", "brain necrosis" and "nodule". From the treatment planning system, the patients' brain dose distributions were manually reviewed by the candidate to exclude those patients not meeting the brain dose criteria, whereas the medical records (Epic Systems Corporation, Verona, WI) were used to identify and exclude patients with prior radiotherapy and to look for reports on clinical symptoms on radiation necrosis. After this procedure, a total of 127 patients were identified. The disease sites included mainly nasopharyngeal cancers, cancers in the paranasal sinuses and sinonasal cancers, periorbital cancers, parotid cancers and skin

cancers, but also some skull base tumors including chordoma and chondrosarcoma (Figure 3.1).
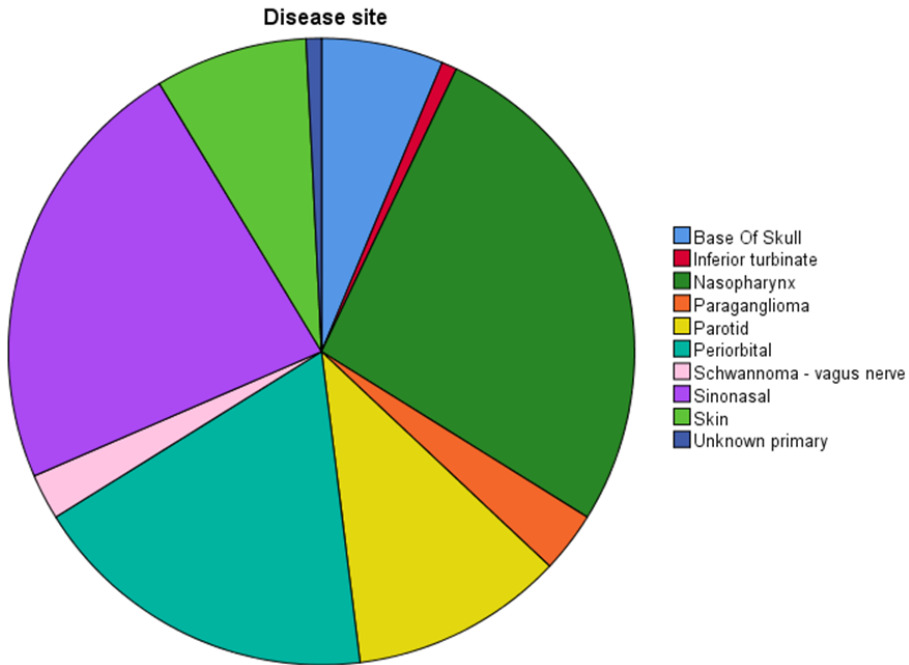
Figure 3.1: Disease sites for 127 patients.

Twenty two of these patients were diagnosed with radiation associated brain necrosis in the MR reports, however for all 127 patients the MRIs and reports where reviewed for RAIC a second time by the candidate in order to identify potential patients with RAIC not captured by the automatic query procedure. The MRIs with reports diagnosing radiation necrosis where finally reviewed by two board- certified radiation oncologist in order to confirm the diagnosis (GBG and SJF).

Figure 3.2 gives and overview of the patient inclusion process and the study cohort in each of the individual studies. In paper I, the study cohort consisted of all 127 patients. The study cohort in paper II consisted of 45 of patients treated with IMPT. These were

patients with available variable RBE weighted doses from Monte Carlo simulations and at least 24 months of follow-up time. Paper III consisted of 15 patients with verified RAIC after treatment with IMPT. Sixteen patients where initially diagnosed with RAIC after treatment with IMPT, however, technical issues hindered extraction of the Monte Carlo doses at voxel level for one patient whom was excluded from the analysis.
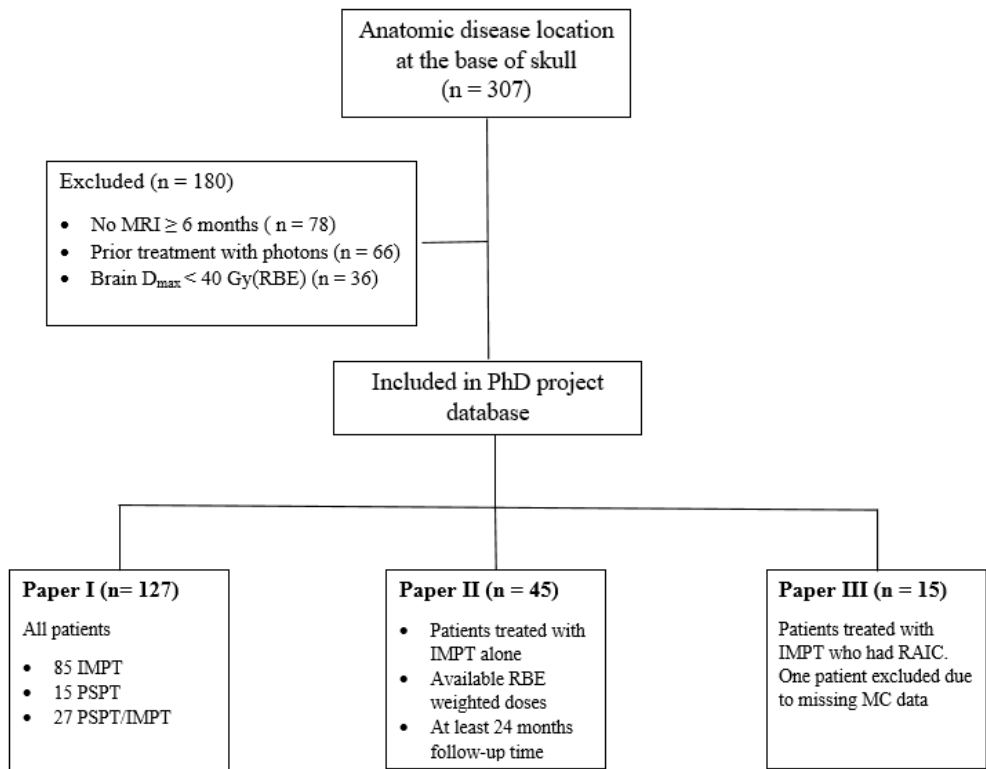
Figure 3.2: Overview over the patient material included in the project data base and the study cohort in each individual study.

3.1.1 Loss to follow-up

In the current project follow-up time was defined as time from the last day of proton therapy to last available follow-up MRI, regardless of any medical consultations the patients might have had after this date. The follow-up MRIs took place regularly at every 3 to 4 months the first and second year, every 6 months until 5 years, and annually thereafter. For the patients diagnosed with RAIC, a median of 6 (min-max: 1-18) follow-up MRIs were available. For the total cohort (n=127) a median of 5 (min-max: 1-18) follow-up MRIs were available. Ten of the patients had died of which two were diagnosed with RAIC. For eight of the patients still alive, it was more than 24 months since the last MRI, four of these had been followed with imaging for 24 months or longer. For 18 of the patients still alive it was 12 months since the last MRI, this was also the case for six of the patients with RAIC.

3.2 The fast dose calculator

For study II and III a recalculation of the patients' treatment plans was required in order to obtain the LET distributions, Monte Carlo dose distributions (RBE = 1.1) and variable RBE weighted dose distributions. The Digital Imaging and Communications in Medicine (DICOM) files including the treatment planning CT, the treatment plans, the structure sets and the treatment planning dose distribution were exported by the candidate from the treatment planning system and imported in to an in-house developed Monte Carlo system, the fast dose calculator (FDC) (126-129). The FDC uses a database of pre-computed proton trajectories discretized in ≤ 1 mm in water in order to calculate the dose distribution in other materials by scaling methods. The FDC algorithm calculates the dose and unrestricted dose averaged LET (LET_d) based on the patient's treatment plan and the assigned planning CT. The LET_d includes primary and secondary protons and is computed using a step-by-step approach previously described by Cortes-Giraldo and Carabe (method 3) (130), and where LET_d is calculated from pre-generated tables of stopping power obtained from GEANT4 (131).

3.2.1 RBE models

In paper II, two phenomenological models were used predict RBE and estimate variable RBE weighted doses (RWD$_{var}$), both taking LET$_d$, dose and α/β as input parameters.

The RBE model from McNamara et al. (RBE$_{McN}$) (132) is based on the experimental data for numerous cell lines extracted from 76 studies and previously summarized and reviewed in Paganetti et al (70). The data set consisted of 285 data points with a range of LET values < 20 keV/µm and α/β < 30 Gy. The RBE model from Wedenberg et al (RBE$_{Wed}$) (133) are based on experimental data from 10 different cell lines. The data set consisted of 24 data points with LET values ranging from 6 to 30 keV/µm and with α/β ranging from 2.7-69.5 Gy. The equation 2.1 were used to predict the RBE using a previously published α/β value for brain necrosis of 2.0 Gy (134). The model assumptions and parameter values are displayed in Table 3.1.

Table 3.1: Assumptions for RBE$_{min}$ and RBE$_{max}$ including corresponding parameter estimates from the original publications on the RBE models from Wedenberg et al. (RBE$_{Wed}$) and McNamara et al.(RBE$_{McN}$).

Modell	Model assumptions		Parameter values			
	RBE$_{max}$	RBE$_{min}$	P$_0$	P$_1$	P$_2$	P$_3$
RBE$_{McN}$	$p_0 + p_1 \dfrac{LET_d}{(\alpha/\beta)_x}$	$p_2 + p_3\sqrt{(\alpha/\beta)_x}LET_d$	0.99064	0.35605	1.1012	-0.0039
RBE$_{Wed}$	$p_0 + p_1 \dfrac{LET_d}{(\alpha/\beta)_x}$	1.0	1.0	0.434	-	-

3.3 Data analysis and statistical methods

The statistical analysis were performed in the software R (R Foundation for Statistical computing, version 3.6 and 4.01) (135) and in IBM SPSS statistics for Windows, Version 24 and 26 (IBM Corp., Armonk, NY, USA).

In all papers, data were summarized using descriptive statistics. Measures of central tendency were presented using mean and median values, whereas measures of variability were reported as standard deviations (SD), interquartile ranges (IQR) and minimum to maximum values (range). Boxplots were used for graphical presentation of descriptive statistics.

Non-parametric test for group comparison included Mann-Whitney-U test for continuous variables and Chi-Square Test/Fishers Exact test for categorical variables (paper I and II).

For comparisons between three related groups, Friedman's Two-way Analysis of Variance by Ranks were applied including pairwise comparisons using Wilcoxon signed-rank test and Bonferroni corrections to adjust the p-values (paper II).

In all statistical tests $p < 0.05$ were considered statistical significant.

3.3.1 Paper I

The study cohort consisted of 127 patients. The Kaplan-Meier method were applied to estimate RAIC-free survival (136). Commonly, a proportion of asymptomatic RAIC will resolve spontaneously. In order to estimate the probability of RAIC over time, when also accounting for transient events of RAIC, multistate analyses was applied (137). For the current analysis the event of interest was RAIC, and data were censored if patients were alive and RAIC free at last available follow-up MRI. Univariate and multivariate Cox Proportional Hazards regression analysis were used to investigate the effect of candidate variables on RAIC.

Recursive Partitioning Analysis (RPA) (chapter 1.3.4) was used to identify volume-dose (V_D) indices predictive of RAIC (65). The Gini index was used as splitting criteria, and with number of observations in the terminal node constrained to 10% of the dataset and a maximum depth of the tree set to 1.

3.3.2 Paper II

Paper II investigated the influence of RBE variations on estimated risk of developing temporal lobe necrosis. The study cohort consisted of 45 patients. After excluding the contralateral lobes from patients with unilateral treatments, 75 temporal lobes were included in the analysis. The endpoint was temporal lobed image changes (TLIC) defined as necrosis, which was present in 16 out of 75 temporal lobes.

The fixed (RWD_{Fix}) and variable RBE weighted (RWD_{Var}) temporal lobe doses were calculated using RBE = 1.1 (RBE_{Fix}), RBE_{McN} and RBE_{Wed}, and the difference in several dose indices between RWD_{Fix} and RWD_{Var} were compared (Table 3.2). For the dose volume indices the predicted RBE was estimated by dividing the RWD_{Var} with RWD_{Fix}.

Table 3.2: Investigated dose indices, $D_{Volume\ (cc)}$ is the dose delivered to x volume of the temporal lobes, $V_{Dose\ (Gy[RBE])}$ is the volume of temporal lobes receiving x dose.

$D_{Volume\ (cc)}$	$V_{Dose\ (Gy[RBE])}$
D_{max}	V_{40}
$D_{1.0}$	V_{45}
$D_{2.0}$	V_{50}
$D_{3.0}$	V_{55}
$D_{4.0}$	V_{60}
$D_{5.0}$	V_{65}
D_{mean}	V_{70}

In clinical treatment plan evaluation, dose constraints and objectives are applied in order to limit risk of developing temporal lobe necrosis. Suggested dose constraints from the literature (Table 3.3) were evaluated according to RWD_{Fix} and RWD_{Var} by calculating the proportion of TLIC in temporal lobes meeting the different dose constraints. These were considered as low-risk temporal lobes of which the proportion of TLIC should not exceed 5%.

Furthermore, in order to investigate the influence of variable RBE on the estimated probability of temporal lobe necrosis, univariate logistic regression NTCP models were fitted using selected dosimetric predictor variables from Table 3.3. The reference NTCP models were fitted based on RWD_{Fix}, whereupon the NTCP were calculated using both RWD_{Fix} and RWD_{Var}. The calculated difference in NTCP (ΔNTCP) between RWD_{Fix} and RWD_{Var} was compared.

Table 3.3:Dose constrains for temporal lobe necrosis

Dose constraints	Reference
$D_{Max} \leq 72.0$ Gy*	Quantitative Analysis of Normal Tissue Effects in the Clinic (105)
$D_{0.5cc} \leq 65.05$ Gy	Wen et al. (115)
$D_{1.0cc} \leq 62.4$ Gy	Kong et al. (109)
$D_{2.0cc} \leq 60.3$ Gy	Feng et al. (106)
$V_{60.0} \leq 3.0$ cc*	The European Particle Therapy Network consensus (120)
$V_{65.0} \leq 0.03$ cc	International Guideline on Dose Prioritization and Acceptance Criteria in Radiation Therapy Planning for Nasopharyngeal Carcinoma (121)
$V_{70.0} \leq 0.03$ cc**	

3.3.3 Paper III

The specific aim of paper III was to investigate voxel-wise dose- and LET_d correlations with RAIC after IMPT. The patient material consisted of 15 patients with RAIC. Monte Carlo simulations were performed using the Fast Dose Calculator (FDC). The DICOM files with the treatment plan, as well as the Monte Carlo calculated dose-and LET_d distributions were imported into an in-house developed MATLAB script. The script allows assigning binary values to user defined structures (i.e. 0 of 1), and for extraction of dose- and LET_d at voxel level. The result were exported as CSV files where each row represented one single voxel.

The contrast enhanced lesions observed on the first follow-up MRI where used as endpoint, therefore voxels within and at the border of the contoured lesions were considered as an event and assign the value 1. Voxels outside the lesions were considered non-events and assign the value 0. Since data were nested, univariate and multivariate mixed effect logistic regression were used to investigate associations

between LET_d, dose and RAIC. The independent variables (dose and LET_d) were normalized (center and scaled) before analysis. During modelling a few assumptions were made. We expected that the difference in number of voxels (both inside and outside RAIC) between the patients would affect the baseline levels and hence the average effects. We further assumed that both the effect of dose and LET_d varied between the patients. The random effects were therefore estimated for both the intercept, dose and the LET_d, assuming uncorrelated random effects. After multivariate modelling with LET_d and dose as predictors, we included an interaction term and repeated the analysis. The reason for this was that we hypothesized that the dose required to induce image change would be reduced if LET_d increased.

Internal model validation including estimating of 95% confidence intervals were performed using cluster bootstrapping with resampling of patients, rather than resampling of individual observations. Modelling were performed on two different data set, where voxels with physical doses below 15 Gy and 40 Gy were excluded, respectively.

3.4 Ethics

All patients had received information and signed written informed consent for data collection and analysis before enrollment in two Institutional Review Board approved prospective studies at MD Anderson Cancer Center, Houston, Texas, USA, Clinicaltrials.gov identifier: NCT 00991094 and Clinicaltrials.gov identifier: NCT 01627093, respectively.

The specific PhD project was approved by The National Committee for Medical and Health Research Ethics in Norway (2020/105).

4. Summary of results

4.1 Paper I

In paper I (138) we reported the incidence and patterns of RAIC in patients treated with proton therapy for HNC at the skull base region. We further identified dosimetric factors associated with RAIC. The median follow-up time was 29 months (6-97). Twenty-two (17.3%) out of 127 patients developed RAIC in median 24 months (9-37) after completion of PT. The Kaplan Meier estimates of the RAIC-free survival were 86%. 72% and 70% at two, three and five years, respectively.

The majority of RAIC developed in patients with nasopharyngeal or sinonasal cancers (77.3%), in patients treated for T4 tumors or unresectable disease (68.2%) or in patients with intracranial disease extent (63.6%) (Table 4.1). The lesions were found in the temporal lobes (14), frontal lobe (6) and cerebellum (2) (Figure 4.1), and were located inside the CTV in two cases, outside in seven cases and overlapping with the CTV in 13 cases.

All lesions were asymptomatic, however, three patients received treatment due to progression of the lesions on follow-up MRIs. Therefore, the RAIC were graded as Grade 1 brain necrosis in 19 of the patients and Grade 3 in three of the patients, respectively. In the last available MRIs, we found that the lesions had resolved in six patients, therefore the estimated probability of RAIC at two, three and five years where 14.3%, 25.4% and 23.1%[1], respectively.

In the univariate Cox Regression analysis only dosimetric variables were significantly associated with the development of RAIC (Table 4.2). In order to limit risk, we suggested that $V_{67Gy(RBE)}$ to the brain should be restricted to 0.2cc.

---

[1] This was reported as 8.7%, 14.3% and 12.7% in paper I. The error occurred during analysis, when the censored observations were wrongly coded.

Table 4.1: Patient characteristics for the entire cohort and by RAIC group.

Characteristic	All patients (n = 127)		No RAIC (n = 105)		RAIC (n = 22)		p
	n	%	n	%	n	%	
Sex							0.98
Male	67	52.8	57	54.3	10	45.5	
Female	60	47.2	48	45.7	12	54.3	
Age							0.69
Median (Q1-Q3)	51 (39-64)		50 (37-63)		54 (41-61)		
Anatomic Site							0.16
Base of Skull, NOS	7	6.3	6	5.7	1	4.5	
Nasopharynx	35	26.8	27	25.7	8	36.4	
Sinonasal	29	22.8	20	19.0	9	40.9	
Parotid	14	11	14	13.3	-	-	
Orbital	23	18.1	21	20.0	2	9.1	
Skin	10	7.9	9	8.6	1	4.5	
Other	9	7.1	8	7.6	1	4.5	
T-category							0.77
T1-T2	28	22	24	22.9	4	18.2	
T3-T4	53	41.7	41	39	12	54.5	
Recurrent	29	22.8	25	23.8	4	18.2	
Tx	5	3.9	5	4.8	-	-	
No stage	12	9.4	10	9.5	2	9.1	
Surgery							0.23
No	49	38.6	38	36.2	11	50	
Yes	78	61.4	67	63.8	11	50	
Induction chemotherapy							0.76
No	106	83.5	86	81.9	20	90.9	
Yes	21	16.5	19	18.1	2	9.1	
Concurrent chemotherapy							0.04
No	54	42.5	49	46.7	5	22.7	
Yes	73	57.5	56	53.3	17	77.3	
PT technique							0.72
IMPT	85	69.9	69	65.7	16	72.7	
PSPT	15	11.8	12	11.4	3	13.6	
IMPT/PSPT	27	21.3	24	22.9	3	13.6	
Prescribed dose							
Median (Q1-Q3)	64.0 (60.1-69.7)		64.0 (60.1-68.3)		69.3 (63.1-70.0)		0.04
Brain D_{max} < 60 Gy(RBE)							0.01
No	95	74.8	74	70.5	21	96.9	
Yes	32	25.2	31	29.5	1	3.1	
Brain D_{max} > 70 Gy(RBE)							< 0.01
No	89	70.1	81	77.1	8	36.4	
Yes	38	29.9	24	22.9	14	63.6	

Q1: 25 percentile, Q3: 75 percentile. Base of Skull: Adenoid cystic carcinoma, adenocarcinoma, neuro-endocrine carcinoma, chondrosarcoma, ameloblastoma, osteosarcoma. Other: vagus nerve schwannoma, paraganglioma, melanoma inferior turbinate, unknown primary site. IMPT: Intensity Modulated Proton Therapy, PSPT: Passive Scattering Proton Therapy

Figure 4.1: Proportion of RAIC in different brain regions according to disease site.

Table 4.2: Results from the uni-and multivariate cox regression analysis.

	Univariate analysis		Multivariate analysis	
	HR (95% CI)	*p*	HR (95% CI)	*p*
Age	1.02 (0.99-1.04)	> 0.1		
Anatomical site*	2.52 (0.99-6.45)	0.054	1.23 (0.41-4.05)	> 0.1
T3-T4**	1.83 (0.79-4.25)	> 0.1	0. 44 (0.12-1.66)	> 0.1
Surgery	0.56 (0.24-1.30)	> 0.1	2.46 (0.41-4.05)	> 0.1
Induction chemotherapy	0.67 (0.20-2.28)	> 0.1		
Concurrent chemotherapy	2.22 (0.82-6.03)	> 0.1	1. 99 (0.42-9.33)	> 0.1
PT technique***	1.06 (0.41-2.72)	> 0.1		
Prescribed dose	1.11 (1.01-1.23)	0.035	1.03 (0.88-1.20)	> 0.1
D_{max}	1.15 (1.07-1.24)	< 0.01	1.06 (0.92-1.21)	> 0.1
$D1_{CC}$	1.11 (1.05-1.18)	< 0.01		
$D2_{CC}$	1.10 (1.04-1.16)	< 0.01		
$D3_{CC}$	1.08 (1.03-1.13)	< 0.01		
$D4_{CC}$	1.07 (1.02-1.12)	< 0.01		
$D5_{CC}$	1.07 (1.02-1.12)	< 0.01		
$V_{40\ GY(RBE)}$	1.01 (0.998-1.02)	0.061	0.99 (0.98-1.01)	> 0.1
$V_{50\ GY(RBE)}$	1.01 (0.996-1.03)	0.080		
$V_{60\ GY(RBE)}$	1.01 (0.985-1.04)	> 0.1		
$V_{70\ Gy(RBE)}$	1.18 (1.03-1.34)	< 0.01	1.06 (0.87-1.29)	> 0.1
$V_{67\ Gy(RBE)} \geq 0.2$ CC	7.72 (2.84-21.0)	< 0.01	7.41 (1.48-38.76)	0.02

* Nasopharyngeal carcinoma/sinonasal vs other, **T3/T4 vs other. *** IMPT vs other, HR: Hazard Ratio

4.2 Paper II

In paper II (139) we studied the impact of variable RBE on temporal lobe dose distributions. We further investigated how uncertainty associated with variable RBE can affect the assessment of risk of developing temporal lobe necrosis (i.e. temporal lobe image change). The variable RBE weighted doses (RWD_{Var}) were significantly higher ($p < 0.05$) than doses calculated using RBE = 1.1 (RWD_{Fix}), thus the RBE in general exceeded 1.1 for the temporal lobes. Overall, the estimated RBE ranged from 1.20 to 1.25 depending on dose indices, but with lower RBE in temporal lobes with image changes (TLIC) compared to those without TLIC (Table 4.3) (The RBE values were not included in the publication).

Violation of the different dose constraints occurred in 21% to 43% of the temporal lobes for RWD_{Fix}, and in 33% to 66% for RWD_{Var} (numbers not included in the publication). In low-risk temporal lobes, defined as temporal lobes meeting the individual dose constraints, observed proportion of image changes ranged 4.0% and 13.1% for RWD_{Fix} and between 1.3% and 5.3% for RWD_{Var}. For $V_{65Gy(RBE)} \leq 0.03cc$ the proportion was less than 5% for both RWD_{Fix} and RWD_{Var} (Figure 4.2).

All NTCP models had good predictive performance (Table 4.4). Variable RBE resulted in an increase in estimated NTCP of temporal lobe necrosis that varied greatly in magnitude depending on dosimetric predictor used in the model. The median ΔNTCP was less than 10% for all models, with the exception of the model with D_{max} as predictor, where the median ΔNTCP was approximately 20%. Largest interpatient variations in ΔNTCP was seen with D_{max} and $V_{65Gy(RBE)}$ as model predictors (Figure 4.4).

Table 4.3: *The median (range) estimated RBE values for relevant dose indices displayed according to temporal lobes with (TLIC) and without image changes (no TLIC), respectively. RBE_{McN} and RBE_{Wed} refers to the RBE models from McNamara et al and Wedenberg et al which were used to calculate the RWD_{var}. For each of the dose indices, the RBE is estimated by RWD_{var}/RWD_{Fix}.*

	no TLIC		TLIC	
	RBE_{McN}	RBE_{Wed}	RBE_{McN}	RBE_{Wed}
D_{max}	1.27 (1.11-1.59)	1.29 (1.11-1.69)	1.18 (1.11-1.31)	1.17 (1.10-1.31)
$D_{0.5cc}$	1.23 (1.12-1.63)	1.24 (1.11-1.73)	1.16 (1.10-1.28)	1.16 (1.10-1.28)
$D_{1.0cc}$	1.22 (1.10-1.67)	1.22 (1.10-1.80)	1.15 (1.10-1.28)	1.15 (1.10-1.28)
$D_{2.0cc}$	1.23 (1.11-1.72)	1.24 (1.11-1.86)	1.17 (1.10-1.29)	1.17 (1.10-1.30)
$D_{3.0cc}$	1.23 (1.13-1.80)	1.25 (1.12-1.94)	1.18 (1.10-1.29)	1.17 (1.10-1.31)
$D_{4.0cc}$	1.24 (1.14-1.88)	1.25 (1.14-2.03)	1.19 (1.11-1.31)	1.17 (1.11-1.33)
$D_{5.0cc}$	1.24 (1.16-1.93)	1.26 (1.14-2.10)	1.20 (1.12-1.32)	1.19 (1.12-1.35)
D_{mean}	1.23 (1.13-1.72)	1.25 (1.12-1.85)	1.21 (1.12-1.35)	1.22 (1.12-1.40)
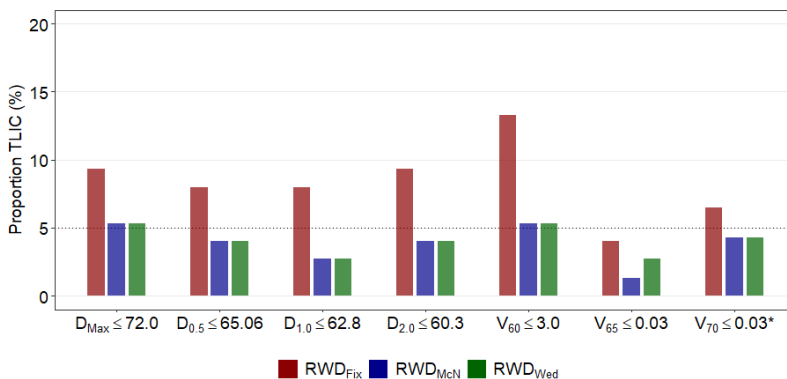
Figure 4.2: *Observed rates of image change in so-called low risk temporal lobes defined as temporal lobes meeting the dose constraints.*

Table 4.4: Odds ratio (OR) and performance statistics for the NTCP models

	Estimates		Performance				
Predictor	OR (95% CI)	p value	AUC	Intercept	Slope	R^2	Brier
$D_{0.5\,cc}$	1.14 (0.06-1.23)	< 0.01	0.838	0.039	0.997	0.35	0.14
D_{Max}	1.19 (1.07-1.33)	< 0.01	0.833	0.042	0.994	0.35	0.14
$D_{1.0cc}$	1.12 (1.05-1.20)	< 0.01	0.829	0.040	1.000	0.34	0.14
$D_{2.0cc}$	1.10 (1.05-1.16)	< 0.01	0.826	0.040	1.003	0.33	0.14
$V_{60GyRBE}$	1.27 (1.03-1.59)	< 0.05	0.813	0.001	0.983	0.11	0.16
$V_{65GyRBE}$	1.52 (1.08-2.15)	< 0.05	0.785	0.223	1.118	0.13	0.16
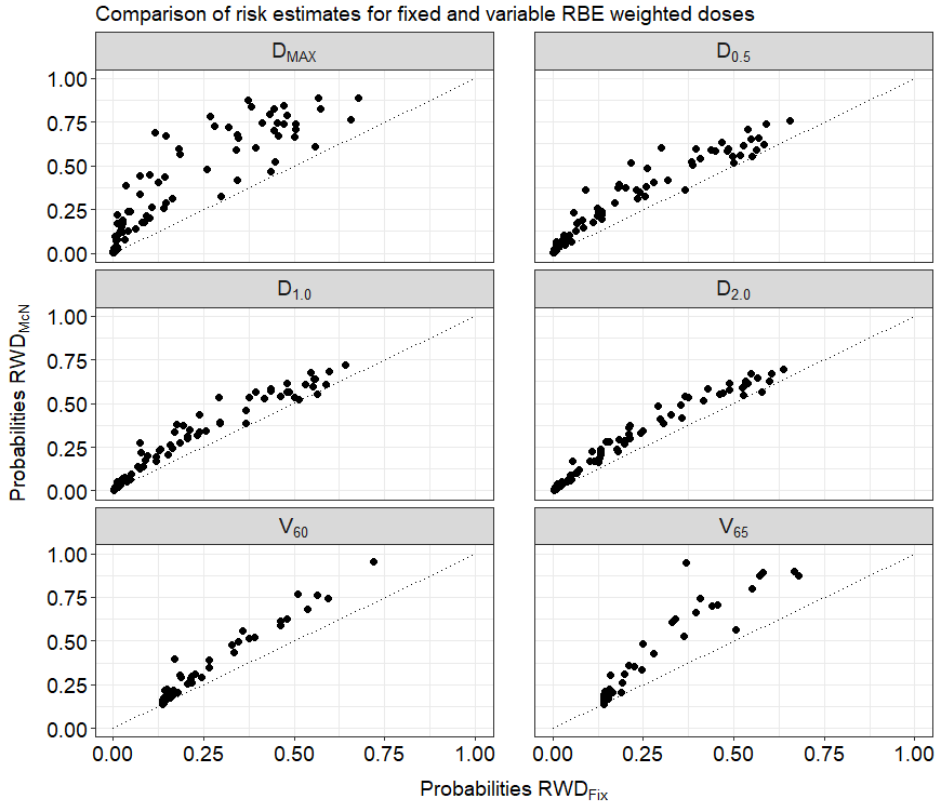
Figure 4.3: Estimated probability of temporal lobed necrosis using RWD$_{Fix}$ and RWD$_{McN}$.

.

4.3 Paper III

In paper III (140) we explored the spatial dose- and LET_d correlations with the RAIC in 15 patients treated with intensity modulated proton therapy using a mixed model methodology. An example of dose and LET_d distribution is displayed in Figure 4.5.

The median (range) LET_{mean} and D_{mean} in the lesions were 3.6 keV/um (2.8-5.6 keV/µm) and 63.5 Gy(RBE) (42.2-69.0 Gy[RBE]), respectively. The highest LET_d in the RAIC lesions and brain tissue were 8.0 keV/µm and 10.7 keV/µm, respectively.

Significant correlation between LET_d and RAIC were found for all models. The model which included both dose and LET_d as predictors had the best model performance with and AUROC of 0.95 (95% CI: 0.92-0.97). When voxel dose exceeded 60 Gy, the increase in probability of RAIC was rapid, also for low LET_d values (i.e. $LET_d = 1$ keV/um).

Patient heterogeneity was considerable, with substantial difference in the effect of both dose and LET_d between patients and where the effect of LET_d was negative for three patients (Figure 4.6).

Figure 4.4: Dose- and LET_d distribution. RAIC (red contour): Contrast enhancement from $T1_W$ MRI sequence.

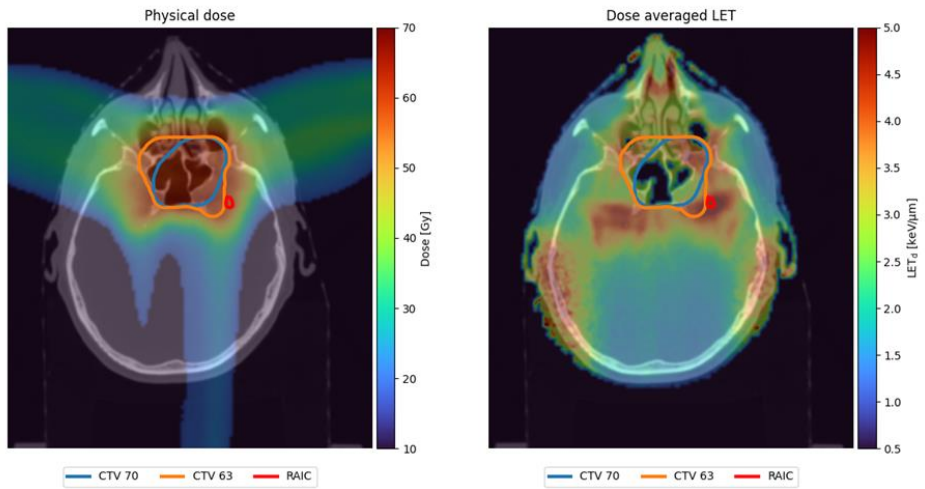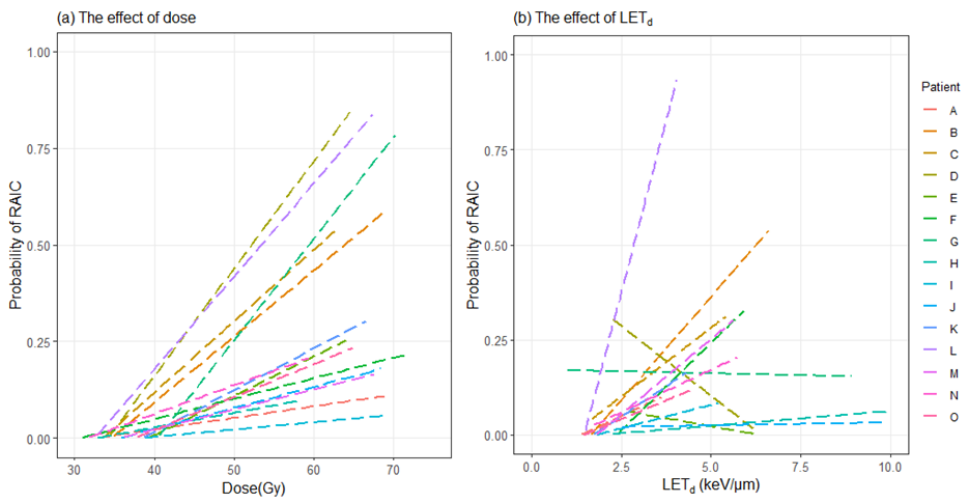Figure 4.5: Dose a) and LET_d b) is plotted versus estimated risk of RAIC, and individual trend lines are generated for all values of LETd and dose using a glm smoothing function (y~x)

5. Discussion

5.1 Methodological considerations

Retrospective studies are amongst other appropriate for studying rare diseases or outcomes, and for events that develop over a long time period. Findings from retrospective studies can be hypothesis generating and further form the basis for clinical trials. Retrospective studies are however limited since data were not collected for the specific research aim in question. Bias, such as selection bias or measurement bias, affect both the internal and the external validity of the results (141).

5.1.1 Paper I

Patient selection

The patient cohort consisted mainly of various HNCs, however also some other cancers at the skull base considered relevant for the endpoint of interest in this work where included. The anatomical tumor location and hence the delivered radiation dose to the brain varies widely for HNC. In the study we aimed at including patients at risk of developing brain necrosis and ensure the detection of all events in a very heterogeneous group of patients. As brain dose is the main risk factor for developing brain necrosis we excluded patients with brain D_{max} less than 40 Gy(RBE). Based on a review of published data, we considered it reasonable to assume that patients with a D_{max} to the brain less than 40 Gy(RBE) were at no risk of developing radiation-induced brain necrosis. Although we consider it unlikely, there is a risk that relevant patients have been excluded by this dose criteria. However, if the dose threshold is unreasonably low, non-risk patients have been included with subsequent overestimation of the incidence.

Follow-up time

Follow-up time was calculated as time from end of radiotherapy until last available MRI. We included patients with follow-up times from 6 months or older. The median follow-up time was 29 months (range: 6-29) and the median time to first MRI with observed RAIC was 24 months (9-37). Radiation necrosis is known to develop from a few months to several years after treatment (142), it is therefore likely that we included patients who

had not yet developed RAIC or radiation necrosis, which introduces a bias in the estimated incidence rates. From the literature, the inclusion of patients in similar studies in general follow the same approach with including patients starting from six months post-treatment. Median follow-up time in the current project are comparable to other proton cohorts, however shorter than photon cohorts.

Loss to follow-up

A hundred and five of the patients have not been diagnosed with radiation necrosis in the MRI reports. For 18 of the patients still alive and not diagnosed with RAIC (i.e. 18%), it was 12 months or longer since the last MRI, while it was 24 months or longer since the last MRI for 8 of the patients (8%). This is a limitation since RAIC and radiation necrosis could have developed in these patients after the last available MRI. Loss to follow-up may have resulted in underestimation of the probability of RAIC.

Death as a competing risk to RAIC

A competing risk is an event that either prevent the outcome of interest to occur, or modify the probability of it happening (143). Ten of the patients in the current cohort had died, of which eight were RAIC free. However, as RAIC develop months to several years after treatment, the death of a patient may have hindered the development of RAIC. Thus, disregarding death as a competing risk in the survival analysis lead to a slightly overestimation of the probability of RAIC.

MRI and diagnosis of radiation necrosis

Patients diagnosed with radiation necrosis were identified through a screening of the MRI reports, as described in chapter 3.1. Since this was a retrospective analysis, no information about the criteria for the initial diagnosis besides what was described in the MRI reports were available. However, a retrospective review of the contrast enhanced T1 weighted and the T2 sequences of the MRIs were performed and where the imaged changes were evaluated according to published recommendations for radiographically diagnosis of cerebral necrosis (chapter 1.5.1).

Limitations of decision trees

One of the aims in paper I was to suggest practical brain dose constraints for proton therapy, and RPA was used to identify a DVH cut-point. One of the main limitation of a single decision tree is its sensitivity to small changes in the training data, which can result in both the selection of a different splitting variable as well as the identification of the optimal variable cut-point. The first split in RPA is decisive for the subsequent splitting of the observations; a different distribution of the variable values and observations in the data set can therefore generate a completely different decision tree. Furthermore, information is lost when the continuous variables are dichotomized. The predictive power of single decision trees is highly variable (65).

5.1.2 Paper II

Patient selection

A subgroup of the patients in Paper I treated with IMPT was selected for this study. IMPT is state-of art proton therapy technique for patients with complex target volumes with adjacent critical structure, such as the patients in our material. We further excluded patients with less than 24 months of follow-up time, in order to limit bias due to inclusion of patients not yet having developed RAIC.

Selection of RBE modeller

The use of only two RBE models is a weakness of our study; including multiple RBE models would provide a broader and more complete description of the potential dose variation caused by variable RBE. However, the RBE models used in the study were chosen because these were already included in the FDC, and it was out of the scope of this thesis to implement more models.

5.1.3 Paper III

Patient selection

As in paper II we only included patients treated with IMPT for this analysis. Initially it was sixteen IMPT patients with RAIC in the patients material, however due to technical difficulties during the Monte Carlo simulations and extraction of the dose- and LET_d distributions, one patient were excluded from the analysis.

Selection of lesions for analysis

The majority of the contrast enhanced lesions in our material underwent an initial progressive phase, before stabilization or regression, and in some cases complete recovery, an evolutionary pattern which is typical for RAIC (101). We considered the first available MRI with observed contrast enhanced lesions to best correspond to the region where the damage first occurred, thus dose and LET_d distributions in these lesions were used for analysis.

5.2 Discussion of main findings

5.2.1 The insidence of RAIC

Recent years there has been a growing concern that increased RBE may result in a higher incidence of radiation induced brain necrosis and RAIC after proton therapy than one should expect. In paper I, RAIC in the brain were observed in 22 (17%) out of 127 patients of which 11% of the patients had temporal lobe lesions. The incidence of RAIC plateaued after approximately three years; the actuarial RAIC-free survival were 86%. 72% and 70% at two, three and five years, respectively.

The ability to compare the incidence of RAIC in the brain for extracranial tumors is complex owing to differences in patient populations, endpoint definitions, treatment modalities and follow-up times. Proton cohorts are in general heterogeneous and consist of various types of cancers sited at the skull base region. Kitpanit et al (108) published the results from 234 patients treated with either proton therapy alone (86.3%) or proton boost after IMRT (13.7%). The cohort included patients with a wide range of head and neck malignancies. The primary endpoint in the study was radiographically diagnosed temporal lobe necrosis, however the authors also reported observed non-temporal lobe lesions. During a median follow-up time of 23 months, 17 out of 234 patients (7.3%) developed RAIC either in the temporal lobes (n=13) or in the frontal lobes (n=4), of which ~ 40% presented with symptomatic lesions. The estimated two years RAIC free survival (brain) was 93% as compared to 86% in our cohort. This discrepancy in incidence, can possibly be explained by differences in the composition of the patient cohorts. Specifically, a fewer proportion of major salivary gland tumors were included in our cohort (11% vs 33%), with no observed toxicity in this disease site in neither theirs nor our study. Secondly, unlike Kitpanit et al, we applied a brain dose threshold which excluded patients with a brain $D_{max} < 40$ Gy(RBE) from the study. Thus, it is likely that their cohort included more patients not at risk of developing radiation necrosis. Unfortunately, dose statistics were given only for the temporal lobes, which complicates direct comparison of dose variables. Furthermore, during analysis the authors included the four cases of frontal lobe necrosis in the non-necrotic group, while these were included in the RAIC group in our study.

In the study from Niazy et al (144), the endpoint was symptomatic RAIC, corresponding to CTCAE ≥ G2 brain necrosis. The patient cohort (n = 179) was a mixture of patients treated with PSPT for extracranial (skull base and HNC tumors) and intracranial tumors. The authors found a significant difference in observed rates of brain necrosis between the intracranial (8%) and the extracranial group (31%). The estimated two and five year incidence of RAIC in the extracranial group were 25% and 42%, respectively. This seems a high rate compared to ours, however the extracranial patient cohort in Niazy et al. can be considered as high risk patients, all with tumor extension into the paranasal sinuses/clivus and with a maximum dose to the brain or dura of at least 59.4 Gy. Noteworthy, 97% of the patients with RAIC in our material had a D_{max} to the brain of at least 60 Gy(RBE), and 64% had intracranial tumor extension.

In a recent publication from Schrøder et al., temporal lobe image changes were found in 21% of the patients (n = 277) treated with PBS for tumors at the skull base and head and neck region (145). It is worth noting that the patients in their study had a longer follow-up time (median 51 months) and a generally higher prescribed dose (median 74 Gy [RBE]) than the patients in our cohort. Longer follow-up time and higher prescribed dose was also suggested by the authors as a possible explanations for the higher incidence than most of the studies it seemed reasonable to compare to.

Zhang et al. (118) recently published the result from a study where the primary aim was to determine a proton specific RBE for contrast enhancement in the temporal lobes. It is nevertheless worth mentioning in this context, because it reports long-term outcomes of temporal lobe image change for well-matched groups of patients with nasopharyngeal cancer treated with either PSPT or IMRT. The proton cohort consisted of 60 patients whereas the IMRT group included 506 patients. Median follow-up time was > 5 years in both groups. They reported that RAIC developed in 10% of the patients in the proton cohort and in 4% of the patients treated with IMRT. In our material, considering the nasopharynx patients (n= 34) only, the corresponding incidence of temporal lobe image change was 24%. One distinction which may be of relevance is that our patients were treated with IMPT, whereas their patients received PSPT.

Compared to proton therapy for extracranial tumor sites at the skull base, IMRT cohorts are in general more homogeneous. Numerous studies have addressed temporal lobe necrosis after IMRT for nasopharyngeal cancer reporting crude rates ranging between 4.6% and 12.9% (106, 107, 109, 110, 112-116, 119, 146, 147). The largest report from Wen et al. reported outcome of temporal lobe injuries (TLI) in 8194 patients who received IMRT based radiotherapy for nasopharyngeal cancer between 2009 and 2015 (115). As in the current study, patients were diagnosed based on follow-up MRIs which were taken every 3 months the first three years and then every 6 months thereafter. During a median follow-up time of 66.8 months, 989 patients (12.1%) developed TLI, thus slightly lower than reported in ours and most proton series, and comparable the incidence rates in the abovementioned publication for Zhang et al (118).

An interesting aspect when reviewing the literature, is that in almost all publications, temporal lobe necrosis is the endpoint of interest, which is important considering the potential cognitive decline severe radiation necrosis in the temporal lobes may induce (148). However, in our material we found that more than 30% of the lesions were located in other parts of the brain. The majority of these non-temporal lesion were located in the frontal lobe in patients treated for sinonasal cancer. In fact, for this patient group, more image changes were found in the frontal lobe then in the temporal lobes. Frontal lobe damages may result in personality and behavioral changes, and could also affect communication skills and muscle strength, all symptoms that can have a severe impact on the patient's quality of life.

Thus, to summarize, published rates of RAIC after proton therapy for various cancers at the skull base region range between 7% and 31% (88, 108, 111, 118, 144, 145, 149-151), and between 2% and 13% after IMRT for nasopharyngeal cancers (106, 107, 109, 110, 112-116, 119, 146, 147). The results in paper I are therefore within the range of the observations from the proton series, however higher than observed after IMRT.

Often reported incidences of RAIC in HNC and skull base tumors include both symptomatic and asymptomatic lesions, and number of patients with symptoms are not always specified. However, when these are reported, the proportions of symptomatic

lesions are typically around 30-40% (108, 111, 145, 150, 151). In our cohort (paper I), none of the patients had yet presented with any clinical symptoms associated with radiation necrosis. Three patients, however, received treatment due to observed progression of the lesions on follow-up MRIs, which might have prevented a possible development of clinical symptoms in the future. Secondly, the favorable result could most likely be explained by small lesion volumes and small regions with edema in our material. Moreover, for six of the patients with RAIC it were more than 12 months since the last follow-up MRI. Thus, for these patients we have no information regarding possible progression of the lesions with potential development of symptoms.

5.2.2 Dose-response relationship and the impact of variable RBE

For treatment plan evaluation, clinicians are amongst other guided by inspecting the DVHs, often in terms of evaluating dosimetric cut-off values assumed to be predictive of brain necrosis. As previously mentioned, most of these dose constraints are derived from photon data, but a few publications have identified dose volume thresholds (RBE = 1.1) associated with brain necrosis from proton data. A 15% probability of temporal lobe necrosis at three years post-treatment was estimated for $V_{60Gy(RBE)}$ exceeding 5.5cc or $V_{70Gy(RBE)}$ exceeding 1.7cc (111). In another publication, the authors found that temporal lobe necrosis increased from 1.6% to 23.1% when $V_{50Gy(RBE)}$ exceeded 11cc, and from 0.6% to 14% when D_{2cc} exceeded 62 Gy(RBE) (108). In comparison, we proposed to apply $V_{67Gy(RBE)}$ < 0.2cc to the brain (paper I), and although this is slightly stricter than the above mentioned suggestions, it is in line with the recommendation of limiting the volume of brain receiving high doses (105, 120, 121, 152).

As mentioned in chapter 1.5.1, a large variety of dose and volume thresholds have been suggested of which the cut-off point associated with toxicity may vary by several Gy and cc for the same variables. Although international consensus have been reach and provide recommendations on brain and temporal lobe dose constraints (105, 120, 121), the exact relationship between dose and the development of RAIC and brain necrosis is still unclear. For proton therapy, the variable RBE adds an additional uncertainty to this

question. As addressed in paper II, variable RBE resulted in significantly higher temporal lobe doses compared to $RBE_{1.1}$, and RBE values that in general exceeded 1.1 for several temporal lobe dose indices. Similar trends have been shown by several others who have simulated the effect of variable RBE for various disease sites, and for different clinical scenarios (76, 153-168). Yepes et al. (162) recalculated 400 treatment plans belonging to 4 different patient groups treated with IMPT, and found that the variable RBE models consistently predicted higher RBE than 1.1 for most OARs. Garbacz et al (166) recalculated 95 treatment plans from patients with brain and skull base tumors previously treated with IMPT. They found that variable RBE resulted in enlarged high dose volumes in the brain and an averaged biological range extensions of > 0.4 cm. Studies comparing PSPT versus IMPT (155) or IMPT versus IMRT (157, 161) found that favorable doses to the OAR using $RBE_{1.1}$ were diminished when applying variable RBE.

As in our analysis (paper II), most studies on variable RBE have applied phenomenological models derived from data on clonogenic cell survival. Typically these describe an RBE dependency on LET_d, fraction dose and the radiosensitivity parameters α and β (69). In our data, there were only small differences in the estimated RBE weighted doses to the temporal lobes between the RWD_{McN} and RWD_{Wed}. Others have shown substantial differences in estimated RBE and variable RBE weighted doses between RBE models, with greatest variations for simultaneously low $(\alpha/\beta)_x$ and high LET_d (76, 158). Despite that the RBE models show large differences in estimated absolute values, they still are consistent in showing a clear trend of increased doses in OARs especially when these are located distally in the proton beam. However, since these models predict RBE for cell survival it is unknown if any of the models would give reliable predictions of the clinical RBE, specifically for normal tissue toxicity endpoints. Currently, proton RBE derived from clinical data are almost lacking. However, recently an RBE of 1.18 for temporal lobe contrast enhancements (i.e. for $D_{1.0\%}$) were determined based on DVH analysis of treatment plans from patients treated with proton therapy and IMRT for NPC (118). In comparison, the overall predicted RBE for the high-dose indices in our material ranged from 1.20-1.22 for $D_{0.5cc}$-$D_{2.0cc}$, whereas

the predicted RBE for the temporal lobes with RAIC ranged from 1.16-1.17, respectively.

In recent years, the use of NTCP models in clinical practice has gained increased acceptance. The first clinical experience with model-based patient selection to proton therapy has recently been published (53), and currently the model based approach is used for identifying patients for inclusion in a clinical trial, randomizing patients between photon and proton therapy for head and neck cancer (56). Given the difference in proton and photon dose distributions to OARs, dose-toxicity relationship may also be different. Therefore, NTCP models for proton therapy must either be validated photon models, or developed based on proton data (57). The univariate NTCP models in paper II, which all showed good discriminative ability (AUC from 0.79 to 0.84), were fitted using several different dose variables from the literature, either previously used in photon-based NTCP models or generally agreed to be predictive of brain necrosis. As shown in other studies for other endpoints (165, 167, 168), variable RBE resulted in a substantial increase in estimated NTCP compared to RBE_{Fix}. In a model based approach, selection of patients are determined whether the absolute difference in NTCP exceeds a specific threshold or not (54), thus disregarding variable RBE, could lead to wrong decisions/conclusions.

Interestingly, the variations in estimated NTCP caused by variable RBE were largely dependent on the dosimetric variable in the NTCP model. The increase was twice as high for D_{max} compared to the other predictor variables. There was also a greater interpatient spread in individual NTCP values as a result of variable RBE in the model with D_{max}. Thus, the choice of variables for NTCP models, is not straightforward, and one should be cautious only relying only on automatic variable selection during NTCP model development. Furthermore, for IMPT treatment plans, simulation studies have shown that equal dose distributions may have completely different LET_d distributions (169), which adds and additional uncertainty in actual biological dose. Thus, evaluating NTCP also in terms of RWD_{Var} in clinical practice may give useful information.

5.2.3 The spatial correlation between LET and RAIC

In lack of long-term follow-up of the patients and due to loss to follow-up, the clinical significance of asymptomatic lesions is unclear. However, from a scientific point of view, these lesion are of importance as they represent an objective and easy measurable biomarker of the clinical effect of irradiation. This is especially true for proton therapy, where the knowledge gap is large regarding the potential influence of variable RBE on the incidence and development of radiation-induced toxicity. Recent years there have been an emerging number of studies addressing RBE effects in pediatric and adult patient cohorts for various normal tissue endpoints (10, 13-15, 170-181). Similar to Paper III (140), some of these studies analyzed brain image changes observed on post-treatment MRIs, and spatially correlated them to dose and/or LET (Table 5.1). The conclusions drawn about the power of LET as predictor of brain necrosis and hence its significance as surrogate for RBE, are however contradictive. In three of the publications, the authors concluded that their data provided clinical evidence for the so-called LET effect. The first study from Peeler et al (13) included 34 pediatric patients with ependymoma treated with PSPT. The endpoint was T2-FLAIR hyperintensity, which was observed and contoured on post-treatment MRIs for 14 of the 34 patients. The spatial correlations between dose and LET_t were analyzed using a generalized linear model with a probit link function. The probit model estimated a rapid increase in the probability of image change in a voxel as a function of LET_t. In the publication from Bahn et al (170), the patient cohort consisted of 110 patents with low-grade gliomas, of which contrast enhanced brain lesions (CEBL) were observed on follow-up MRIs in 23 patients. In a voxel-based multivariate logistic regression model, the location of CEBL were significantly associated with dose and LET_d. Furthermore, a significantly higher risk of developing CEBL in the periventricular (PVR) region were found, suggesting an increase in radiosensitivity in this region (170). Similar findings were reported in a publication from Eulitz et al (173). As in Bahn et al., contrast-enhanced lesions accumulated at the edge of the CTV, in regions of both high dose and LET_d, and multivariate logistic regression models including dose, LET_d and PVR were superior in predicting locations of lesions, compared to the univariate models. However, the statistical analysis applied in these publications assume independent and identically

distributed observations, while the presented data was hierarchical. As the nested nature of the data was not accounted for in the analysis it could have led to and underestimation of the variance and too low p-values (182).

As presented in paper III, we were able to demonstrate an overall statistically significant association between LET_d and image change using mixed effect modelling. In a study including 50 patients treated with PSPT for intra-and extracranial tumors, Niemierko et al. used a similar model without finding LET_d to be significantly correlated to necrotic regions/voxels (176). In addition to the mixed effect modelling, the authors matched voxels inside and outside the lesions by dose, generating a data set where, in principle, the distributions of the LET_d were the only difference between the necrotic and non-necrotic regions. When adjusted for dose, no significant difference in LET_d values between necrotic and non-necrotic regions could be found. The authors reported that the interpatient variations in the LET_d effect were high, and suggested that difference in patient radiosensitivity, timing of MRI scans, lesions size and other confounding factors could obscure any LET_d effect. Similar tendency, with LET_d effects ranging from negative to positive, could also be observed in our material. However, comparing the estimated ICCs, patient heterogeneity was higher in Niemierko et al, which directly affects the estimated variance and p-values, and thus may explain the different results. Patient heterogeneity was also highlighted as potentially overshadowing a clear LET_d effect in the study from Garbacz et al (174). They analyzed seven cases of contrast enhanced lesions in 45 patients treated with PBS for skull base tumors. Adjusted for dose, higher LET_d was found in non-necrotic voxels in one patients, whereas more or less identical LET_d were found in two of the patients. Overall, only slightly higher LET_d was observed in necrotic voxels (~0.2 keV/µm). Similar results were reported in Bertolet et al (171). They analyzed T2-FlAIR image changes (ICA) in 26 patients treated with PBS for meningioma, finding higher LET_d in the ICAs for only 11 of the patients. In contrast to this, Harrabi et al (175) found significantly higher LET_d in 22 out of 23 CEBLs when analyzing dose matched voxels in the patient material first described in Bahn et al. (170).

Tabell 5.1: Overview over publications investigating spatial correlations between LET and RBE with RAIC in the brain. Studies include patient populations with intracranial- and extracranial tumor sites.

Publication	Disease site	Nb pt/ events	RAIC/endpoint	Technique	Statistical methods	Findings and conclusions
Peeler et al. 2016 (13)	Intracranial* (glioma)	34/14	T2$_{Flair}$ hyperintensity	PSPT	Probit regression	Dose for 50 % risk decreases with increasing LET. First clinical study demonstrating a correlation between LET$_t$ and RAIC
Eulitz et al. 2019 (173)	Intracranial (glioma)	6/6	T1w contrast enhancement	PSPT	Logistic regression	Model with dose and LET indicate variable RBE different from RBE = 1.1
Niemierko et al. 2020 (176)	Intra-and extracranial (HNC. Skull base.)	50/50	Regions of necrosis	PSPT	Logistic regression. Mix effect logistic regression. Comparison dose-matched voxels (I^2)	Let$_d$ not correlated to necrotic lesions. Difference in radiosensitivity could overshadow the LET effect
Bahn et al. 2020** (170). Harrabi et al. 2021** (175)	Intracranial (glioma)	110/23	T1$_w$ contrast enhancement	PBS	Logistic regression Comparison dose-matched voxels (one-sided t-test)	RAIC does not occur at random. But in proximity to ventricular system and in regions of both high dose and LET$_d$. Significant difference in mean LET$_d$ for 22 out of 23 patients. Clinical evidence for an increased risk in ventricular proximity and for a proton RBE that increases significantly with increasing LET
Garbacz et al. 2021 (174)	Extracranial (skull base)	45/7	T1$_w$ contrast enhancement. T2$_{Flair}$ hyperintensity	IMPT/ PBS	Comparison dose-matched voxels (I^2)	Large patient heterogeneity. Slightly higher average LET$_d$ in RAIC
Bertolet et al. (2022) (171)	Intracranial (glioma)	228/26	T2$_{Flair}$ hyperintensity	PBS (SFUD)	Dose-matching	Most patients did not show a spatial correlation between their image changes and the LETd values
* Pediatric. ** same patient cohort						

The large interpatient variations in our cohort was especially pronounced for the LET$_d$. Compared to dose, the SD of the random effects where substantially higher for LET$_d$. Most likely this can be explained by the combination of patients in our material, having both a strongly positive and negative LET$_d$ effect, whereas the effect of dose was overall more consistent across the patients, as illustrated in Figure 4.6. Our work and others are in general burdened with several uncertainties and limitations. Accurate knowledge about the delivered dose- and LET distribution is lacking due to treatment variations leading to range deviations which may influence both the dose- and the LET distributions. It has previously been showed that uncertainties in the proton range could

lead to changes in the LET_d of up to 2 keV/µm at the distal end of the beam range (183). In addition, emphasis is placed on creating treatment plans that are robust against range uncertainties, which in turn may very well lead to an increased robustness against RBE uncertainties as well. Furthermore, concerns about a potential unwanted biological effect of increased RBE due to elevated LET at the end-of-range are in general handled during treatment planning, mostly by increasing number of total beams in the treatment plan, as well as restraining number of distal beam edge extending into critical organs (16, 183, 184). Clinically, one can expect LET_d values > 15 keV/um, where typically the highest LET_d will occur in low dose regions (70, 169). In our material, the mean LET_d in RAIC ranged from 2.8 to 5.6 keV/µm. This agrees well with the findings from Niemierko et al (176) who reported mean LET_d values ranging from 2.2 keV/µm to 5.6 keV/µm in the necrotic regions. Slightly lower LET_d values (2.5-3.6 keV/µm) were found in the RAIC by Garbacz et al (174). In contrast, Bahn et al (170) reported higher mean LET_d in the CEBLs, ranging from 3.6-8.8 keV/µm. Not knowing any details about treatment planning and beam composition, it is still interesting to note that in Bahn et al. treatments were delivered using either a single (n=24) or two beams (n=85) with one exception, whereas in Garbacz et al, which reported the lowest mean LET_d in the lesions, median number of beams was four.

6. Conclusions

The incidence of brain image changes in this patient cohort were comparable to other proton series consisting of HNC and skull base tumors, however slightly higher than reported after IMRT for NPC. The image changes were primarily observed in patients treated for NPC or sinonasal cancers with locally advanced disease. Although the majority of RAIC developed in the temporal lobes, almost one third of the lesions were found in the frontal lobes, emphasizing that the risk of developing brain necrosis in this part of the brain may also be significant.

The dosimetric analysis and the predictive modelling are in line with previous publications and confirm the significance of high dose for the development of RAIC and radiation necrosis. Furthermore, our results from paper II show that risk may be underestimated if variations in RBE are disregarded; thus including variable RBE weighted doses in treatment plan evaluation could provide valuable clinical information and should be considered. Our results further indicate that uncertainties from variable RBE are highest for D_{max}, we therefore recommend to avoid using D_{max} as dose constraint in clinical treatment plan evaluation, or implementing NTCP models with D_{max} as a model predictor.

The results in paper III showed that LET_d were significantly correlated to RAIC. Our results suggest that the LET_d effect could be of clinical significance for some patients. LET_d assessment in clinical treatment plans should therefore be taken into considerations.

7. Future perspective

The results from this work strongly support the need for integrating visualization of LET_d distribution and variable RBE-weighted doses into treatment planning systems, as well as optimization tools based on LET_d data and the physical dose. This would allow for minimizing the LET_d in critical OARs, as well as identifying patients one would expect to be at higher risk of toxicity due to increased RBE of protons. Furthermore, although large uncertainties are associated with absolute values derived from variable RBE models, they still may be useful for comparing relative risks (i.e. when comparing two different treatment plans for the same patient), specifically for IMPT treatment plans where the LET_d distributions may differ largely between treatment plans with similar dose distributions.

A revise of RBE related guidelines would require stronger clinical evidence of a correlation between clinical outcome measures and biological effective dose or RBE surrogates such as LET_d. In addition to retrospective and prospective single outcome studies, high quality systematic reviews and meta-analysis should be performed as well as pooled analysis of spatial correlations between LET_d and RAIC.

Potentially RBE-related treatment effects should be kept in mind during planning and design of randomized clinical trials, which preferably should be multicenter studies. E.g. clinical trials comparing treatment outcome from photon- and proton therapy for extracranial and intracranial tumors should include RAIC as secondary endpoint, and have follow-up imaging protocols appropriate for early and accurate detection of image changes.

8. Bibliography

1.   Sung H, Ferlay J, Siegel RL, Laversanne M, Soerjomataram I, Jemal A, et al. Global Cancer Statistics 2020: GLOBOCAN Estimates of Incidence and Mortality Worldwide for 36 Cancers in 185 Countries. CA: A Cancer Journal for Clinicians. 2021;71(3):209-49.

2.   Delaney GP, Barton MB. Evidence-based Estimates of the Demand for Radiotherapy. Clinical Oncology. 2015;27(2):70-6.

3.   Röntgen WC. Ueber eine neue Art von Strahlen. Annalen der Physik. 1898;300(1):12-7.

4.   Grubbé EH. Priority in the Therapeutic Use of X-rays. Radiology. 1933;21(2):156-62.

5.   Lederman M. The early history of radiotherapy: 1895-1939. Int J Radiat Oncol Biol Phys. 1981;7(5):639-48.

6.   Coutard H. PRINCIPLES OF X RAY THERAPY OF MALIGNANT DISEASES. The Lancet. 1934;224(5784):1-8.

7.   Bragg WH, Kleeman R. LXXIV. On the ionization curves of radium. The London, Edinburgh, and Dublin Philosophical Magazine and Journal of Science. 1904;8(48):726-38.

8.   Goitein M. Radiation Oncology: A Physicist's-Eye View. 1 ed: Springer New York, NY; 2008. XII, 330 p.

9.   Allen AM, Pawlicki T, Dong L, Fourkal E, Buyyounouski M, Cengel K, et al. An evidence based review of proton beam therapy: The report of ASTRO's emerging technology committee. Radiotherapy and Oncology. 2012;103(1):8-11.

10.   Giantsoudi D, Sethi RV, Yeap BY, Eaton BR, Ebb DH, Caruso PA, et al. Incidence of CNS Injury for a Cohort of 111 Patients Treated With Proton Therapy for Medulloblastoma: LET and RBE Associations for Areas of Injury. Int J Radiat Oncol Biol Phys. 2016;95(1):287-96.

11.   Gunther JR, Sato M, Chintagumpala M, Ketonen L, Jones JY, Allen PK, et al. Imaging Changes in Pediatric Intracranial Ependymoma Patients Treated With Proton

Beam Radiation Therapy Compared to Intensity Modulated Radiation Therapy. Int J Radiat Oncol Biol Phys. 2015;93(1):54-63.

12.   Indelicato DJ, Flampouri S, Rotondo RL, Bradley JA, Morris CG, Aldana PR, et al. Incidence and dosimetric parameters of pediatric brainstem toxicity following proton therapy. Acta Oncol. 2014;53(10):1298-304.

13.   Peeler CR, Mirkovic D, Titt U, Blanchard P, Gunther JR, Mahajan A, et al. Clinical evidence of variable proton biological effectiveness in pediatric patients treated for ependymoma. Radiother Oncol. 2016;121(3):395-401.

14.   Underwood TSA, Grassberger C, Bass R, MacDonald SM, Meyersohn NM, Yeap BY, et al. Asymptomatic Late-phase Radiographic Changes Among Chest-Wall Patients Are Associated With a Proton RBE Exceeding 1.1. Int J Radiat Oncol Biol Phys. 2018;101(4):809-19.

15.   Wang CC, McNamara AL, Shin J, Schuemann J, Grassberger C, Taghian AG, et al. End-of-Range Radiobiological Effect on Rib Fractures in Patients Receiving Proton Therapy for Breast Cancer. Int J Radiat Oncol Biol Phys. 2020;107(3):449-54.

16.   Heuchel L, Hahn C, Pawelke J, Sørensen BS, Dosanjh M, Lühr A. Clinical use and future requirements of relative biological effectiveness: Survey among all European proton therapy centres. Radiotherapy and Oncology. 2022;172:134-9.

17.   Wilson RR. Radiological Use of Fast Protons. Radiology. 1946;47(5):487-91.

18.   Lawrence JH, Tobias CA, Born JL, Mc CR, Roberts JE, Anger HO, et al. Pituitary irradiation with high-energy proton beams: a preliminary report. Cancer Res. 1958;18(2):121-34.

19.   Newhauser WD, Zhang R. The physics of proton therapy. Phys Med Biol. 2015;60(8):R155-209.

20.   Slater JM, Archambeau JO, Miller DW, Notarus MI, Preston W, Slater JD. The proton treatment center at Loma Linda University Medical Center: Rationale for and description of its development. Int J Radiat Oncol Biol Phys. 1992;22(2):383-9.

21.   PTCOG. Patient statistics per end of 2020: Particle Therapy Co-Operative Group; 2021 [Patient statistics per end of 2020]. Available from: https://www.ptcog.ch/index.php/patient-statistics.

22.   Bethe H. Zur Theorie des Durchgangs schneller Korpuskularstrahlen durch Materie. Annalen der Physik. 1930;397(3):325-400.

23.   ICRU. International Commission on Radiation Units and Measurements. Report 78: Prescribing, Recording and Reporting Proton-Beam Therapy. Oxford: International Commission on Radiation Units and Measurements; 2007.

24.   ICRU. Report 16. Journal of the International Commission on Radiation Units and Measurements. 2016;os9(1):NP-NP.

25.   Deng W, Yang Y, Liu C, Bues M, Mohan R, Wong WW, et al. A Critical Review of LET-Based Intensity-Modulated Proton Therapy Plan Evaluation and Optimization for Head and Neck Cancer Management. International journal of particle therapy. 2021;8(1):36-49.

26.   ICRU. Report 85. Journal of the International Commission on Radiation Units and Measurements. 2011;11(1):NP-NP.

27.   Gottschalk B. Physics of Proton Interactions with Matter. In: Paganetti H, editor. Proton Therapy Physics (2end ed). Series in Medical Physics and Biomedical Engineering. Boca Raton: CRC Press; 2019. p. 27-68.

28.   Lu H-M, Flanz J. Characteristics of Clinical Proton Beams. In: Paganetti H, editor. Proton Therapy Physics. Boca Raton: CRC Press; 2019. p. 113-36.

29.   Sloepsma R. Beam Delivery Using Passive Scattering. In: Paganetti H, editor. Proton Therapy Physics (2end ed): CRC Press; 2019. p. 137-68.

30.   Flanz J. Particle Beam Scanning. In: Paganetti H, editor. Proton Therapy Physics (2end ed): CRC Press; 2019. p. 169-206.

31.   Paganetti H. Proton therapy physics (1st ed): CRC press; 2012.

32.   Joiner M, Kogel AVD, Steel G. Introduction: the significance of radiogiology and radiotherapy for cancer treatment. In: Joiner M, Kogel AVD, editors. Basic Clinical Radiobiology: Hodder Arnold; 2009. p. 1-10.

33.   Wouters B, Begg A. Irradiation-induced damage and teh DNA damage response. In: Joiner M, Kogel AVD, editors. Basic Clinical Radiobiology (4th ed): Hodder Arnold; 2009. p. 11-26.

34.   Hall EJ, Giaccia AJ. Radiobiology for the radiologist. Philadelphia: Wolters Kluwer Health/Lippincott Williams & Wilkins; 2012.

35.   Sage E, Shikazono N. Radiation-induced clustered DNA lesions: Repair and mutagenesis. Free Radical Biology and Medicine. 2017;107:125-35.

36.   Hill MA. Radiation Track Structure: How the Spatial Distribution of Energy Deposition Drives Biological Response. Clinical Oncology. 2020;32(2):75-83.

37.   Paganetti H. Mechanisms and Review of Clinical Evidence of Variations in Relative Biological Effectiveness in Proton Therapy. Int J Radiat Oncol Biol Phys. 2022;112(1):222-36.

38.   Joiner M. Quantifying cell kill and cell survival. In: Joiner M, Kogel AVD, editors. Basic Clinical Radiobiology (4th ed): Hodder Arnold; 2009. p. 41-55.

39.   McMahon SJ. The linear quadratic model: usage, interpretation and challenges. Physics in Medicine & Biology. 2018;64(1):01TR.

40.   Doerr W, Schmidt M. Normal Tissue Radiobiology. Comprehensive Biomedical Physics. 2014;7:75-95.

41.   Jung H, Beck-Bornholdt HP, Svoboda V, Alberti W, Herrmann T. Quantification of late complications after radiation therapy. Radiother Oncol. 2001;61(3):233-46.

42.   Dörr W. Radiobiology of tissue reactions. Annals of the ICRP. 2015;44(1_suppl):58-68.

43.   Dörr W, Hendry JH. Consequential late effects in normal tissues. Radiotherapy and Oncology. 2001;61(3):223-31.

44.   Langendijk JA, Lambin P, De Ruysscher D, Widder J, Bos M, Verheij M. Selection of patients for radiotherapy with protons aiming at reduction of side effects: the model-based approach. Radiother Oncol. 2013;107(3):267-73.

45.   Kutcher GJ, Burman C. Calculation of complication probability factors for non-uniform normal tissue irradiation: the effective volume method. Int J Radiat Oncol Biol Phys. 1989;16(6):1623-30.

46.   Kutcher GJ, Burman C, Brewster L, Goitein M, Mohan R. Histogram reduction method for calculating complication probabilities for three-dimensional treatment planning evaluations. International Journal of Radiation Oncology*Biology*Physics. 1991;21(1):137-46.

47.   Källman P, Agren A, Brahme A. Tumour and normal tissue responses to fractionated non-uniform dose delivery. Int J Radiat Biol. 1992;62(2):249-62.

48. Lyman JT. Complication Probability as Assessed from Dose-Volume Histograms. Radiation Research Supplement. 1985;8:S13-S9.

49. Nathanson BH, Higgins TL. An introduction to statistical methods used in binary outcome modeling. Semin Cardiothorac Vasc Anesth. 2008;12(3):153-66.

50. Niemierko A, Goitein M. Calculation of normal tissue complication probability and dose-volume histogram reduction schemes for tissues with a critical element architecture. Radiother Oncol. 1991;20(3):166-76.

51. Niemierko A, Goitein M. Modeling of normal tissue response to radiation: the critical volume model. Int J Radiat Oncol Biol Phys. 1993;25(1):135-45.

52. Kierkels RGJ, Korevaar EW, Steenbakkers RJHM, Janssen T, van't Veld AA, Langendijk JA, et al. Direct use of multivariable normal tissue complication probability models in treatment plan optimisation for individualised head and neck cancer radiotherapy produces clinically acceptable treatment plans. Radiotherapy and Oncology. 2014;112(3):430-6.

53. Tambas M, Steenbakkers RJHM, van der Laan HP, Wolters AM, Kierkels RGJ, Scandurra D, et al. First experience with model-based selection of head and neck cancer patients for proton therapy. Radiotherapy and Oncology. 2020;151:206-13.

54. Langendijk JA, Hoebers FJP, de Jong MA, Doornaert P, Terhaard CHJ, Steenbakkers RJHM, et al. National Protocol for Model-Based Selection for Proton Therapy in Head and Neck Cancer. International Journal of Particle Therapy. 2021;8(1):354-65.

55. Widder J, van der Schaaf A, Lambin P, Marijnen CA, Pignol JP, Rasch CR, et al. The Quest for Evidence for Proton Therapy: Model-Based Approach and Precision Medicine. Int J Radiat Oncol Biol Phys. 2016;95(1):30-6.

56. DAHANCA 35: Proton Versus Photon Therapy for Head-neck Cancer [Internet]. National Library of Medicine. 2020. Available from: https://clinicaltrials.gov/ct2/show/NCT04607694.

57. Moons KG, Altman DG, Reitsma JB, Ioannidis JP, Macaskill P, Steyerberg EW, et al. Transparent Reporting of a multivariable prediction model for Individual Prognosis or Diagnosis (TRIPOD): explanation and elaboration. Ann Intern Med. 2015;162(1):W1-73.

58.   Steyerberg EW. Overfitting and optimism in prediction models. Clinical Prediction Models: A Practical Approach to Development, Validation, and Updating. New York, NY: Springer New York; 2009. p. 83-100.

59.   Steyerberg EW, Vickers AJ, Cook NR, Gerds T, Gonen M, Obuchowski N, et al. Assessing the performance of prediction models: a framework for traditional and novel measures. Epidemiology. 2010;21(1):128-38.

60.   Vergouwe Y, Nieboer D, Oostenbrink R, Debray TPA, Murray GD, Kattan MW, et al. A closed testing procedure to select an appropriate method for updating prediction models. 2017;36(28):4529-39.

61.   JL D, KN B. Modern Mathematical Statistics with Applications. 2 ed: Springer New York, NY; 2012. XII, 845 p.

62.   Devore JL, Berk KN. Regression and Correlation. Modern Mathematical Statistics with Applications. New York, NY: Springer New York; 2012. p. 613-722.

63.   Bolker BM, Brooks ME, Clark CJ, Geange SW, Poulsen JR, Stevens MHH, et al. Generalized linear mixed models: a practical guide for ecology and evolution. Trends in Ecology & Evolution. 2009;24(3):127-35.

64.   Harrison XA, Donaldson L, Correa-Cano ME, Evans J, Fisher DN, Goodwin CED, et al. A brief introduction to mixed effects modelling and multi-model inference in ecology. PeerJ. 2018;6:e4794.

65.   Strobl C, Malley J, Tutz G. An introduction to recursive partitioning: Rationale, application, and characteristics of classification and regression trees, bagging, and random forests. Psychological Methods. 2009;14(4):323-48.

66.   IAEA. Relative Biological Effectiveness in Ion Beam Therapy. Vienna: INTERNATIONAL ATOMIC ENERGY AGENCY; 2008.

67.   Paganetti H. The physics of Proton Biology. In: Paganetti H, editor. Proton Therapy Physics (1st edt): CRC Press; 2012. p. 593-626.

68.   Sørensen BS. Commentary: RBE in proton therapy – where is the experimental in vivo data? Acta Oncologica. 2019;58(10):1337-9.

69.   McNamara AL, Willers H, Paganetti H. Modelling variable proton relative biological effectiveness for treatment planning. The British journal of radiology. 2020;93(1107):20190334-.

70. Paganetti H. Relative biological effectiveness (RBE) values for proton beam therapy. Variations as a function of biological endpoint, dose, and linear energy transfer. Phys Med Biol. 2014;59(22):R419-72.

71. Paganetti H, Niemierko A, Ancukiewicz M, Gerweck LE, Goitein M, Loeffler JS, et al. Relative biological effectiveness (RBE) values for proton beam therapy. Int J Radiat Oncol Biol Phys. 2002;53(2):407-21.

72. Carabe A, Moteabbed M, Depauw N, Schuemann J, Paganetti H. Range uncertainty in proton therapy due to variable biological effectiveness. Phys Med Biol. 2012;57(5):1159-72.

73. Sørensen BS, Overgaard J, Bassler N. In vitro RBE-LET dependence for multiple particle types. Acta Oncologica. 2011;50(6):757-62.

74. Paganetti H, Blakely E, Carabe-Fernandez A, Carlson DJ, Das IJ, Dong L, et al. Report of the AAPM TG-256 on the relative biological effectiveness of proton beams in radiation therapy. Med Phys. 2019;46(3):e53-e78.

75. Gerweck LE, Kozin SV. Relative biological effectiveness of proton beams in clinical therapy. Radiother Oncol. 1999;50(2):135-42.

76. Rorvik E, Fjaera LF, Dahle TJ, Dale JE, Engeseth GM, Stokkevag CH, et al. Exploration and application of phenomenological RBE models for proton therapy. Phys Med Biol. 2018;63(18):185013.

77. Carabe-Fernandez A, Dale RG, Jones B. The incorporation of the concept of minimum RBE (RbEmin) into the linear-quadratic model and the potential for improved radiobiological analysis of high-LET treatments. Int J Radiat Biol. 2007;83(1):27-39.

78. Luhr A, von Neubeck C, Pawelke J, Seidlitz A, Peitzsch C, Bentzen SM, et al. "Radiobiology of Proton Therapy": Results of an international expert workshop. Radiother Oncol. 2018;128(1):56-67.

79. Mody MD, Rocco JW, Yom SS, Haddad RI, Saba NF. Head and neck cancer. The Lancet. 2021;398(10318):2289-99.

80. Vai A, Molinelli S, Rossi E, Iacovelli NA, Magro G, Cavallo A, et al. Proton Radiation Therapy for Nasopharyngeal Cancer Patients: Dosimetric and NTCP Evaluation Supporting Clinical Decision. Cancers (Basel). 2022;14(5).

81.   Nguyen ML, Cantrell JN, Ahmad S, Henson C. Intensity-modulated proton therapy (IMPT) versus intensity-modulated radiation therapy (IMRT) for the treatment of head and neck cancer: A dosimetric comparison. Med Dosim. 2021;46(3):259-63.

82.   Lewis GD, Holliday EB, Kocak-Uzel E, Hernandez M, Garden AS, Rosenthal DI, et al. Intensity-modulated proton therapy for nasopharyngeal carcinoma: Decreased radiation dose to normal structures and encouraging clinical outcomes. Head Neck. 2016;38 Suppl 1:E1886-95.

83.   Widesott L, Pierelli A, Fiorino C, Dell'Oca I, Broggi S, Cattaneo GM, et al. Intensity-Modulated Proton Therapy Versus Helical Tomotherapy in Nasopharynx Cancer: Planning Comparison and NTCP Evaluation. Int J Radiat Oncol Biol Phys. 2008;72(2):589-96.

84.   Taheri-Kadkhoda Z, Björk-Eriksson T, Nill S, Wilkens JJ, Oelfke U, Johansson K-A, et al. Intensity-modulated radiotherapy of nasopharyngeal carcinoma: a comparative treatment planning study of photons and protons. Radiation Oncology. 2008;3(1):4.

85.   Gunn GB, Garden AS, Ye R, Ausat N, Dahlstrom KR, Morrison WH, et al. Proton Therapy for Head and Neck Cancer: A 12-Year, Single-Institution Experience. International Journal of Particle Therapy. 2021;8(1):108-18.

86.   Holliday EB, Garden AS, Rosenthal DI, Fuller CD, Morrison WH, Gunn GB, et al. Proton Therapy Reduces Treatment-Related Toxicities for Patients with Nasopharyngeal Cancer: A Case-Match Control Study of Intensity-Modulated Proton Therapy and Intensity-Modulated Photon Therapy. International Journal of Particle Therapy. 2015;2(1):19-28.

87.   Jiří K, Vladimír V, Michal A, Matěj N, Silvia S, Pavel V, et al. Proton pencil-beam scanning radiotherapy in the treatment of nasopharyngeal cancer: dosimetric parameters and 2-year results. European Archives of Oto-Rhino-Laryngology. 2021;278(3):763-9.

88.   Dagan R, Bryant C, Li Z, Yeung D, Justice J, Dzieglewiski P, et al. Outcomes of Sinonasal Cancer Treated With Proton Therapy. Int J Radiat Oncol Biol Phys. 2016;95(1):377-85.

89.   Yu NY, Gamez ME, Hartsell WF, Tsai HK, Laramore GE, Larson GL, et al. A Multi-Institutional Experience of Proton Beam Therapy for Sinonasal Tumors. Adv Radiat Oncol. 2019;4(4):689-98.

90.   Lee A, Kitpanit S, Chilov M, Langendijk JA, Lu J, Lee NY. A Systematic Review of Proton Therapy for the Management of Nasopharyngeal Cancer. International Journal of Particle Therapy. 2021;8(1):119-30.

91.   Patel SH, Wang Z, Wong WW, Murad MH, Buckey CR, Mohammed K, et al. Charged particle therapy versus photon therapy for paranasal sinus and nasal cavity malignant diseases: a systematic review and meta-analysis. The Lancet Oncology. 2014;15(9):1027-38.

92.   Tambas M, van der Laan HP, Steenbakkers RJHM, Doyen J, Timmermann B, Orlandi E, et al. Current practice in proton therapy delivery in adult cancer patients across Europe. Radiotherapy and Oncology. 2022;167:7-13.

93.   Fischer AW, Holfelder. Lokales Amyloid im Gehirn. Deutsche Zeitschrift für Chirurgie. 1930;227(1):475-83.

94.   Furuse M, Nonoguchi N, Kawabata S, Miyatake S-I, Kuroiwa T. Delayed brain radiation necrosis: pathological review and new molecular targets for treatment. Medical Molecular Morphology. 2015;48(4):183-90.

95.   Ali FS, Arevalo O, Zorofchian S, Patrizz A, Riascos R, Tandon N, et al. Cerebral Radiation Necrosis: Incidence, Pathogenesis, Diagnostic Challenges, and Future Opportunities. Current Oncology Reports. 2019;21(8):66.

96.   Zhou X, Liu P, Wang X. Temporal Lobe Necrosis Following Radiotherapy in Nasopharyngeal Carcinoma: New Insight Into the Management. Front Oncol. 2020;10:593487.

97.   Kłos J, van Laar PJ, Sinnige PF, Enting RH, Kramer MCA, van der Weide HL, et al. Quantifying effects of radiotherapy-induced microvascular injury; review of established and emerging brain MRI techniques. Radiother Oncol. 2019;140:41-53.

98.   Miyatake S, Nonoguchi N, Furuse M, Yoritsune E, Miyata T, Kawabata S, et al. Pathophysiology, diagnosis, and treatment of radiation necrosis in the brain. Neurol Med Chir (Tokyo). 2015;55(1):50-9.

99.   Brandsma D, Stalpers L, Taal W, Sminia P, van den Bent MJ. Clinical features, mechanisms, and management of pseudoprogression in malignant gliomas. The Lancet Oncology. 2008;9(5):453-61.

100.   Verma N, Cowperthwaite MC, Burnett MG, Markey MK. Differentiating tumor recurrence from treatment necrosis: a review of neuro-oncologic imaging strategies. Neuro Oncol. 2013;15(5):515-34.

101.   Wang YX, King AD, Zhou H, Leung SF, Abrigo J, Chan YL, et al. Evolution of radiation-induced brain injury: MR imaging-based study. Radiology. 2010;254(1):210-8.

102.   NHI. NCI Common Terminology Criteria for Adverse Events (CTCAE): National Cancer Institute 2010 [Available from: https://evs.nci.nih.gov/ftp1/CTCAE/CTCAE_4.03/CTCAE_4.03_2010-06-14_QuickReference_5x7.pdf.

103.   Rahmathulla G, Marko NF, Weil RJ. Cerebral radiation necrosis: a review of the pathobiology, diagnosis and management considerations. Journal of clinical neuroscience : official journal of the Neurosurgical Society of Australasia. 2013;20(4):485-502.

104.   Delishaj D, Ursino S, Pasqualetti F, Cristaudo A, Cosottini M, Fabrini MG, et al. Bevacizumab for the Treatment of Radiation-Induced Cerebral Necrosis: A Systematic Review of the Literature. J Clin Med Res. 2017;9(4):273-80.

105.   Lawrence YR, Li XA, el Naqa I, Hahn CA, Marks LB, Merchant TE, et al. Radiation dose-volume effects in the brain. Int J Radiat Oncol Biol Phys. 2010;76(3 Suppl):S20-7.

106.   Feng M, Huang Y, Fan X, Xu P, Lang J, Wang D. Prognostic variables for temporal lobe injury after intensity modulated-radiotherapy of nasopharyngeal carcinoma. Cancer Med. 2018;7(3):557-64.

107.   Huang J, Kong FF, Oei RW, Zhai RP, Hu CS, Ying HM. Dosimetric predictors of temporal lobe injury after intensity-modulated radiotherapy for T4 nasopharyngeal carcinoma: a competing risk study. Radiat Oncol. 2019;14(1):31.

108.   Kitpanit S, Lee A, Pitter KL, Fan D, Chow JCH, Neal B, et al. Temporal Lobe Necrosis in Head and Neck Cancer Patients after Proton Therapy to the Skull Base. Int J Part Ther. 2020;6(4):17-28.

109.   Kong C, Zhu XZ, Lee TF, Feng PB, Xu JH, Qian PD, et al. LASSO-based NTCP model for radiation-induced temporal lobe injury developing after intensity-modulated radiotherapy of nasopharyngeal carcinoma. Sci Rep. 2016;6:26378.

110.   Lu L, Sheng Y, Zhang G, Li Y, OuYang P-Y, Ge Y, et al. Temporal lobe injury patterns following intensity modulated radiotherapy in a large cohort of nasopharyngeal carcinoma patients. Oral Oncology. 2018;85:8-14.

111.   McDonald MW, Linton OR, Calley CS. Dose-volume relationships associated with temporal lobe radiation necrosis after skull base proton beam therapy. Int J Radiat Oncol Biol Phys. 2015;91(2):261-7.

112.   Su SF, Huang SM, Han F, Huang Y, Chen CY, Xiao WW, et al. Analysis of dosimetric factors associated with temporal lobe necrosis (TLN) in patients with nasopharyngeal carcinoma (NPC) after intensity modulated radiotherapy. Radiat Oncol. 2013;8:17.

113.   Su SF, Huang Y, Xiao WW, Huang SM, Han F, Xie CM, et al. Clinical and dosimetric characteristics of temporal lobe injury following intensity modulated radiotherapy of nasopharyngeal carcinoma. Radiother Oncol. 2012;104(3):312-6.

114.   Sun Y, Zhou GQ, Qi ZY, Zhang L, Huang SM, Liu LZ, et al. Radiation-induced temporal lobe injury after intensity modulated radiotherapy in nasopharyngeal carcinoma patients: a dose-volume-outcome analysis. BMC cancer. 2013;13:397.

115.   Wen D-W, Lin L, Mao Y-P, Chen C-Y, Chen F-P, Wu C-F, et al. Normal tissue complication probability (NTCP) models for predicting temporal lobe injury after intensity-modulated radiotherapy in nasopharyngeal carcinoma: A large registry-based retrospective study from China. Radiotherapy and Oncology. 2021;157:99-105.

116.   Zeng L, Huang SM, Tian YM, Sun XM, Han F, Lu TX, et al. Normal Tissue Complication Probability Model for Radiation-induced Temporal Lobe Injury after Intensity-modulated Radiation Therapy for Nasopharyngeal Carcinoma. Radiology. 2015;276(1):243-9.

117.   Zeng L, Tian YM, Sun XM, Chen CY, Han F, Xiao WW, et al. Late toxicities after intensity-modulated radiotherapy for nasopharyngeal carcinoma: patient and treatment-related risk factors. British Journal of Cancer. 2014;110(1):49-54.

118.   Zhang YY, Huo WL, Goldberg SI, Slater JM, Adams JA, Deng XW, et al. Brain-Specific Relative Biological Effectiveness of Protons Based on Long-term Outcome of Patients With Nasopharyngeal Carcinoma. Int J Radiat Oncol Biol Phys. 2021;110(4):984-92.

119.   Zhou X, Ou X, Xu T, Wang X, Shen C, Ding J, et al. Effect of dosimetric factors on occurrence and volume of temporal lobe necrosis following intensity modulated radiation therapy for nasopharyngeal carcinoma: a case-control study. Int J Radiat Oncol Biol Phys. 2014;90(2):261-9.

120.   Lambrecht M, Eekers DBP, Alapetite C, Burnet NG, Calugaru V, Coremans IEM, et al. Radiation dose constraints for organs at risk in neuro-oncology; the European Particle Therapy Network consensus. Radiother Oncol. 2018;128(1):26-36.

121.   Lee AW, Ng WT, Pan JJ, Chiang CL, Poh SS, Choi HC, et al. International Guideline on Dose Prioritization and Acceptance Criteria in Radiation Therapy Planning for Nasopharyngeal Carcinoma. Int J Radiat Oncol Biol Phys. 2019;105(3):567-80.

122.   Bentzen SM, Constine LS, Deasy JO, Eisbruch A, Jackson A, Marks LB, et al. Quantitative Analyses of Normal Tissue Effects in the Clinic (QUANTEC): an introduction to the scientific issues. Int J Radiat Oncol Biol Phys. 2010;76(3 Suppl):S3-9.

123.   Marks LB, Ten Haken RK, Martel MK. Guest Editor's Introduction to QUANTEC: A Users Guide. Int J Radiat Oncol Biol Phys. 2010;76(3, Supplement):S1-S2.

124.   Marks LB, Yorke ED, Jackson A, Ten Haken RK, Constine LS, Eisbruch A, et al. Use of normal tissue complication probability models in the clinic. Int J Radiat Oncol Biol Phys. 2010;76(3 Suppl):S10-9.

125.   Emami B, Lyman J, Brown A, Coia L, Goitein M, Munzenrider JE, et al. Tolerance of normal tissue to therapeutic irradiation. Int J Radiat Oncol Biol Phys. 1991;21(1):109-22.

126. Yepes P, Randeniya S, Taddei PJ, Newhauser WD. A Track-Repeating Algorithm for Fast Monte Carlo Dose Calculations of Proton Radiotherapy. Nuclear technology. 2009;168(3):736-40.

127. Yepes P, Randeniya S, Taddei PJ, Newhauser WD. Monte Carlo fast dose calculator for proton radiotherapy: application to a voxelized geometry representing a patient with prostate cancer. Phys Med Biol. 2009;54(1):N21-8.

128. Yepes PP, Eley JG, Liu A, Mirkovic D, Randeniya S, Titt U, et al. Validation of a track repeating algorithm for intensity modulated proton therapy: clinical cases study. Phys Med Biol. 2016;61(7):2633-45.

129. Yepes PP, Mirkovic D, Taddei PJ. A GPU implementation of a track-repeating algorithm for proton radiotherapy dose calculations. Phys Med Biol. 2010;55(23):7107-20.

130. Cortes-Giraldo MA, Carabe A. A critical study of different Monte Carlo scoring methods of dose average linear-energy-transfer maps calculated in voxelized geometries irradiated with clinical proton beams. Phys Med Biol. 2015;60(7):2645-69.

131. Agostinelli S, Allison J, Amako K, Apostolakis J, Araujo H, Arce P, et al. Geant4—a simulation toolkit. Nuclear Instruments and Methods in Physics Research Section A: Accelerators, Spectrometers, Detectors and Associated Equipment. 2003;506(3):250-303.

132. McNamara AL, Schuemann J, Paganetti H. A phenomenological relative biological effectiveness (RBE) model for proton therapy based on all published in vitro cell survival data. Phys Med Biol. 2015;60(21):8399-416.

133. Wedenberg M, Lind BK, Hardemark B. A model for the relative biological effectiveness of protons: the tissue specific parameter alpha/beta of photons is a predictor for the sensitivity to LET changes. Acta Oncol. 2013;52(3):580-8.

134. Frese MC, Wilkens JJ, Huber PE, Jensen AD, Oelfke U, Taheri-Kadkhoda Z. Application of constant vs. variable relative biological effectiveness in treatment planning of intensity-modulated proton therapy. Int J Radiat Oncol Biol Phys. 2011;79(1):80-8.

135.   Team RC. R: A language and environment for statistical computing Vienna, Austria: R Foundation for Statistical Computing; 2020 [Available from: https://www.R-project.org/.

136.   Rich JT, Neely JG, Paniello RC, Voelker CCJ, Nussenbaum B, Wang EW. A practical guide to understanding Kaplan-Meier curves. Otolaryngology–Head and Neck Surgery. 2010;143(3):331-6.

137.   Meira-Machado L, de Uña-Álvarez J, Cadarso-Suárez C, Andersen PK. Multi-state models for the analysis of time-to-event data. Statistical Methods in Medical Research. 2009;18(2):195-222.

138.   Engeseth GM, Stieb S, Mohamed ASR, He R, Stokkevåg CH, Brydøy M, et al. Outcomes and patterns of radiation associated brain image changes after proton therapy for head and neck skull base cancers. Radiother Oncol. 2020;151:119-25.

139.   Engeseth GM, Hysing LB, Yepes P, Pettersen HES, Mohan R, Fuller CD, et al. Impact of RBE variations on risk estimates of temporal lobe necrosis in patients treated with intensity-modulated proton therapy for head and neck cancer. Acta Oncol. 2022;61(2):215-22.

140.   Engeseth GM, He R, Mirkovic D, Yepes P, Mohamed ASR, Stieb S, et al. Mixed Effect Modeling of Dose and Linear Energy Transfer Correlations With Brain Image Changes After Intensity Modulated Proton Therapy for Skull Base Head and Neck Cancer. Int J Radiat Oncol Biol Phys.2021;111(3):684-92.

141.   Talari K, Goyal M. Retrospective studies - utility and caveats. J R Coll Physicians Edinb. 2020;50(4):398-402.

142.   Valk PE, Dillon WP. Radiation injury of the brain. AJNR Am J Neuroradiol. 1991;12(1):45-62.

143.   Austin PC, Lee DS, Fine JP. Introduction to the Analysis of Survival Data in the Presence of Competing Risks. Circulation. 2016;133(6):601-9.

144.   Niyazi M, Niemierko A, Paganetti H, Sohn M, Schapira E, Goldberg S, et al. Volumetric and actuarial analysis of brain necrosis in proton therapy using a novel mixture cure model. Radiother Oncol. 2019.

145.   Schröder C, Köthe A, De Angelis C, Basler L, Fattori G, Safai S, et al. NTCP modelling for high-grade temporal radionecrosis in a large cohort of patients receiving

pencil beam scanning proton therapy for skull base and head and neck tumors. Int J Radiat Oncol Biol Phys. 2022;113 (2):448-55

146. Wang J, Miao Y, Ou X, Wang X, He X, Shen C, et al. Development and validation of a model for temporal lobe necrosis for nasopharyngeal carcinoma patients with intensity modulated radiation therapy. Radiat Oncol. 2019;14(1):42.

147. Zhou GQ, Yu XL, Chen M, Guo R, Lei Y, Sun Y, et al. Radiation-induced temporal lobe injury for nasopharyngeal carcinoma: a comparison of intensity-modulated radiotherapy and conventional two-dimensional radiotherapy. PloS one. 2013;8(7):e67488.

148. Cheung MC, Chan AS, Law SC, Chan JH, Tse VK. Impact of radionecrosis on cognitive dysfunction in patients after radiotherapy for nasopharyngeal carcinoma. Cancer. 2003;97(8):2019-26.

149. Gillmann C, Lomax AJ, Weber DC, Jäkel O, Karger CP. Dose–response curves for MRI-detected radiation-induced temporal lobe reactions in patients after proton and carbon ion therapy: Does the same RBE-weighted dose lead to the same biological effect? Radiotherapy and Oncology. 2018;128(1):109-14.

150. Miyawaki D, Murakami M, Demizu Y, Sasaki R, Niwa Y, Terashima K, et al. Brain injury after proton therapy or carbon ion therapy for head-and-neck cancer and skull base tumors. Int J Radiat Oncol Biol Phys. 2009;75(2):378-84.

151. Pehlivan B, Ares C, Lomax AJ, Stadelmann O, Goitein G, Timmermann B, et al. Temporal lobe toxicity analysis after proton radiation therapy for skull base tumors. Int J Radiat Oncol Biol Phys. 2012;83(5):1432-40.

152. Jensen K, Friborg J, Hansen CR, Samsøe E, Johansen J, Andersen M, et al. The Danish Head and Neck Cancer Group (DAHANCA) 2020 radiotherapy guidelines. Radiotherapy and Oncology. 2020;151:149-51.

153. Carabe A, Espana S, Grassberger C, Paganetti H. Clinical consequences of relative biological effectiveness variations in proton radiotherapy of the prostate, brain and liver. Phys Med Biol. 2013;58(7):2103-17.

154. Fjæra LF, Indelicato DJ, Ytre-Hauge KS, Muren LP, Lassen-Ramshad Y, Toussaint L, et al. Spatial Agreement of Brainstem Dose Distributions Depending on

Biological Model in Proton Therapy for Pediatric Brain Tumors. Adv Radiat Oncol. 2021;6(1):100551.

155.   Giantsoudi D, Adams J, MacDonald S, Paganetti H. Can differences in linear energy transfer and thus relative biological effectiveness compromise the dosimetric advantage of intensity-modulated proton therapy as compared to passively scattered proton therapy? Acta Oncol. 2018;57(9):1259-64.

156.   Giovannini G, Bohlen T, Cabal G, Bauer J, Tessonnier T, Frey K, et al. Variable RBE in proton therapy: comparison of different model predictions and their influence on clinical-like scenarios. Radiat Oncol. 2016;11:68.

157.   Gutierrez A, Rompokos V, Li K, Gillies C, D'Souza D, Solda F, et al. The impact of proton LET/RBE modeling and robustness analysis on base-of-skull and pediatric craniopharyngioma proton plans relative to VMAT. Acta Oncol. 2019;58(12):1765-74.

158.   Otterlei OM, Indelicato DJ, Toussaint L, Ytre-Hauge KS, Pilskog S, Fjaera LF, et al. Variation in relative biological effectiveness for cognitive structures in proton therapy of pediatric brain tumors. Acta Oncol. 2021;60(2):267-74.

159.   Resch AF, Landry G, Kamp F, Cabal G, Belka C, Wilkens JJ, et al. Quantification of the uncertainties of a biological model and their impact on variable RBE proton treatment plan optimization. Physica Medica. 2017;36:91-102.

160.   Tilly N, Johansson J, Isacsson U, Medin J, Blomquist E, Grusell E, et al. The influence of RBE variations in a clinical proton treatment plan for a hypopharynx cancer. Phys Med Biol. 2005;50(12):2765-77.

161.   Wedenberg M, Toma-Dasu I. Disregarding RBE variation in treatment plan comparison may lead to bias in favor of proton plans. Med Phys. 2014;41(9):091706.

162.   Yepes P, Adair A, Frank SJ, Grosshans DR, Liao Z, Liu A, et al. Fixed- versus Variable-RBE Computations for Intensity Modulated Proton Therapy. Adv Radiat Oncol. 2018;4(1):156-67.

163.   Ytre-Hauge KS, Fjaera LF, Rorvik E, Dahle TJ, Dale JE, Pilskog S, et al. Inter-patient variations in relative biological effectiveness for cranio-spinal irradiation with protons. Sci Rep. 2020;10(1):6212.

164. Ödén J, Eriksson K, Toma-Dasu I. Inclusion of a variable RBE into proton and photon plan comparison for various fractionation schedules in prostate radiation therapy. Med Phys. 2017;44(3):810-22.

165. Ödén J, Eriksson K, Toma-Dasu I. Incorporation of relative biological effectiveness uncertainties into proton plan robustness evaluation. Acta Oncol. 2017;56(6):769-78.

166. Garbacz M, Gajewski J, Durante M, Kisielewicz K, Krah N, Kopeć R, et al. Quantification of biological range uncertainties in patients treated at the Krakow proton therapy centre. Radiat Oncol. 2022;17(1):50.

167. Marteinsdottir M, Paganetti H. Applying a variable relative biological effectiveness (RBE) might affect the analysis of clinical trials comparing photon and proton therapy for prostate cancer. Physics in Medicine & Biology. 2019;64(11):115027.

168. Marteinsdottir M, Wang CC, McNamara A, Depauw N, Shin J, Paganetti H. The impact of variable relative biological effectiveness in proton therapy for left-sided breast cancer when estimating normal tissue complications in the heart and lung. Phys Med Biol. 2021;66(3):035023.

169. Grassberger C, Trofimov A, Lomax A, Paganetti H. Variations in linear energy transfer within clinical proton therapy fields and the potential for biological treatment planning. Int J Radiat Oncol Biol Phys. 2011;80(5):1559-66.

170. Bahn E, Bauer J, Harrabi S, Herfarth K, Debus J, Alber M. Late Contrast Enhancing Brain Lesions in Proton-Treated Patients With Low-Grade Glioma: Clinical Evidence for Increased Periventricular Sensitivity and Variable RBE. Int J Radiat Oncol Biol Phys. 2020;107(3):571-8.

171. Bertolet A, Abolfath R, Carlson DJ, Lustig RA, Hill-Kayser C, Alonso-Basanta M, et al. Correlation of LET With MRI Changes in Brain and Potential Implications for Normal Tissue Complication Probability for Patients With Meningioma Treated With Pencil Beam Scanning Proton Therapy. Int J Radiat Oncol Biol Phys. 2022;112(1):237-46.

172. Eulitz J, Lutz B, Wohlfahrt P, Dutz A, Enghardt W, Karpowitz C, et al. A Monte Carlo based radiation response modelling framework to assess variability of clinical RBE in proton therapy. Phys Med Biol. 2019.

173. Eulitz J, Troost EGC, Raschke F, Schulz E, Lutz B, Dutz A, et al. Predicting late magnetic resonance image changes in glioma patients after proton therapy. Acta Oncol. 2019:1-4.

174. Garbacz M, Cordoni FG, Durante M, Gajewski J, Kisielewicz K, Krah N, et al. Study of relationship between dose, LET and the risk of brain necrosis after proton therapy for skull base tumors. Radiotherapy and Oncology. 2021;163:143-9.

175. Harrabi SB, von Nettelbladt B, Gudden C, Adeberg S, Seidensaal K, Bauer J, et al. Radiation induced contrast enhancement after proton beam therapy in patients with low grade glioma - how safe are protons? Radiother Oncol. 2021.

176. Niemierko A, Schuemann J, Niyazi M, Giantsoudi D, Maquilan G, Shih HA, et al. Brain Necrosis in Adult Patients After Proton Therapy: Is There Evidence for Dependency on Linear Energy Transfer? Int J Radiat Oncol Biol Phys. 2020;109(1):10.

177. Skaarup M, Lundemann MJ, Darkner S, Jørgensen M, Marner L, Mirkovic D, et al. A framework for voxel-based assessment of biological effect after proton radiotherapy in pediatric brain cancer patients using multi-modal imaging. Med Phys. 2021;48(7):4110-21.

178. Ödén J, Toma-Dasu I, Witt Nyström P, Traneus E, Dasu A. Spatial correlation of linear energy transfer and relative biological effectiveness with suspected treatment-related toxicities following proton therapy for intracranial tumors. Med Phys. 2020;47(2):342-51.

179. Roberts KW, Wan Chan Tseung HS, Eckel LJ, Harmsen WS, Beltran C, Laack NN. Biologic Dose and Imaging Changes in Pediatric Brain Tumor Patients Receiving Spot Scanning Proton Therapy. Int J Radiat Oncol Biol Phys. 2019;105(3):664-73.

180. Wagenaar D, Schuit E, van der Schaaf A, Langendijk JA, Both S. Can the mean linear energy transfer of organs be directly related to patient toxicities for current head and neck cancer intensity-modulated proton therapy practice? Radiotherapy and Oncology. 2021;165:159-65.

181. Bolsi A, Placidi L, Pica A, Ahlhelm FJ, Walser M, Lomax AJ, et al. Pencil beam scanning proton therapy for the treatment of craniopharyngioma complicated with radiation-induced cerebral vasculopathies: A dosimetric and linear energy transfer (LET) evaluation. Radiother Oncol. 2020;149:197-204.

182. Dowding I, Haufe S. Powerful Statistical Inference for Nested Data Using Sufficient Summary Statistics. Front Hum Neurosci. 2018;12:103-.

183. Hahn C, Eulitz J, Peters N, Wohlfahrt P, Enghardt W, Richter C, et al. Impact of range uncertainty on clinical distributions of linear energy transfer and biological effectiveness in proton therapy. Med Phys. 2020;47(12):6151-62.

184. Sørensen BS, Pawelke J, Bauer J, Burnet NG, Dasu A, Høyer M, et al. Does the uncertainty in relative biological effectiveness affect patient treatment in proton therapy? Radiother Oncol. 2021;163:177-84.
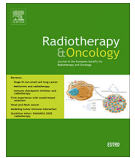
Original Article

Outcomes and patterns of radiation associated brain image changes after proton therapy for head and neck skull base cancers

Grete May Engeseth [a,b,c,d], Sonja Stieb [a], Abdallah Sherif Radwan Mohamed [a], Renjie He [a], Camilla Hanquist Stokkevåg [b], Marianne Brydøy [a], Clifton Dave Fuller [a], Adam S. Garden [a], David I. Rosenthal [a], Jack Phan [a], William H. Morrison [a], Jay P. Reddy [a], Richard Wu [a], Xiaodong Zhang [a], Steven Jay Frank [a], Gary Brandon Gunn [a,*]

[a] Department of Radiation Oncology, University of Texas MD Anderson Cancer Center, Houston, USA; [b] Department of Oncology and Medical Physics, Haukeland University Hospital, Bergen; [c] Department of Clinical Science; and [d] Department of Physics and Technology, University of Bergen, Norway

ARTICLE INFO

ABSTRACT

Background and purpose: To characterize patterns and outcomes of brain MR image changes after proton therapy (PT) for skull base head and neck cancer (HNC).

Material and methods: Post-treatment MRIs ≥6 months were reviewed for radiation-associated image changes (RAIC) in 127 patients. All patients had received at least a point dose of 40 Gy(RBE) to the brain. The MRIs were rigidly registered to planning CTs and RAIC lesions were contoured both on T1 weighted (post-contrast) and T2 weighted sequences, and dose–volume parameters extracted. Probability of RAIC was calculated using multistate survival analysis. Univariate/multivariate analyses were performed using Cox Regression. Recursive partitioning analysis was used to investigate dose–volume correlates of RAIC development.

Results: 17.3% developed RAIC. All RAIC events were asymptomatic and occurred in the temporal lobe (14), frontal lobe (6) and cerebellum (2). The median volume of the contrast enhanced RAIC lesion was 0.5 cc at their maximum size. The RAIC resolved or improved in 45.5% of the patients and were stable or progressed in 36.4%. The 3-year actuarial rate of developing RAIC was 14.3%. RAIC was observed in 63% of patients when $V_{67\ Gy(RBE)}$ of the brain ≥0.17 cc.

Conclusion: Small RAIC lesions after PT occurred in 17.3% of the patients; the majority in nasopharyngeal or sinonasal cancer. The estimated dose–volume correlations confirm the importance of minimizing focal high doses to brain when achievable.

© 2020 Elsevier B.V. All rights reserved. Radiotherapy and Oncology 151 (2020) 119–125

Radiation therapy for head neck cancers (HNCs) at the skull base can result in high doses of radiation delivered to the brain, potentially leading to radiation-associated image changes (RAIC) [1]. Often the diagnosis of RAIC is based solely on radiographic findings on post-treatment MRIs obtained for routine cancer surveillance purposes. For HNCs, information on RAIC stems largely from studies in patients with nasopharyngeal cancers (NPC) treated with Intensity Modulated Radiation Therapy (IMRT), with reported incidences of temporal lobe RAIC ranging between 2% and 14% [2–12]. From patients treated proton therapy (PT) a few mixed cohort studies including selected HNCs report incidences of brain RAIC of 11–31% [13–16]. In studies evaluating the dose–response relationship for RAIC development, constraints have been suggested for several dose–volume parameters as well as for the Equivalent Uniform Dose (EUD) (Table 1), whereas the recently published international consensus guideline for NPC radiotherapy recommend to aim for a temporal lobe $D_{0.03cc} \leq 65$ Gy and $D_{0.03cc} \leq 70$ Gy for T1–T2 and T3–T4 tumors, respectively [17].

Owing to the proximity to Central Nervous System (CNS) critical structures, HNCs with tumor at the skull base or with intracranial extension are often selected for treatment with PT to improve or maintain target volume coverage while respecting normal tissues

* Corresponding author at: Department of Radiation Oncology, University of Texas MD Anderson Cancer Center, 1840 Old Spanish Trail, 77054 Houston, USA.

E-mail addresses: grete.may.engeseth@helse-bergen.no (G.M. Engeseth), SMStieb@mdanderson.org (S. Stieb), ASMohamed@mdanderson.org (A.S.R. Mohamed), RHe1@mdanderson.org (R. He), hanquist.stokkevag@helse-bergen.no (C.H. Stokkevåg), marianne.brydoy@helse-bergen.no (M. Brydøy), CDFuller@mdanderson.org (C.D. Fuller), agarden@mdanderson.org (A.S. Garden), dirosenthal@mdanderson.org (D.I. Rosenthal), jphan@mdanderson.org (J. Phan), whmorrison@mdanderson.org (W.H. Morrison), JReddy@mdanderson.org (J.P. Reddy), rywu@mdanderson.org (R. Wu), xizhang@mdanderson.org (X. Zhang), sjfrank@mdanderson.org (S.J. Frank), GBGunn@mdanderson.org (G. Brandon Gunn).

Table 1
Outcome and dose volume constraints reported in literature.

Author (# pat)	Incidence	Grading/clinical symptoms (% of diagnosed RAIC)	Actuarial rates	Median FU in months (range)	Median latency months (range)	Prescribed dose Gy/Gy (RBE) (# fx)	D-V constraints/ features/ probabilities
IMRT							
Zeng et al. (351) [10]	8.3% T4: 28.0%	CTCAE V3.0: G1: 58.6%, G2: 31.0%, G3: 3%	3y: 5.6%, 5y: 9.7%	76 (6–100)	33 (12–83)	66 (30)	TD5/5: D_{1cc}: 62.8 Gy TD50/5: D_{1cc}: 77.6 Gy
Kong et al. (132) [4]	12.9%	8 out of 17 symptomatic (47.1%)	5y: 4.7% (T3)	64 (11–106)	43 (19–68)	64–75 (32–34)	TD5/5: D_{1cc}: 62.8 Gy TD50/5: D_{1cc}: 80.9 Gy
		Vertigo, headache, memory detoriation, muscle weakness and personality changes	32.8% (T4 tumors only)				TD5/5: D_{max}: 69.0 Gy TD50/5: D_{max}: 82.1 Gy
Feng et al. (695) [2]	8.5%	28.8%: Headache, memory detoriation, emotion disorder	NR	73 (22–108)	38 (22–55)	66–76 (30–33)	TD5/5: D_{2cc}: 60.3 Gy TD50/5: D_{2cc}: 76.9 Gy
SU et al. (870) [6]	4.6%	22%: Dizziness, headaches, memory detoriation, muscle weakness, epileptic attack	NR	40 (6–104)	30 (6–56)	68 (30)	2.7% risk 5 years: V_{40Gy} < 11cc
Zhou et al. (1887) [12]	2.3%	Symptomatic : 30.2%	3y : 3.5%, 5y: 7.0%	28 (6–60)	30 (10–54)	60–70.4 (30–32)	Lesion volume < 5 cc: V_{45Gy} < 15.1 cc
Wang et al (749) [9]	5.1%	100% according to RTOG/ EORTC: G1: 84.2%, G2:5.3%, G3:10.5%	NR	48.8 (3.5–75.1)	NR	66–70.4 (30–32)	Identified features by LASSO*: $D_{0.5cc}$, D_{10cc}
Huang et al (506) (stage T4 only) [3]	12.5%	CTCAE: G1: 72.4%, G2: 17.4%, G3: 10.3% Total 46.3%: headache, dizziness, memory impairment, epileptic attacks personality changes, consciousness	Cumulative incidence: 3 y: 5.4%, 5 y: 13.2%	40.1 (6–120.1)	NR	66–70.4(32)	5y: 13.2%: D_{1cc} ≤71.1 Gy, 63.3% : D_{1cc} >71.1 Gy
Takiar et al (66) [8]	14.0%	2 cognitive impairment	NR	35 (1–124)	NR	66–70 (33–35)	NR
Proton							
Pehlivan (62) [16]	11.3%	G1:5, G3: 2	NR	38 (14–92)	19 (10–38)	68.4–73.5 (4 fx/week)	NR
McDonald et al. (66) [13]	18.2%	G1: 12.4%, G2: 5.7%	3 y: 12.4%, G2+ at 3 Y: 5.7%. G1: 9, G2: 1, G3: 4, G4: 2	31 (6–96)	21 (8–51)	62.0–79.2 (31–44)	15% risk 3 year: $V_{40Gy(RBE)}$ > 16.55cc $V_{60Gy(RBE)}$ > 55.0cc $V_{70Gy(RBE)}$ > 1.7cc
Niyazi et al. (179) [14] (intracranial and extracranial tumors)	20.7% (only G2 necrosis)	Grade 2 (CTCAE 4.0): total: 20.7%; intracranial: 8.4%, extracranial :31.3%	2 y: Intracranial: 2.5%, extracranial: 25.5% 5 y: intracranial: 4.5% extracranial: 42.4%.	4.4 years (0.–13.0)	1.5 years (0.2–6.9)	Intracranial: 59.4 (NR) Extracranial: 70.0 (NR)	Intracranial: EUD_{50} 57.7 Gy(RBE) Extracranial: EUD_{50}: 39.5 Gy (RBE)
Dagan et al (84) [15]	16.7%**	G2: 11 %, G3: 4% G5: 1.7%	NR	29 (5–86)	NR	74.4 Gy(RBE)	NR

D–V: dose volume, CTCAE: Common terminology Criteria for Adverse Events, FU: follow up, y: year.
  * Least Absolute Shrinkage and Selection Operator.
  ** Only symptomatic patients reported; results not based on MRI findings.

tolerance and reducing the toxicities and symptoms associated with the greater integral dose with IMRT. However, studies on the development of RAIC after PT for HNCs are limited. Thus, as part of a broader effort to better define the role and value of PT for HNC and to provide PT-specific dose recommendations to guide clinicians and the PT community, the specific aims of this study were to:

Characterize the incidence and patterns of RAIC after PT for skull base HNCs
Identify candidate clinical and dose–volume parameters associated with RAIC
Propose practical dose constraints to minimize the risk of RAIC

Methods and materials

Patient cohort

Adult patients treated with PT for HNC at University of Texas MD Anderson Cancer Center were eligible for participation in two consecutive Institutional Review Board-approved prospective studies (ClinicalTrials.org identifiers: NCT 00991094 and NCT 01627093). Eligibility included: (1) Anatomic tumor location at the base of skull, including primary tumors of the nasopharynx, sinonasal, periorbital, parotid, and skin, (2) A point dose of at least 40 Gy to the brain (relative biological effectiveness = 1.1), and (3) one or more follow-up MRI ≥6 months after completion of PT. Patients with prior radiation therapy to the region or who had

received photon-based treatment as part of therapy were excluded.

Treatment

All PT plans were based on non-contrast CT images and generated in the Eclipse treatment planning system (TPS) (Varian Medical Systems, Palo Alto, CA, USA) using either Intensity Modulated Proton Therapy (IMPT), Passive Scattered Proton Therapy (PSPT) or a combination of IMPT/PSPT. For dose prescription a proton relative biological effectiveness (RBE) value of 1.1 was used as recommended by the ICRU [18]. Dose (prescribed to CTV) and fractionation regimens were generally 60 Gy(RBE) in 30 fractions or 63–66 Gy(RBE) in 30–33 fractions in the postoperative PT setting or 66–70 Gy(RBE) in 33–35 fractions in the definitive PT setting. Induction chemotherapy regimens used were typically 3 cycles with taxane and platinum or taxane, platinum and fluorouracil (TPF), and concurrent chemotherapy was usually platinum-based.

Follow-up and diagnosis of RAIC

Follow-up MRIs took place regularly at 8–12 weeks after therapy completion and then every 3 months in the first year, every 4 months in the second year, every 6 months until 5 years, and annually thereafter. Defined as RAIC were (i) contrast enhanced lesions on T1 weighted (T1w) MRIs located in previously irradiated brain tissue and/or (ii) cysts or white matter lesions manifested as high signal intensity on the T2 weighted (T2w) sequences [19]. All RAICs were initially diagnosed by a radiologist during routine disease surveillance and were, for this analysis, identified through review of all MRI reports, and retrospectively reassessed by two board certified radiation oncologists (GBG and SJF). No additional RAIC to those already diagnosed in the MRI reports was discovered. The clinical grading of RAIC was performed retrospectively by chart review according to CTCAE v4.03 [20].

Extraction of clinical and treatment related data

Patient, tumor and treatment characteristics were retrieved from the patients' medical records (Epic Systems Corporation, Verona, WI) and the TPS. The MRIs were rigid registered to the initial treatment planning CT and qualitatively evaluated through visual inspection and further manually corrected if deemed necessary. To detect the extent of the RAIC, gadolinium contrast enhanced lesions on T1w sequences (T1w lesions) and hyperintensities including visible edema from T2w sequences (T2w lesions) were contoured as individual structures and propagated to the planning CT. dose–volume histograms (DVHs) for all patients were exported using bin size of 0.1 Gy(RBE) from where candidate dose volume parameters for the brain tissue were retrieved, including: the maximum dose (D_{max}), the dose delivered to 0.5cc ($D_{0.5cc}$) and 1cc (D_{1cc}) to 5cc (D_{5cc}) of the brain in 1cc steps, as well as the volume of brain receiving 40–70 Gy(RBE) in 1 Gy(RBE) steps ($V_{40Gy(RBE)}$ to $V_{70Gy(RBE)}$). The selection of candidate variables were based on (a) previously identified dose–volume parameters judged as important in predicting RAIC and (b) applicability to clinical practice and plan optimization and evaluation. In addition, for each patient the T1w and T2w lesion volumes with the corresponding minimum dose (D_{min}), the mean dose (D_{mean}) and the D_{max} were extracted for the first MRI and the MRI with the largest volume of RAIC ("worst" MRI).

Statistical analysis

The follow-up time was calculated as the time between the last PT fraction and the patient's last follow-up MRI. The RAIC latency time was calculated as the time between the last PT fraction and first MRI with RAIC. Time to resolution from RAIC was calculated from date of the first MRI with RAIC and the date of the first MRI where lesion had resolved.

In a course where the event of interest can transient between different states, multistate analysis can provide better accuracy of events reporting. As RAIC resolution is common in a considerable proportion of patients, multistate analysis was used to estimate the probability of RAIC over time [21]. For the current analysis the event of interest was RAIC, and data were censored if patients were alive and RAIC free at last available follow-up MRI. Bootstrapping (n = 1000) was used to estimate the 95% confidence intervals [22,23].

Comparisons between patients with and without RAIC were performed using the Mann Whitney U test, the Chi Square and Fishers exact test. All tests were two-sided with a significance level of 0.05. Correlations between the clinical and dosimetric predictor variables were calculated using Spearman's rank correlation and Pearson's correlation coefficient. Univariate and multivariate analysis of the association between RAIC and candidate predictors were performed using Cox Proportional Hazards Regression Analysis [24,25]. Covariates with p value <0.2 from the univariate analysis were considered for inclusion in the multivariate analysis. However, since DVH parameters are highly correlated, the dose volume variables with the lowest significance level from variables where the correlation coefficient were >0.8 were chosen for the analysis.

To identify important V_D parameters, recursive partitioning analysis (RPA) was applied. The chosen endpoint was RAIC three years post-treatment; dose–volume statistics from patients with three years follow-up time or more were included in the analysis. RPA was performed using bootstrapping (n = 1000) with number of observations in the terminal node constrained to 10% of the dataset and splitting of nodes based on the Gini index [26,27]. Statistical analyses were performed in SPSS version 24 (IBM SPSS Statistics for Windows, Version 24.0. Armonk, NY: IBM Corp, US) and R version 3.6 (R Foundation for Statistical Computing, Vienna, Austria).

Results

One-hundred and ninety-three patients treated from 12/2010 through 06/2018 met the inclusion criteria. Of these, 66 were excluded due to prior photon treatment to the same region. The remaining 127 patients formed the cohort.

Patient, tumor and treatment characteristics are displayed in Table 2. Eighty-five patients (66.9%) were treated exclusively with IMPT, 15 patients (11.8%) exclusively with PSPT and 27 patients (21.3%) with a combination of PSPT and IMPT. Thirty eight patients (29.9%) had one adaption of the treatment plan and 6 patients (4.7%) had two. Twenty patients (15.7%) received both induction and concurrent chemotherapy.

Median follow-up time was 29 months (range: 6-97). Twenty-two patients (17.3%) developed RAIC with a median latency of 24 months (9–37); all but one RAIC had developed within three years after PT. Median follow-up time after diagnosis of RAIC was 14 months (0–70). All patients with RAIC were asymptomatic at initial diagnoses and subsequent follow-up visits. However, due to progression of the image changes on the follow-up MRIs, two patients were treated with pentoxifylline and vitamin E (one of whom also received dexamethasone), and a third patient was treated with bevacizumab [28]. A decision to initiate treatment suggests that the lesions were considered to be clinically severe enough to warrant medical intervention, therefore, 3 patients were rated to have Grade 3 and 19 patients Grade 1 CNS necrosis according to CTCAE 4.03 (Supplementary material Table 1). At last available MRI the lesions had resolved in six patients, progressed in four, regressed

Table 2
Patient, treatment and tumor characteristics for the entire cohort and by RAIC group.

Characteristic	All patients (n = 127)		No RAIC (n = 105)		RAIC (n = 22)		p
	n	%	n	%	n	%	
Sex							0.98
Male	67	52.8	57	54.3	10	45.5	
Female	60	47.2	48	45.7	12	54.3	
Age							0.69
Median (Q1–Q3)	51 (39–64)		50 (37–63)		54 (41–61)		
Anatomic Site							0.16
Base of Skull, NOS	7	6.3	6	5.7	1	4.5	
Nasopharynx	35	26.8	27	25.7	8	36.4	
Sinonasal	29	22.8	20	19.0	9	40.9	
Parotid	14	11	14	13.3	–	–	
Orbital	23	18.1	21	20.0	2	9.1	
Skin	10	7.9	9	8.6	1	4.5	
Other	9	7.1	8	7.6	1	4.5	
T-category							0.77
T1–T2	28	22	24	22.9	4	18.2	
T3–T4	53	41.7	41	39	12	54.5	
Recurrent	29	22.8	25	23.8	4	18.2	
Tx	5	3.9	5	4.8	–	–	
No stage	12	9.4	10	9.5	2	9.1	
Surgery							0.23
No	49	38.6	38	36.2	11	50	
Yes	78	61.4	67	63.8	11	50	
Induction chemotherapy							0.76
No	106	83.5	86	81.9	20	90.9	
Yes	21	16.5	19	18.1	2	9.1	
Concurrent chemotherapy							0.04
No	54	42.5	49	46.7	5	22.7	
Yes	73	57.5	56	53.3	17	77.3	
PT technique							0.72
IMPT	85	69.9	69	65.7	16	72.7	
PSPT	15	11.8	12	11.4	3	13.6	
IMPT/PSPT	27	21.3	24	22.9	3	13.6	
Prescribed dose							
Median (Q1–Q3)	64.0 (60.1–69.7)		64.0 (60.1–68.3)		69.3 (63.1–70.0)		0.04
Brain D_{max} < 60 Gy(RBE)							0.01
No	95	74.8	74	70.5	21	96.9	
Yes	32	25.2	31	29.5	1	3.1	
Brain D_{max} > 70 Gy(RBE)							<0.01
No	89	70.1	81	77.1	8	36.4	
Yes	38	29.9	24	22.9	14	63.6	

Q1: 25 percentile, Q3: 75 percentile. Base of Skull: Adenoid cystic carcinoma, adenocarcinoma, neuro-endocrine carcinoma, chondrosarcoma, ameloblastoma, osteosarcoma. Other: vagus nerve schwannoma, paraganglioma, melanoma inferior turbinate, unknown primary site. IMPT: Intensity Modulated Proton Therapy, PSPT: Passive Scattering Proton Therapy.

in four, were stable in four and four patients had yet to have a follow-up MRI. A case example of the observed RAIC evolution including overview of evolution timeline can be found in Supplementary Material Figs. 1 and 2. Overall, the estimated probability of RAIC at two, three and five years was 8.7% (95% CI: 3.8%, 13.7%), 14.3% (95% CI: 8.2%, 20.4%), and 12.7% (95% CI: 6.9%, 18.5%), respectively (Supplementary Fig. 3).

Tumor and treatment characteristics for patients with RAIC including dose–volume summary statistics for the contoured lesions are provided in Supplementary Materials (Table 2–4). Of patients diagnosed with RAIC, 68.2% patients had been treated for T4 or unresectable disease, and 63.6% had intracranial tumor extension. RAIC was located in the temporal lobe (14 patients), frontal lobe (six patients) and in the cerebellum (two patients). The majority of RAIC developed in patients with NPC or sinonasal cancers (77.3%); all (eight) RAIC occurred in the temporal lobe for the NPCs and for the patients with sinonasal cancer RAIC was found both in the temporal lobe (four) and the frontal lobe (five) (Supplementary Material Fig. 4). Two of the contrast-enhanced

T1w lesions were inside and seven were outside the CTV, the remaining 13 were overlapping with the CTV. At first MRI 92% of the T1w contrast-enhanced lesions were 1cc or less, with a median volume of 0.3cc (punctuate to 1.1cc); on the MRIs where the RAIC was at its largest size, 77% of the T1w lesions were less than 1cc with a median volume of 0.5cc (0.1–3.1cc). The T1w lesion doses were highest in lesions located in the temporal lobe and for lesions inside the CTV (Fig. 1).

Statistical significant differences by RAIC group were only found for prescribed dose and brain dose–volume parameters (Tables 2–3). $V_{40\ Gy(RBE)}$–$V_{70\ Gy(RBE)}$ for the brain were included in the RPA. The result showed that 63.1% of the patients with $V_{67\ Gy(RBE)} \geq 0.17$cc developed RAIC (Fig. 2/Supplementary Material Table 5). Based on the result from RPA, we included $V_{67\ Gy(RBE)} \geq 0.17$cc in the univariate cox regression analysis. From this analysis prescribed dose, D_{max}, D_{1-5cc}, $V_{70\ (Gy RBE)}$ and $V_{67\ Gy(RBE)} \geq 0.17$cc were significantly associated with the development of RAIC. In the multivariate analysis; $V_{67\ Gy(RBE)} \geq 0.17$cc was the only statistically significant predictive factor (HR: 7.57, 95% CI: 1.48, 38.76, p = 0.015) (Table 4).
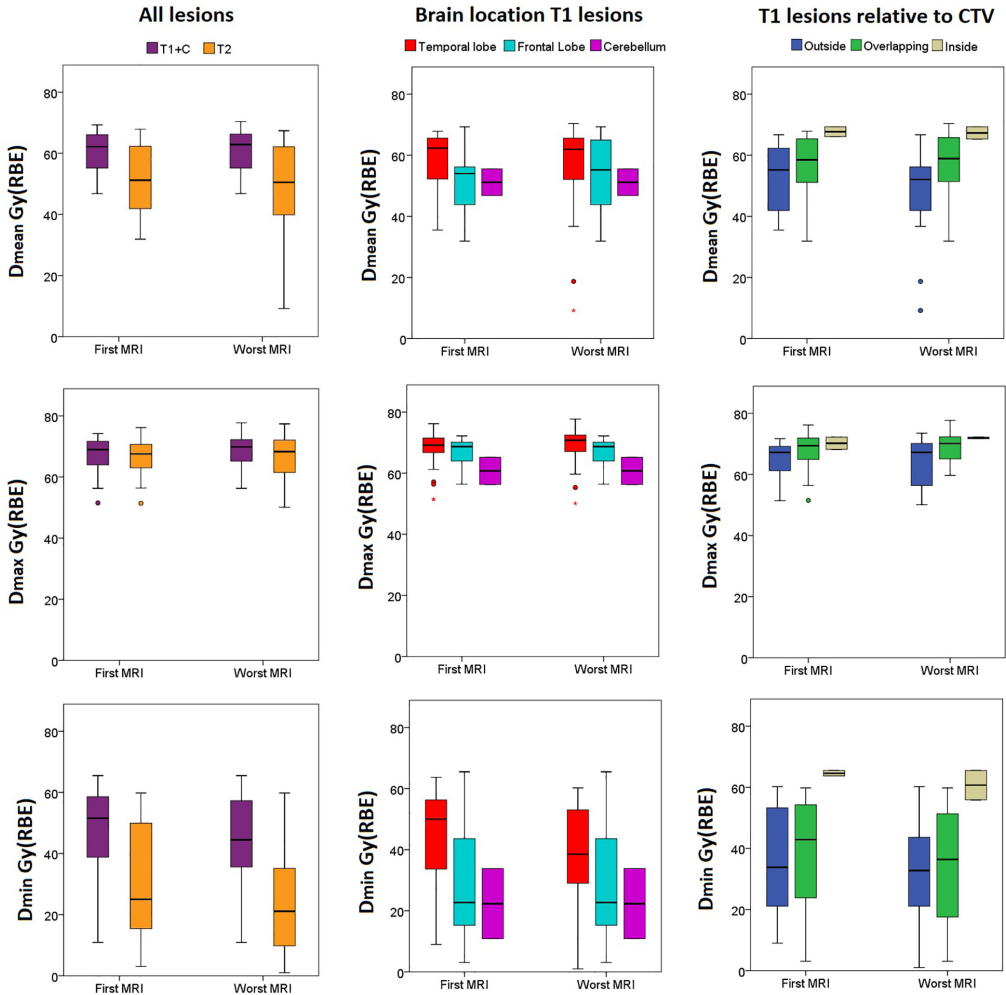
Fig. 1. RAIC lesion doses for all lesions (left column), according to location in the brain (middle column) and location relative to the CTV (right column).

Table 3
Dose volume statistics for those with and without RAIC. Median (Q1–Q3) reported.

	No RAIC (n = 105)	RAIC (n = 22)	p
Dose parameters brain	Median Gy[RBE] (Q1–Q3)		
D_{max}	64.3 (58.6–69.6)	73.1(67.7–75.8)	<.001
$D_{1.0\ cc}$	59.1 (51.4–64.7)	67.0(62.8–72.1)	<.001
$D_{2.0\ cc}$	56.7 (49.8–63.9)	66.2 (58.7–70.5)	<.001
$D_{3.0\ cc}$	54.3 (48.2–64.4)	64.7 (57.9–69.0)	<.001
$D_{4.0\ cc}$	51.9 (46.5–61.5)	63.7 (57.4–67.8)	<.001
$D_{5.0\ cc}$	50.3 (45.3–60.7)	63.0 (56.3–66.7)	<.001
Volume parameters brain	Median cc (Q1–Q3)		
$V_{40\ Gy(RBE)}$	16.3 (7.7–41.4)	40.4 (25.8–63.9)	0.001
$V_{45\ Gy(RBE)}$	10.0 (5.2–31.5)	30.2 (17.3–49.9)	0.001
$V_{50\ Gy(RBE)}$	5.1 (1.8–21.1)	23.7 (10.7–36.2)	<.001
$V_{55\ Gy(RBE)}$	2.7 (0.11–13.6)	14.3 (6.2–25.1)	<.001
$V_{60\ Gy(RBE)}$	0.5 (0–6.9)	9.2 (1.5–16.7)	0.001
$V_{65\ Gy(RBE)}$	0.0 (0.0–0.9)	2.4 (0.4–6.8)	<.001
$V_{70\ Gy(RBE)}$	0.0 (0.0–0.0)	0.14 (0.0–2.7)	<.001

Discussion

In the current study, we characterized the patterns and clinical outcomes of RAIC after PT in a relatively large and heterogeneous cohort of patients with HNCs at the skull base. The crude incidence rate of RAIC in our study was 17.3%, but given the transient nature of observed lesions, the estimated probability of RAIC at 2, 3, and 5-years was 9%, 14%, and 13%, respectively.

In contrast to reported elsewhere, the patients in our study where asymptomatic. There are several possible explanations for our findings in contradistinction to other series. Both higher doses and larger RAIC volumes have been suggested to have an impact on the development of clinical symptoms [1,28,29]. In the current study the median T1w and T2w lesion volumes were 0.5cc and 2.9cc at its worst, whereas lesion volumes reported in other studies were considerable larger. Zhou et al. [12] found mean T1w and T2w lesion volumes of 4.2cc and 21.7cc, and 30% clinical symptoms. Su et al. [6] reported mean T1w and T2w lesion volumes of
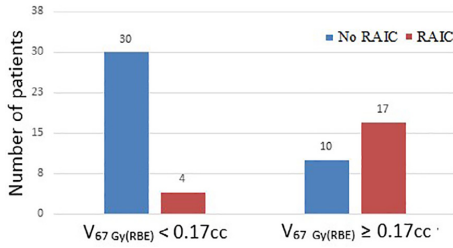
Fig. 2. Results from RPA: 17 out of 27 patients with $V_{67\ Gy(RBE)} \geq 0.17cc$ developed RAIC, whereas 4 out of 30 patients with $V_{67\ Gy(RBE)} < 0.17cc$ developed RAIC.

7.7cc and 21.2cc and 22% clinical symptoms. McDonald et al. [13] found significant difference in the mean and maximum lesion doses between Grade 1 vs. Grade 2 lesions. In the McDonald study the D_{mean} and D_{max} for symptomatic contrast enhancing lesions were 73.0 Gy(RBE) and 82.9 Gy(RBE), respectively, compared to 62.2 Gy(RBE) and 69.0 Gy(RBE) for asymptomatic lesions in the current study. Secondly, asymptomatic RAIC could be considered an early sign of impending symptomatic progression, future development of clinical symptoms in our cohort cannot be ruled out. Thirdly, as no formal assessment of neuro-cognitive function was routinely performed, it is possible that the clinical impact of the lesions and corresponding edema is underestimated.

In RPA all possible combinations of thresholds among the V_D parameters were evaluated and showed that 63% of the patients with $V_{67\ Gy(RBE)} \geq 0.17cc$ developed RAIC; the $V_{67\ Gy(RBE)}$ therefore provides practical and useful reference to support clinical decision making, particularly in difficult cases where higher dose to the brain is unavoidable and where the risk of developing RAIC is high. Our result is in good agreement with the recently published international consensus guideline for NPC, that recommend avoiding $V_{65\ Gy} \geq 0.03cc$ and $V_{70\ Gy} \geq 0.03cc$ for T1–T2 and T3–T4 tumors, respectively [17]. The result agrees reasonable well with the proposed dose constraint from McDonald et al. [13], who identified of $V_{70\ Gy(RBE)} < 1.7cc$ for 15% probability of RAIC using Generalized Estimating Equation modelling of dose response relationship with

RAIC in 66 patients treated with PT. Niyazi et al. [14] used DVH reduction methods when developing a mixture NTCP model for patients with intracranial- and extracranial tumors treated with PT. An a-value of 9 fitted their data best, and they estimated an $EUD_9 = 39.5$ Gy for 50% probability of symptomatic CNS necrosis. It is not possible to directly compare this to our result, however, an a-value of 1 equals the mean dose, while with increasing a-values the high dose area of the DVH curve are more weighted and the calculated EUD gets closer to the near-maximum dose.

An important goal of the current study was to provide a comprehensive overview over the incidence of RAIC in HNC treated with proton therapy. HNC are a heterogeneous patient group with varying dose to the brain, depending on both dose prescription and tumor location; a brain dose threshold as one of the inclusion criteria was therefore considered appropriate. Previous studies have identified V_{40Gy} as one predictor of RAIC and in order to ensure identification of all RAIC events in the cohort, we selected $D_{max} \geq 40$ Gy(RBE) as the minimum cut-off point.

Although all MRI reports and images in the current study were retrospectively reviewed and diagnoses verified, inherent limitations of retrospective review apply. Other limitations in our study exist, including a relatively short follow-up time, as RAIC can develop at a later time point or existing lesions could potentially progress. The MRIs in our study were acquired for standard post treatment surveillance purposes, and T2 flair sequences were not routinely available, thus standard T2w sequences were used for contouring of the brain image changes as T2w edema signal, which can be less accurate than T2 flair. Differences in scanner types and image acquisition protocols inherently influence image quality, sensitivity and specificity and could influence the interpretation of the images. However, as the MRIs were only used for detection and contouring of the brain image changes the uncertainty should therefore be small with simple sequences as T1w and T2w. Further, since the lesions were very small, accuracy of the calculation of the lesion doses may be influenced by uncertainties in the image registration procedure. Finally, our material included a variety of tumor sites treated with both PSPT and IMPT. PSPT generally has a larger irradiated volume, whereas IMPT is conformal, but more sensitive to uncertainties. Although PT technique was not significantly correlated with RAIC development, we cannot rule out that it may influence our results.

Table 4
Results from univariate and multivariate cox regression analysis of clinical and dosimetric variables associations with the development of RAIC.

	Univariate analysis		Multivariate analysis	
	HR (95% CI)	p	HR (95% CI)	p
Age	1.02 (0.99–1.04)	>0.1		
Anatomical site[*]	2.52 (0.99–6.45)	0.054	1.23 (0.41–4.05)	>0.1
T3–T4[**]	1.83 (0.79–4.25)	>0.1	0.44 (0.12–1.66)	>0.1
Surgery	0.56 (0.24–1.30)	>0.1	2.46 (0.41–4.05)	>0.1
Induction chemotherapy	0.67 (0.20–2.28)	>0.1		
Concurrent chemotherapy	2.22 (0.82–6.03)	>0.1	1.99 (0.42–9.33)	>0.1
PT technique[***]	1.06 (0.41–2.72)	>0.1		
Prescribed dose	1.11 (1.01–1.23)	0.035	1.03 (0.88–1.20)	>0.1
D_{max}	1.15 (1.07–1.24)	<0.01	1.06 (0.92–1.21)	>0.1
$D1_{CC}$	1.11 (1.05–1.18)	<0.01		
$D2_{CC}$	1.10 (1.04–1.16)	<0.01		
$D3_{CC}$	1.08 (1.03–1.13)	<0.01		
$D4_{CC}$	1.07 (1.02–1.12)	<0.01		
$D5_{CC}$	1.07 (1.02–1.12)	<0.01		
$V_{40\ GY(RBE)}$	1.01 (0.998–1.02)	0.061	0.99 (0.98–1.01)	>0.1
$V_{50\ GY(RBE)}$	1.01 (0.996–1.03)	0.080		
$V_{60\ GY(RBE)}$	1.01 (0.985–1.04)	>0.1		
$V_{70\ GY(RBE)}$	1.18 (1.03–1.34)	<0.01	1.06 (0.87–1.29)	>0.1
$V_{67\ GY(RBE)} \geq 0.17_{CC}$	7.72 (2.84–21.0)	<0.01	7.41 (1.48–38.76)	0.015

[*] Nasopharyngeal carcinoma/sinonasal vs other.
[**] T3/T4 vs other.
[***] IMPT vs other, HR: Hazard Ratio.

In addition, the study could also have limited power to define dose–volume constraints since our cohort was too small to split into a training and a validation set for RPA. Therefore, our results should be externally validated.

We investigated RAIC in a heterogeneous cohort of skull base HNC and found that 17.3% developed RAIC, the majority of these occurred in nasopharyngeal or sinonasal cancers. The lesions were small and asymptomatic, resolved in 27% of the patients and progressed in 18% of the patients. The estimated dose–volume correlations identified in our study were in agreement with previous studies and confirm the importance of minimizing focal high doses to brain when achievable.

Conflict of Interest

None.

Appendix A. Supplementary data

Supplementary data to this article can be found online at https://doi.org/10.1016/j.radonc.2020.07.008.

References

[1] Lawrence YR, Li XA, el Naqa I, Hahn CA, Marks LB, Merchant TE, et al. Radiation dose-volume effects in the brain. Int J Radiat Oncol Biol Phys 2010;76(3 Suppl): S20–7.
[2] Feng M, Huang Y, Fan X, Xu P, Lang J, Wang D. Prognostic variables for temporal lobe injury after intensity modulated-radiotherapy of nasopharyngeal carcinoma. Cancer Med 2018;7:557–64.
[3] Huang J, Kong FF, Oei RW, Zhai RP, Hu CS, Ying HM. Dosimetric predictors of temporal lobe injury after intensity-modulated radiotherapy for T4 nasopharyngeal carcinoma: a competing risk study. Radiat Oncol 2019;14:31.
[4] Kong C, Zhu XZ, Lee TF, Feng PB, Xu JH, Qian PD, et al. LASSO-based NTCP model for radiation-induced temporal lobe injury developing after intensity-modulated radiotherapy of nasopharyngeal carcinoma. Sci Rep 2016;6:26378.
[5] Su SF, Huang SM, Han F, Huang Y, Chen CY, Xiao WW, et al. Analysis of dosimetric factors associated with temporal lobe necrosis (TLN) in patients with nasopharyngeal carcinoma (NPC) after intensity modulated radiotherapy. Radiat Oncol 2013;8:17.
[6] Su SF, Huang Y, Xiao WW, Huang SM, Han F, Xie CM, et al. Clinical and dosimetric characteristics of temporal lobe injury following intensity modulated radiotherapy of nasopharyngeal carcinoma. Radiother Oncol 2012;104:312–6.
[7] Sun Y, Zhou GQ, Qi ZY, Zhang L, Huang SM, Liu LZ, et al. Radiation-induced temporal lobe injury after intensity modulated radiotherapy in nasopharyngeal carcinoma patients: a dose-volume-outcome analysis. BMC Cancer 2013;13:397.
[8] Takiar V, Ma D, Garden AS, Li J, Rosenthal DI, Beadle BM, et al. Disease control and toxicity outcomes for T4 carcinoma of the nasopharynx treated with intensity-modulated radiotherapy. Head Neck 2016;38(Suppl 1):E925–33.
[9] Wang J, Miao Y, Ou X, Wang X, He X, Shen C, et al. Development and validation of a model for temporal lobe necrosis for nasopharyngeal carcinoma patients with intensity modulated radiation therapy. Radiat Oncol 2019;14:42.
[10] Zeng L, Huang SM, Tian YM, Sun XM, Han F, Lu TX, et al. Normal tissue complication probability model for radiation-induced temporal lobe injury after intensity-modulated radiation therapy for nasopharyngeal carcinoma. Radiology 2015;276:243–9.
[11] Zhou GQ, Yu XL, Chen M, Guo R, Lei Y, Sun Y, et al. Radiation-induced temporal lobe injury for nasopharyngeal carcinoma: a comparison of intensity-modulated radiotherapy and conventional two-dimensional radiotherapy. PLoS One 2013;8:e67488.
[12] Zhou X, Ou X, Xu T, Wang X, Shen C, Ding J, et al. Effect of dosimetric factors on occurrence and volume of temporal lobe necrosis following intensity modulated radiation therapy for nasopharyngeal carcinoma: a case-control study. Int J Radiat Oncol Biol Phys 2014;90:261–9.
[13] McDonald MW, Linton OR, Calley CS. Dose-volume relationships associated with temporal lobe radiation necrosis after skull base proton beam therapy. Int J Radiat Oncol Biol Phys 2015;91:261–7.
[14] Niyazi M, Niemierko A, Paganetti H, Sohn M, Schapira E, Goldberg S, et al. Volumetric and actuarial analysis of brain necrosis in proton therapy using a novel mixture cure model. Radiother Oncol 2020;142:154–61.
[15] Dagan R, Bryant C, Li Z, Yeung D, Justice J, Dziegielewski P, et al. Outcomes of sinonasal cancer treated with proton therapy. Int J Radiat Oncol Biol Phys 2016;95:377–85.
[16] Pehlivan B, Ares C, Lomax AJ, Stadelmann O, Goitein G, Timmermann B, et al. Temporal lobe toxicity analysis after proton radiation therapy for skull base tumors. Int J Radiat Oncol Biol Phys 2012;83:1432–40.
[17] Lee AW, Ng WT, Pan JJ, Chiang CL, Poh SS, Choi HC, et al. International guideline on dose prioritization and acceptance criteria in radiation therapy planning for nasopharyngeal carcinoma. Int J Radiat Oncol Biol Phys 2019;105:567–80.
[18] International Commission on Radiation Units and Measurements. Report 78: prescribing, recording and reporting proton-beam therapy. Oxford: International Commission on Radiation Units and Measurements; 2007.
[19] Shah R, Vattoth S, Jacob R, Manzil FF, O'Malley JP, Borghei P, et al. Radiation necrosis in the brain: imaging features and differentiation from tumor recurrence. Radiographics 2012;32:1343–59.
[20] NCI Common Terminology Criteria for Adverse Events (CTCAE): National Cancer Institute 2010 [Available from: https://evs.nci.nih.gov/ftp1/CTCAE/CTCAE_4.03/CTCAE_4.03_2010-06-14_QuickReference_5x7.pdf.
[21] Wang YX, King AD, Zhou H, Leung SF, Abrigo J, Chan YL, et al. Evolution of radiation-induced brain injury: MR imaging-based study. Radiology 2010;254:210–8.
[22] Aalen OO, Johansen S. An empirical transition matrix for non-homogeneous Markov chains based on censored observations. Scand J Stat 1978;5:141–50.
[23] Datta S, Satten GA. Validity of the Aalen-Johansen estimators of stage occupation probabilities and Nelson-Aalen estimators of integrated transition hazards for non-Markov models. Stat Prob Lett 2001;55:403–11.
[24] Therneau T, Grambsch PM. Modeling survival data: extending the Cox model. New York: Springer; 2000.
[25] Therneau T. A package for survival analysis in R. version 2.38 2015 [Available from: https://CRAN.R-project.org/package=survival].
[26] Kuhn M. caret: Classification and regression training. R package version 6.0-84 2019 [Available from: https://CRAN.R-project.org/package=caret].
[27] Therneau T, Atkinson, B. rpart: Recursive Partitioning and Regression Trees. R package version 4.1-15 2019 [Available from: https://CRAN.R-project.org/package=rpart].
[28] Rahmathulla G, Marko NF, Weil RJ. Cerebral radiation necrosis: a review of the pathobiology, diagnosis and management considerations. J Clin Neurosci 2013;20:485–502.
[29] Cheung MC, Chan AS, Law SC, Chan JH, Tse VK. Impact of radionecrosis on cognitive dysfunction in patients after radiotherapy for nasopharyngeal carcinoma. Cancer 2003;97:2019–26.

Supplementary material

Table I: Grading of central nervous system necrosis according to the National Cancer Institute Common Toxicity Criteria for Adverse Events (CTCAE) v4.03.

Grade 1	Grade 2	Grade 3	Grade 4	Grade 5
Asymptomatic; clinical or diagnostic observations only; intervention not indicated	Moderate symptoms; corticosteroids indicated	Severe symptoms; medical intervention indicated	Life-threatening consequences; urgent intervention indicated	Death

Figure 1: Evolution of RAIC: Male (54 years) with nasopharyngeal cancer, treated with PT and concurrent chemotherapy. 19 months after treatment the patient was diagnosed with bilateral temporal lobe RAIC. The post contrast T1 and T2 weighted MRIs are displayed on top and middle row, respectively. Image a) demonstrates bilateral contrast enhanced temporal lobe lesions on the post contrast T1 weighted MRI, and increased signal intensities on the corresponding T2 sequence (d). b): MRI two months later shows decrease in size on the contrast enhanced lesion in the right temporal lobe and increase in size and enhancement in the left temporal lobe. The area with hyperintensities on the T2 weighted MRIs has correspondingly decreased and increased in volume (e). c) and f): MRI 33 months after diagnosis of RAIC: RAIC lesions have resolved spontaneously without medical intervention. Bottom row: IMPT dose distribution displayed in representative axial (g), coronal (h) sagittal views (i). CTV 1 (70 Gy[RBE]) and CTV 2 (63 Gy[RBE]), CTV 3 (57 Gy[RBE]) shown in orange, blue and yellow, respectively; T1w lesion is contoured in magenta and T2w lesion in cyan.
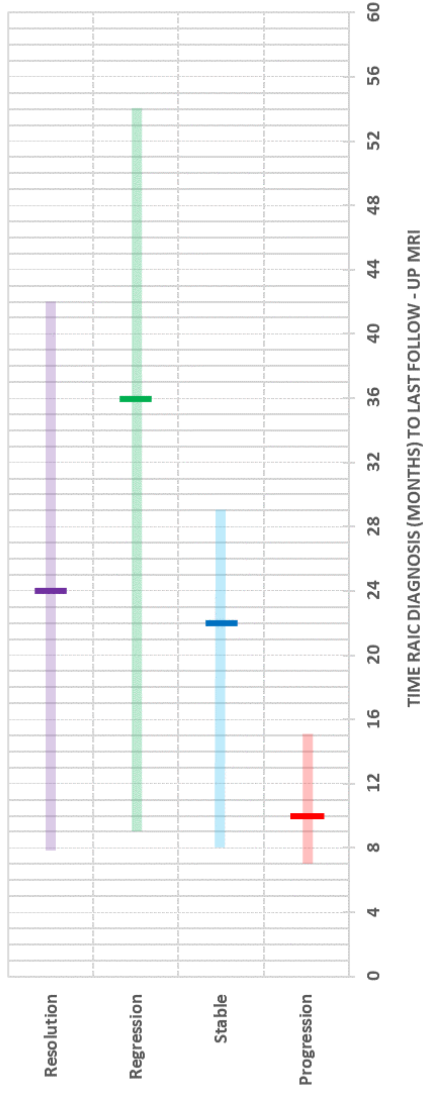
Figure 2: Time from diagnosis to different RAIC states at last follow-up MRI. Median (vertical lines) and range (horizontal bars) displayed.
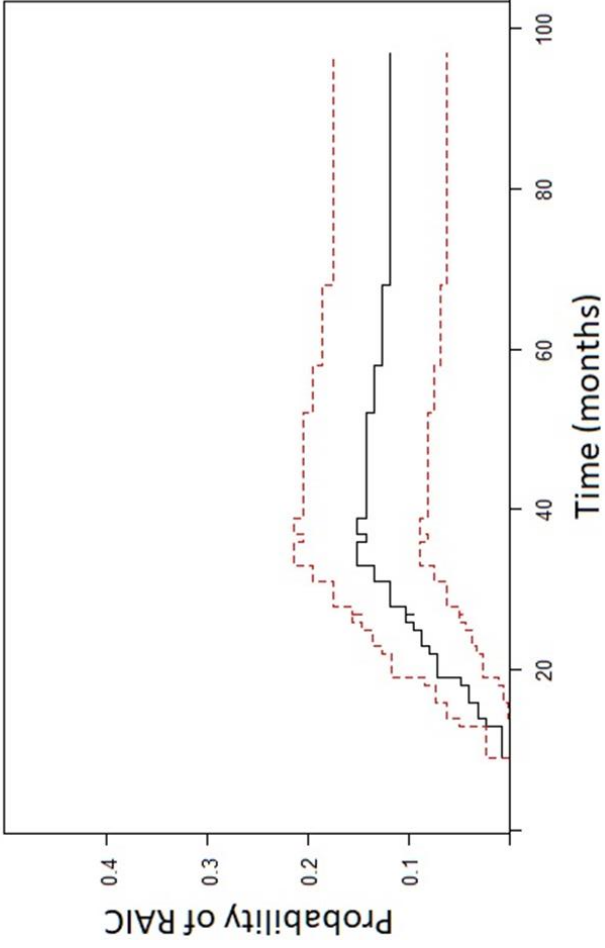
Figure 3: The probability of having RAIC over time (black solid line) including 95% confidence intervals (red dotted lines).

Table II: Anatomical, tumor and treatment characteristics of the patients with RAIC.

Patient	Site/ Histology	T-stage	Resection	PT setting	Chemo	Dose (fx)	Cranial/proximal disease extent	CTCAE
1	BOS / Ameloblastoma	rT4	R1	postop PT	No	66 (30)	Dura, carotid canal, cavernous sinus	G1
2	Nasopharynx / ACC	T4	R3	def PT (unresectable)	CC	70 (33)	Cavernous sinus, dura	G1
3	Nasopharynx / ACC	T4	R3	def PT (unresectable)	CC	70 (33)	Cavernous sinus, dura	G1
4	Vagus nerve / Schwannoma	-	R3	def PT (unresectable)	No	54 (27)	Cerebellar cistern	G1
5	Nasopharynx /NPC	T1	R3	def PT	CC	70 (33)	Base of skull/sphenoid sinus	G1
6	Nasopharynx /NPC	T1	R3	def PT	IC/CC	70 (33)	Base of skull/sphenoid sinus	G3*
7	Lacrimal gland /ACC	T4	R1	postop PT	CC	64 (32)	Orbital apex	G1
8	Paranasal sinus/ ACC	T4	R1	postop PT	CC	66 (30)	Cavernous sinus, sphenoid sinus	G1
9	Nasopharynx/NPC	T4	R3	def PT	IC/CC	70 (33)	Cavernous sinus	G1
10	Paranasal sinus / Esthesioneuroblastoma	rT4	R0	postop PT	No	60 (30)	Cribriform plate, dura	G1
11	Paranasal sinus /ACC	T4	R2	def PT (unresectable)	CC	70 (33)	Cavernous sinus, clivus, ethmoid sinus	G1
12	Periorbital / ACC	T2	R0	postop PT	CC	60 (30)	Cavernous sinus, orbital apex	G1
13	Maxillary sinus /ACC	T4	R3	def PT (unresectable)	CC	70 (33)	Cavernous sinus	G1
14	Paranasal sinus / Esthesioneuroblastoma	rT2	R0	postop PT	No	60 (30)	Dura	G1
15	Nasopharynx / ACC	T4	R3	def PT (unresectable)	CC	70 (33)	Cavernous sinus, sphenoid sinus	G1
16	Nasopharynx / ACC	T4	R2	postop PT	CC	70 (33)	Carotid canal	G3**
17	Palate / Adenosquamous	T4	R3	def PT (unresectable)	CC	70 (33)	Cavernous sinus	G1
18	Skin/SCC	T4	R3	postop PT	CC	70 (33)	Foramen ovale	G1
19	Paranasal sinus / Esthesioneuroblastoma	T3	R0	postop PT	CC	70 (35)	Dura	G3***
20	Nasopharynx / ACC	T4	R3	def PT (unresectable)	CC	70 (33)	Sphenoid sinus, carotid canal, clivus nasoethmoid, anterior skull base,	G1
21	Nasal cavity / SCC	rT3	-	def PT (unresectable)	CC	68 (34)	Frontal bone	G1
22	Nasal cavity / Adenocarcinoma	T2	R0	postop PT	No	60 (30)	Cribriform plate	G1

Treatment: def: definitive, CC: concurrent chemotherapy, IC: induction chemotherapy, Dose: Gy(RBE), fx: fractions, * Bevacizumab, ** Dexamethasone, pentoxifylline, vitamin E, *** pentoxifylline, vitamin E. ACC: adenoid cystic carcinoma, SCC: squamous cell carcinoma, NPC: nasopharyngeal carcinoma

Table III: Summary statistics for all T1 and T2 lesion. Median (Q1-Q3) values reported. Dose in Gy(RBE) and volume in CC.

First MRI	Volume	D_{mean}	D_{max}	D_{min}
T1 lesion	0.3 (0.1-0.6)	62.2 (55.2-66.2)	69.0 (63.8-71.7)	51.6 (38.2-58.8)
T2 lesion	1.0 (0.4-2.8)	51.2 (41.9-62.3)	67.6 (62.1-70.9)	25.0 (15.4-50.0)
Worst MRI	**Volume**	**D_{mean}**	**D_{max}**	**D_{min}**
T1 lesion	0.5 (0.2-1.0)	62.9 (54.5-66.4)	69.9 (64.9-71.9)	44.5 (35.2-57.6)
T2 lesion	2.9 (0.6-9.4)	50.5 (38.8-62.2)	68.3 (61.3-72.2)	21.1 (9.7-36.3)

Table IV: Summary statistics by location of T1 and T2 lesion at first MRI. Median volume and dose statistics for all lesion and according to location relative to CTV. Median (Q1-Q3) values reported. Dose in Gy(RBE), volume in cc.

Location T1 lesion relative to CTV	Volume	D_{mean}	D_{max}	D_{min}
First MRI				
Inside	0.2 (-)	67.7 (-)	70.2 (-)	64.6 (-)
Overlapping	0.4 (0.1-0.8)	61.9 (53.5-66.0)	68.7 (62.8-72.6)	50.4 (37.6-57.7)
Outside	0.2 (0.1-0.7)	56.2 (55.2-64.7)	69.2 (63.2-70.5)	49.6 (33.8-57.7)
Worst MRI				
Inside	0.3 (-)	67.3 (-)	72.0 (-)	60.7 (-)
Overlapping	0.5 (0.3-1.4)	63.8 (55.7-67.0)	69.6 (64.6-73.2)	45.4 (36.0-58.0)
Outside	0.7 (0.1-0.8)	55.2 (52.1-64.7)	69.2 (61.8-70.8)	39.4 (23.8-57.3)
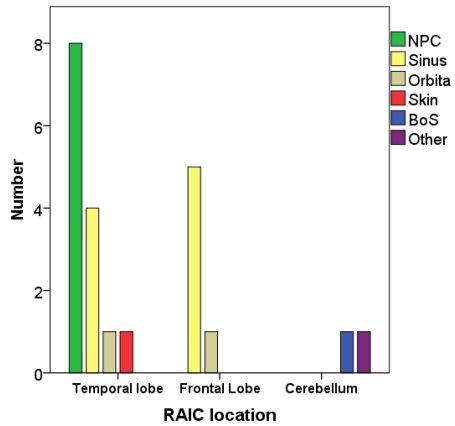
Figure 4: Location of RAIC according to initial disease site.

Table V: Model performance statistics.

Confusion matrix final model		
Observed /predicted	No	Yes
No	49.1%	16.4%
Yes	6.6%	27.9%
Bootstrapped confusion matrix		
Observed /predicted	No	Yes
No	47.6%	16.0%
Yes	17.7%	18.7%
Performance statistics		
	Final model	Bootstrapped
Accuracy	0.770	0.663
AUC	0.780	0.649
Sensitivity	0.875	0.736
Specificity	0.636	0.560

Impact of RBE variations on risk estimates of temporal lobe necrosis in patients treated with intensity-modulated proton therapy for head and neck cancer

Grete May Engeseth, Liv Bolstad Hysing, Pablo Yepes, Helge Egil Seime Pettersen, Radhe Mohan, Clifton Dave Fuller, Camilla Hanquist Stokkevåg, Richard Wu, Xiaodong Zhang, Steven Jay Frank & Gary Brandon Gunn

Physics Contribution

Mixed Effect Modeling of Dose and Linear Energy Transfer Correlations With Brain Image Changes After Intensity Modulated Proton Therapy for Skull Base Head and Neck Cancer

Grete May Engeseth, MSc,*,†,‡ Renjie He, PhD,* Dragan Mirkovic, PhD,§
Pablo Yepes, PhD,‖ Abdallah Sherif Radwan Mohamed, MD, MSc,*
Sonja Stieb, MD,* Clifton Dave Fuller, PhD,* Richard Wu, MSc,*
Xiadong Zhang, PhD,* Liv Bolstad Hysing, PhD,†,#
Helge Egil Seime Pettersen, PhD,† Camilla Hanquist Stokkevåg, PhD,†,#
Radhe Mohan, PhD,§ Steven Jay Frank, MD,* and
Gary Brandon Gunn, MD*

*The University of Texas MD Anderson Cancer Center, Department of Radiation Oncology, Houston,
Texas; †Haukeland University Hospital, Department of Oncology and Medical Physics, Bergen, Norway;
‡The University of Bergen, Department of Clinical Science, Bergen, Norway; §The University of Texas
MD Anderson Cancer Center, Department of Radiation Physics, Houston, Texas; ‖Rice University,
Physics and Astronomy Department, Houston, Texas; and #The University of Bergen, Department of
Physics and Technology, Bergen, Norway

Purpose: Intensity modulated proton therapy (IMPT) could yield high linear energy transfer (LET) in critical structures and increased biological effect. For head and neck cancers at the skull base this could potentially result in radiation-associated

brain image change (RAIC). The purpose of the current study was to investigate voxel-wise dose and LET correlations with RAIC after IMPT.

Methods and Materials: For 15 patients with RAIC after IMPT, contrast enhancement observed on T1-weighted magnetic resonance imaging was contoured and coregistered to the planning computed tomography. Monte Carlo calculated dose and dose-averaged LET (LET_d) distributions were extracted at voxel level and associations with RAIC were modelled using uni- and multivariate mixed effect logistic regression. Model performance was evaluated using the area under the receiver operating characteristic curve and precision-recall curve.

Results: An overall statistically significant RAIC association with dose and LET_d was found in both the uni- and multivariate analysis. Patient heterogeneity was considerable, with standard deviation of the random effects of 1.81 (1.30-2.72) for dose and 2.68 (1.93-4.93) for LET_d, respectively. Area under the receiver operating characteristic curve was 0.93 and 0.95 for the univariate dose-response model and multivariate model, respectively. Analysis of the LET_d effect demonstrated increased risk of RAIC with increasing LET_d for the majority of patients. Estimated probability of RAIC with $LET_d = 1$ keV/μm was 4% (95% confidence interval, 0%, 0.44%) and 29% (95% confidence interval, 0.01%, 0.92%) for 60 and 70 Gy, respectively. The TD_{15} were estimated to be 63.6 and 50.1 Gy with LET_d equal to 2 and 5 keV/μm, respectively.

Conclusions: Our results suggest that the LET_d effect could be of clinical significance for some patients; LET_d assessment in clinical treatment plans should therefore be taken into consideration. © 2021 The Author(s). Published by Elsevier Inc. This is an open access article under the CC BY license (http://creativecommons.org/licenses/by/4.0/)

Introduction

The main rationale for using intensity modulated proton therapy (IMPT) in the treatment of head and neck cancers (HNC) is the ability to create highly conformal treatment plans with reduced normal tissue doses and potentially lower complication rates compared with photon therapy.[1] Protons are considered to be more biologically effective than photons. In proton treatment planning and delivery this is accounted for by using a fixed value of 1.1 for the proton relative biological effectiveness (RBE).[2] However, the RBE of protons is not constant; it varies depending on a complex combination of dose, clinical endpoint, tissue α/β, and the linear energy transfer (LET).[3-5] An approximately linear increase in RBE with increasing LET (keV/μm) has been shown for dose- and energy ranges relevant for clinical use.[5] As LET increases with increasing depth, its maximum is at the end of the proton range, typically close to the clinical target volume (CTV) border. Further, IMPT treatment planning studies have reported elevated LET and increased biological dose in organs at risk (OAR) in close proximity to the CTV.[6] Questions are therefore raised whether increased RBE in OAR adjacent to the CTV could lead to radiation-associated normal tissue injury with subsequent development of adverse effect.

The clinical evidence of a causal effect of LET with radiation-associated side effects is limited and inconclusive. Based on voxel-level analysis of posttreatment imaging data, a few studies have reported correlations between LET and regions of radiation associated brain image change (RAIC) in pediatric and adult patients treated with proton therapy.[7-9] In contrast, no such correlation was found in a recent study including 50 patients treated with passive scattering proton therapy (PSPT), where several different methods were used to investigate LET and RAIC associations.[10]

As HNC near the skull base often consists of complex target volumes surrounded by dose-limiting critical organs, highly modulated proton beams with steep dose gradients are required to create optimal treatment plans. This may potentially lead to high LET and increased biological effect in critical structures compared with what is indicated by the fixed RBE weighted dose distribution.[6,11] Moreover, our group recently characterized a cohort of patients with skull base HNC with RAIC events after treatment with proton therapy.[12] These lesions were overlapping or located just outside the CTV border, indicating a potential increased biological effectiveness of protons due to elevated LET in the dose fall-off area. Therefore, the purpose of the current study was to explore dose and LET correlations with RAIC in a subgroup of patients treated with IMPT for skull base HNC.

Methods and Materials

Patients and treatment

The study cohort included 15 patients with HNC at the skull base who had been diagnosed with RAIC after IMPT. These 15 patients were identified after review of available magnetic resonance (MR) reports and images for development of RAIC in 85 patients previously treated with IMPT at our center between December 2010 and June 2018. All patients were participants in 1 of 2 prospective clinical trials (ClinicalTrials.org identifiers: NCT 00991094 and NCT 01627093) and had provided study-specific written informed consent.

The patients' treatment plans had been generated in the Eclipse Treatment planning system (Varian Medical Systems, Palo Alto, CA). Treatment planning was based on non-contrast CT images acquired with the patient in supine position and immobilized with a posterior customized mold and thermoplastic mask. CTV definitions had been manually performed and peer-reviewed before treatment planning. The typical beam arrangements consisted of multiple beams with large angular separation to spread out the

placement of potential high-LET and with the majority of patients being treated with 1 posterior and 2 left and right anterior oblique beams (Fig. E1). Each treatment plan used a simultaneous integrated boost technique and was individually optimized to obtain optimal CTV coverage while minimizing dose to surrounding normal tissues.

RAIC definition, image registration, and Monte Carlo simulations

RAICs had initially been assessed on posttreatment surveillance MRIs, which were routinely acquired every 3 to 4 months during the first 2 years after treatment completion, then every 6 months until 5 years, and annually thereafter. The MRI findings defined as RAIC included gadolinium contrast-enhanced brain lesions on T1-weighted ($T1_w$) sequences, accompanied by increased signal intensity/edema and/or cysts on T2-weighted ($T2_w$) sequences.[13] Retrospectively, a second review with verification of the RAIC diagnosis was performed by 2 board-certified radiation oncologists (GBG and SJF). Both the radiologists and the oncologists were blinded to the dose and LET distributions and were not involved in the further statistical analysis and modeling of the dose and LET correlations with RAIC. In a typical RAIC evolution, the initial phase is often followed by progression of the lesion.[14] The majority of the patients had several consecutive MRIs after RAIC diagnosis with lesions of varying (increasing/decreasing) size; for the current analysis we considered the contrast enhanced lesions from the earliest $T1_w$ MRI with observed RAIC to be the most appropriate surrogate for the origin of the radiation associated injury. The earliest MRI with RAIC and the treatment planning CTs were automatically registered (rigid), and the result of the image registration was evaluated by visual inspection and manually modified if deemed necessary. Figure E1 shows an example of a contrast enhanced lesion visible on the $T1_w$ MRI sequence and the contoured lesion propagated on the treatment planning CT with the 40 to 70 Gy(RBE) isodose lines overlaid.

For characterization of the proton beam quality either the full LET spectrum or an average LET at each point could be used. The LET average is typically calculated using either the arithmetic mean of the LET fluence spectrum (track averaged [LET_t]) or by weighting the LET by the dose it deposits in each point(dose averaged LET [LET_d]).[15] For therapeutic proton beams, LET_d is considered to be more appropriate than LET_t.[5,16] To obtain accurate dose and LET distributions for the brain tissue and the RAIC lesions, the treatment plans were recalculated using an in-house developed Monte Carlo system: the Fast Dose Calculator (FDC). The FDC is a track-repeating algorithm for proton therapy, validated for scanning beams.[17-19] The FDC algorithm calculates the dose and unrestricted LET_d based on the patient's treatment plan and the assigned planning CT. The LET_d includes primary and secondary protons and is computed using a step-by-step approach previously described

by Cortes-Giraldo and Carabe,[20] where LET_d is calculated from pregenerated tables of stopping power obtained from GEANT4.[21] The resulting Monte Carlo doses and LET_d distributions were extracted at the voxel level for each patient, whereupon each voxel within a contoured lesion was defined as one single RAIC event (ie, binary response value = 1), with the voxels outside the lesions (in the brain tissue) defined as nonevents (ie, binary response value = 0).

Modeling and risk estimation

The data material consisted of multiple voxels from each patient, including the voxel-wise associated dose, LET_d, and binary response values. Because the data were clustered within patients, mixed effect logistic regression was used to investigate the association between RAIC, dose, and LET_d.[22-24] In contrast to a standard logistic regression model, mixed effect logistic regression takes into account patient heterogeneity and the within-patient correlation of the data. It allows for variation of the model intercept and/or predictor coefficients and provides estimates of the effects that are constant across the patients (fixed effects) as well as the effects that vary across patients (random effects). The main predictors in the current models were the physical dose and the LET_d, and we assumed that the effect of these predictors varied between the patients. Therefore, the univariate and multivariate analyses were performed with estimation of the fixed and random effects of both dose and LET_d. In addition to dose and LET_d we included an interaction term (LET_d:dose) in the multivariate model. Interaction terms can be applied during modeling to investigate whether a predictor has a different effect on the outcome depending on the value of another predictor. Because the scale of LET_d and dose differ, Z-standardization of the predictor variables was performed before modeling (mean = 0, standard deviation = 1).

Model fits were evaluated using the Akaike information criterion (AIC), log likelihood, pseudo R^2, and Brier score. The models' ability to discriminate between voxels with and without RAIC was evaluated using the receiver operating characteristic (ROC) curve and the calculated C-index (area under the curve [AUROC]). As an additional discriminative measure, we generated precision-recall (PR) curves, as they are an appropriate and useful supplement to ROC curves for evaluating performance in imbalanced data sets with rare events and where the minority class is of interest, as with the current study.[25] Both ROC curves and PR curves are model-wide evaluations; for a range of different probability thresholds, the ROC curves plot the trade-offs between the true positive rate versus the false positive rate, whereas the PR curves plot the precisian versus the recall.

Cluster bootstrapping was used for internal model validation. The cluster bootstrapping procedure involves resampling of patients with replacement, rather than resampling of individual observations. This resampling strategy has been proven superior over both resampling of individual observations and a 2-level successive resampling of patients

and observations.[26] For the current analysis this implied that patients (including all the voxels from each of the selected patients) were resampled with replacement (number of samples = 1000), whereupon the model was fit on each of the bootstrap samples and performance measures extracted. The modeling was performed in R, version 3.6.0[27], using the *glmer* function from the *lme4* library.[28]

Results

The patient characteristics are presented in Table 1. All patients had skull base and/or intracranial involvement with typical disease extent to sphenoid sinus, cavernous sinus, and dura. Thirteen (86.7%) lesions were in the temporal lobe(s) and 2 (13.3%) in the frontal lobe. The median (range) lesion volume was 0.2 cm^3 (0.1-1.1 cm^3). Ten of the patients had lesion volumes less than 0.3 cm^3. The number of voxels in the lesions ranged between 195 and 5365, whereas the number of voxels in the irradiated brain area ranged between 6157 and 49,238. The proportion of voxels with RAIC in the total data set was 6%. The median (range) LET_{mean} and D_{mean} (RBE = 1.1) in the lesions were 3.61 keV/μm (2.82-5.59 keV/μm) and 63.5 Gy(RBE) (42.2-69.0 Gy[RBE]), respectively. The highest LET_d value in a lesion was 8.04 keV/μm and the highest LET_d value in the brain tissue was 10.69 keV/μm. An example of dose and LET_d distribution including RAIC and CTV contours is displayed in Figure 1.

Table 1 Patient characteristics (15 patients)

Characteristics	No. (%) or median (range)
Female sex	8 (53.3)
Age	53 (24-71)
Disease site	
Nasopharynx	8 (53.3)
Sinonasal	5 (33.3)
Other	2 (13.3)
T category	
T1-T2	3 (20)
T3-T4	10 (66.7)
Recurrent	2 (13.3)
Unresectable disease	7 (46.6)
Chemotherapy	14 (93.3)
CTV 1 volume (cm^3)*	110.6 (25.5-340.0)
CTV 2 volume (cm^3)†	194.0 (3.0-484.0)
Number of beams	3 (2-5)
Prescribed dose (Gy[RBE])	70 (60-70)
Number of fractions	33 (30-33)
Fraction dose (Gy[RBE])	2.12 (2.0-2.20)
Time to RAIC (months)	19 (9-33)

Abbreviations: CTV = clinical target volume; RAIC = radiation-associated brain image change; RBE = relative biological effectiveness.

  * Prescribed dose: 63-70 Gy(RBE).

  † Prescribed dose: 57-63 Gy(RBE).Other: orbital and skin.

The fixed effects represent the overall (constant) effect of the predictors on RAIC. There was a positive and statistically significant correlation between RAIC and dose, as well as between RAIC and LET_d in both the univariate and multivariate models (Table 2). We further found a small but significant interaction between LET_d and dose; that is, as dose increases, the effect of LET_d decreases and vice versa. As shown by the negative coefficient sign, the combined effect of dose and LET_d was therefore less than the sum of the individual effects. The conditional effects of LET_d and dose are illustrated in Figure E2. Based on the multivariate model we generated probability curves for several LET_d values and dose levels (Fig. 2a,b). The corresponding surface plot of the model is displayed in Figure 2c. The TD_{15} (the dose for 15% probability of RAIC) were estimated to be 63.6 and 50.1 Gy with LET_d equal to 2 and 5 keV/μm, respectively (Fig. 2a). A rapid increase in RAIC risk could be observed when doses exceeded 60 Gy even for lower LET_d values; for LET equal to 1 keV/μm the estimated risk of RAIC was 4% (95% confidence interval [CI], 0%-0.44%) at 60 Gy versus 29% (95% CI, 0.01%-0.92%) at 70 Gy (Fig. 2b).

The random effects are associated with patient heterogeneity. The intraclass correlation (ICC) was 0.77. The standard deviations (95% CI) of the random effects were 1.81 (1.30-2.72) for dose and 2.68 (1.93-4.93) for LET_d. The interpatient variation is illustrated in Figure 3, where the risk estimates are plotted as a function of dose and LET_d and with individual trend lines generated for each of the patients. A distinct difference between dose and LET_d could be observed; although the effect of the dose was moderate for some patients, there was still a clear trend of increasing risk with increasing dose (Fig. 3a). For LET_d, on the other hand, the trend was less consistent, with a positive LET_d effect for the majority of the patients; however, with a negative LET_d effect for 3 of the patients (Fig. 3b). Besides an overall lower LET_d in the RAIC regions compared with the rest of the brain tissue in these 3 patients, our analysis revealed nothing specific regarding number of beams (2-3), beam arrangements, dose distribution, CTV location, or disease extent that could explain this finding. The interpatient variation resulted in large uncertainties in RAIC predictions. The probability curves with 95% prediction interval are displayed in Figure E3.

Model fit and performance measures are displayed in Table 2. The AUROC and the area under the precision recall curve (AUPRC) were 0.85 and 0.33 for the univariate model with LET_d as predictor, and 0.93 and 0.54 for the univariate model with dose as predictor, respectively. The performance of the multivariate model was slightly improved with an AUROC and AUPRC of 0.95 and 0.59, respectively (Fig. 4). Cluster bootstrapping was used for internal validation of the multivariate model. The mean AUROC from the cluster bootstrap procedure was 0.95 (95% CI, 0.92-0.97), whereas the mean AUPRC was 0.58 (95% CI, 0.41-0.71).

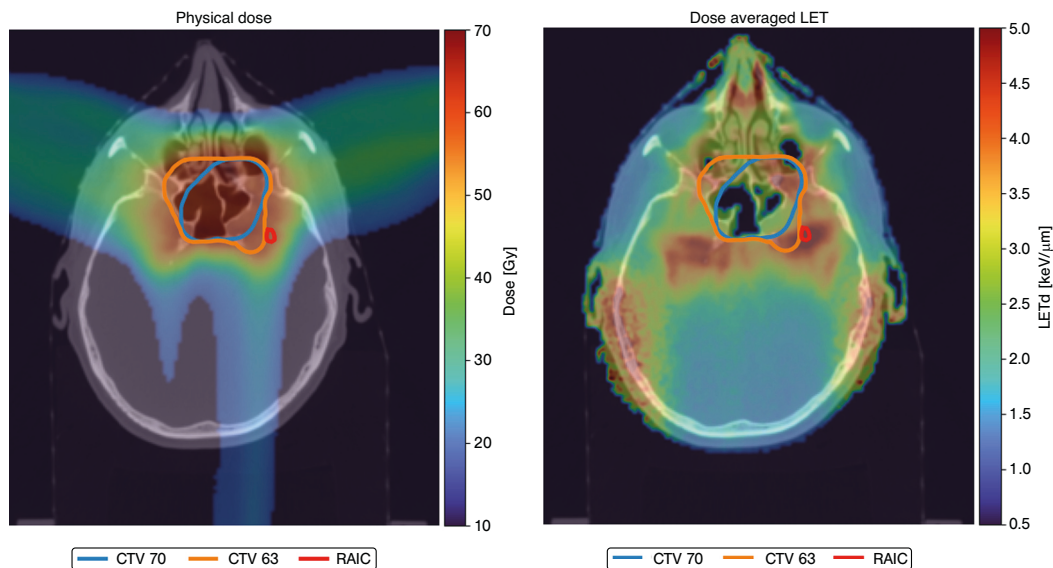We further performed a subgroup analysis to investigate dose and LET_d correlations with RAIC when all

Fig. 1. Example of dose distribution (physical dose) to the left and the dose-averaged linear energy transfer (LET$_d$) distribution to the right. The high LET$_d$ in low-dose regions laterally are due to secondary radiation. Radiation-associated brain image change (RAIC) (red contour): the contoured contrast enhanced lesion from the T1 weighted magnetic resonance imaging (MRI).

voxels with doses below 40 Gy were removed from the data set. The results from this analysis were consistent with the main analysis, with significant associations with dose and LET$_d$ in both the uni- and multivariate analysis, and a significant interaction between LET$_d$ and dose. Compared with the main model, the AUROCs were slightly reduced to 0.84 for both the univariate models and to 0.90 for the multivariate model. The parameter estimates from the analysis are displayed in Table E1 with ROC and PR curves in Figure E4.

Discussion

In the current study, dose and LET$_d$ associations with RAIC in patients treated with IMPT for HNC at the skull base were explored using voxel-level data and mixed effect logistic regression modeling. Our result demonstrated positive and significant dose and LET$_d$ associations with RAIC in all models and a slightly improved ability to discriminate between voxels with and without RAIC when LET$_d$ was included as predictor. We further found that the effect of

Table 2   Parameter estimates (95% confidence intervals in parenthesis) for the univariate and multivariate models including model fit and performance measures

Variables	Univariate model (LET$_d$)	Univariate model (dose)	Multivariate model
LET$_d$ (keV/μm)	1.81 (0.79, 2.84)*	-	1.90 (0.56, 3.20)†
Dose (Gy)	-	2.72 (1.86, 3.58)*	2.90 (2.00, 3.79)*
LET$_d$:dose	-	-	−0.32 (−0.38, -0.26)*
Random effects (SD)			
LET$_d$ (keV/μm)	2.09 (1.51, 3.14)	-	2.68 (1.93, 4.93)
Dose (Gy)	-	1.73 (1.24, 2.61)	1.81 (1.30, 2.72)
Model fit and performance			
AIC	101,671.8	76,704.9	70,106.4
Log likelihood	−50,831.9	−38,348.4	−35,046.2
Pseudo R^2 (fixed effects)	0.37	0.39	0.48
Pseudo R^2 (total)	0.63	0.83	0.88
Brier score	0.05	0.04	0.04

Abbreviations: AIC = Akaike Criteria Information; CI = confidence interval; LET$_d$ = dose-averaged linear energy transfer; SD = standard deviation.

  * $P < .001$.

  † $P < .01$.

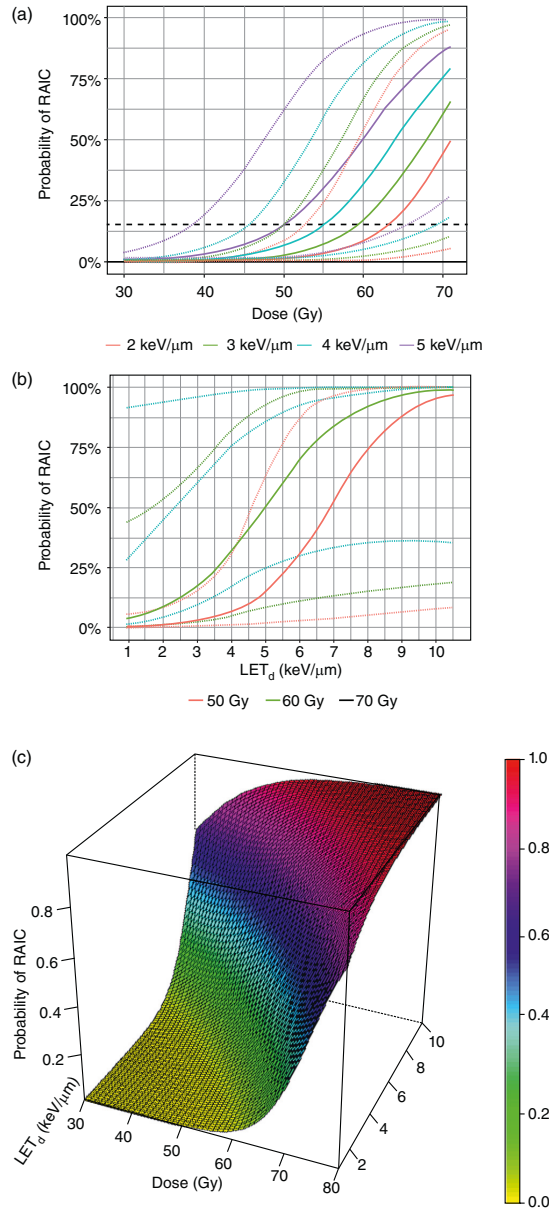LET$_d$:dose: interaction term; Pseudo R^2: Nagelkerke's.

Fig. 2.   Probability curves (solid lines) including 95% confidence intervals (dotted lines) for (a) 4 different dose-averaged linear energy transfer (LET$_d$) values in and for (b) 3 different dose levels in. Dashed horizontal lines correspond to (a) 15% and (b) 5% probability of radiation associated brain image change (RAIC). (c) The corresponding surface plot is displayed. All the plots were generated from the multivariate model.

dose and LET$_d$ varied considerably between patients, resulting in wide CIs and large uncertainties in predictions.

A few previous studies have aimed to investigate the associations between elevated LET and regions with RAIC by analyzing voxel level data. In 34 pediatric patients treated with PSPT for ependymoma, Peeler et al[9] reported a

significant correlation between hyper-intensities on T2-Fluid-attenuated inversion recovery images and LET$_t$. They developed a model with LET$_t$ and dose as predictors and showed that the estimated tolerance dose for 50% risk (TD$_{50}$) of image change in a voxel was reduced when LET$_t$ increased. Similar findings were reported by Eulitz et al,[8,29]
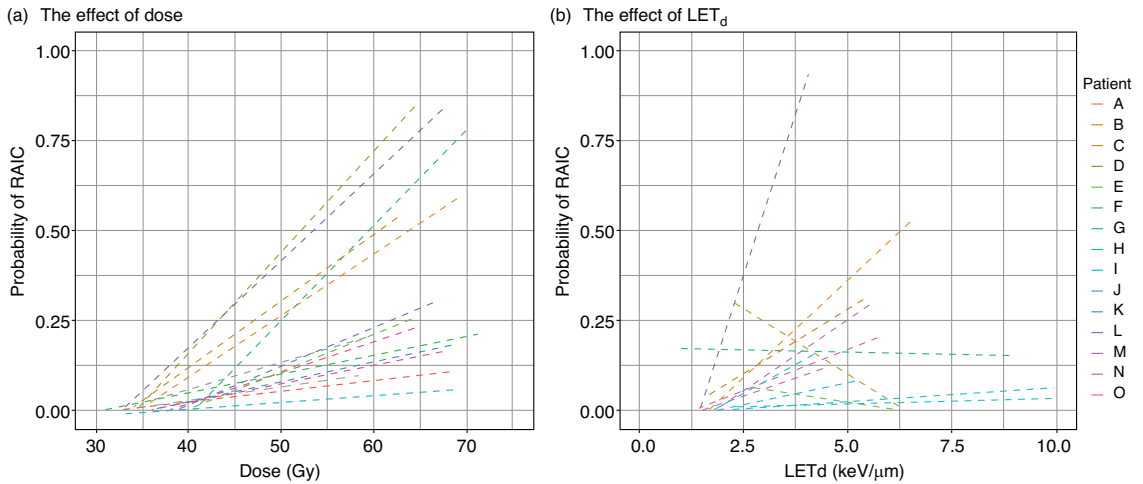
Fig. 3.   (a) Dose and (b) dose-averaged linear energy transfer (LET$_d$) plotted versus estimated risk of radiation associated brain image change (RAIC). Individual trend lines are generated for all values of LET$_d$ and dose using a glm smoothing function (y~x).

investigating correlations between LET$_t$ and contrast enhanced lesions from T1$_w$ MRIs in adult patients treated with PSPT for glioma. They found improved predictive performance when including LET$_t$ in the dose-response models; and, as in Peeler et al, a reduction in TD$_{50}$ was observed with increasing LET$_t$. Bahn et al[7] developed a model for patient-specific predictions of the local risk of image change based on the treatment plan using voxel level data from a large cohort (n = 110) of low-grade gliomas treated with pencil beam scanning. They showed that the location of RAIC mainly occurred in regions with combined high dose and LET$_d$ and not at random. In all these studies, the LET-RAIC associations were analyzed using generalized linear models, assuming uncorrelated observations. Similar to the present study, mixed effect modeling

was used by Niemierko et al[10] when analyzing LET$_d$ associations with RAIC in 50 patients treated with PSPT for brain tumors and HNC. In contrast to our findings, the effect of LET$_d$ was not found to be significantly correlated with RAIC, neither from the analysis using dose-matched voxels nor by mixed effect logistic regression. Compared with the current study, the heterogeneity in their patient material was higher (ICC of 0.96 vs 0.77), which may be one explanation for the difference in the significance of LET$_d$. Further, our patients received treatment with IMPT, which may yield an overall higher LET$_d$ compared with PSPT.[30]

Our result showed a more rapid increase in RAIC risks for doses exceeding 60 Gy even for the lowest LET$_d$ values, confirming that dose is the main determinant in the development of RAIC.[31] However, the ability of the model to distinguish
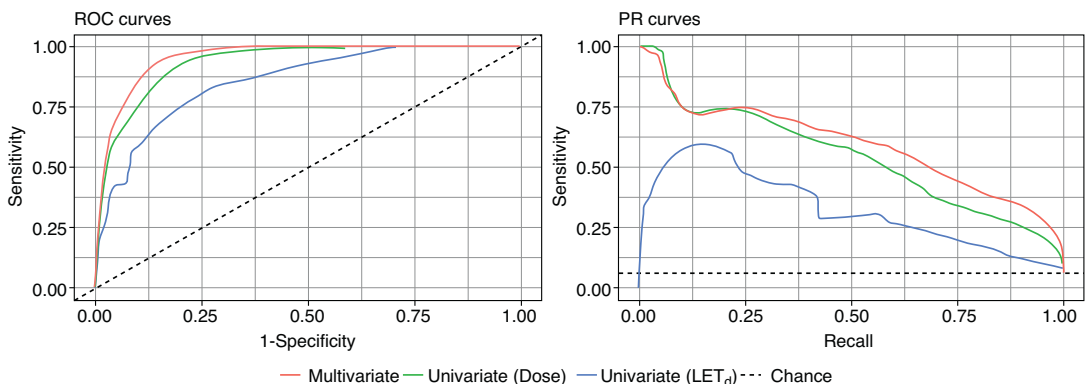

Fig. 4.   Receiver operating characteristic (ROC) curves (left) and precision-recall (PR) curves (right). The dashed lines represent a no-skill model (area under the receiver operating characteristic [AUROC] = 0.5 and area under the precision recall [AUPR] = 0.06).

between voxels with and without RAIC was improved when including the LET_d as predictor. Although our random effect analysis showed large interpatient variation in the LET_d effect, it is relevant to consider assessment of the LET distribution in the evaluation of clinical treatment plans, not least because our result showed a clear LET_d effect for the majority of the patients. For IMPT, where the LET distributions can be very different for seemingly similar dose distributions,[32] studies on LET optimized treatment planning have reported promising results, with reduced high LET values in OARs;[11,33,34] however, this remains an area of active investigation and it is unknown whether this translates into a clinical benefit. Regardless, analyzing clinical outcomes from LET optimized treatment plans may provide useful insight of the importance of LET and increased biologic effectiveness.

Previously, we reported RAIC associations at patient level in a cohort of patients with HNC treated with passive scattering and/or active scanning, finding significant RAIC correlations only for dosimetric variables in the multivariate analysis.[12] For the current study, where we specifically investigated the spatial relationship between dose, LET_d and RAIC, we considered it appropriate to only include patients with RAIC. In future studies, it may be relevant to also include patients without RAIC. To identify potential differences in the LET_d distributions between patients with and without RAIC, a matched design with a large patient cohort would be required.

In the present study, we used a mixed effect logistic regression model to investigate the dose and LET_d correlations with RAIC. A standard logistic regression model would consider each voxel as an independent observation, ignoring the correlation between the voxels in each patient. Neglecting this clustering structure of the data would affect the parameter estimates and in particular the associated P values and CIs. The mixed effect logistic regression model strengthens the result of the current study, as the method controls for nonindependence between voxels.

In addition to the intrinsic shortcomings of a retrospective analysis, the limitations of the present study include the low number of patients in the study cohort and the uncertainties in the dose and LET_d values used for modeling due to potentially image registration inaccuracies, proton range uncertainties, and anatomic deformations. Further, the LET_d was used as input variable in the models instead of the full LET spectrum. Although it is assumed that the LETs in clinical proton beams are in the range where the RBE increases linearly with LET, and hence are below values where the overkill effect is likely to occur, we cannot rule out that this simplification adds additional uncertainty to the models. Finally, there are uncertainties in the identification of the lesion origin location due to the progressive nature of RAIC. As the MRIs are obtained in a certain time interval during clinical follow-up, RAIC could have been in progression for a period at the earliest available MRI.

In conclusion, using a mixed effect method we found an overall statistically significant dose and LET correlation with RAIC after IMPT for HNC. Despite the large interpatient difference in radiosensitivity, our results suggest that the LET_d effect could be of clinical significance for some patients. LET_d assessment in clinical treatment plans should therefore be taken into consideration. Future directions include investigating if LET_d optimization could reduce observed and predicted RAIC risk without compromising treatment plan and target dose coverage.

References

1. Leeman JE, Romesser PB, Zhou Y, et al. Proton therapy for head and neck cancer: Expanding the therapeutic window. *Lancet Oncol* 2017;18:e254–e265.
2. International Commission on Radiation Units and Measurements. *Report 78: Prescribing, Recording and Reporting Proton-Beam Therapy*. Oxford: International Commission on Radiation Units and Measurements; 2007.
3. Luhr A, von Neubeck C, Krause M, Troost EGC. Relative biological effectiveness in proton beam therapy - Current knowledge and future challenges. *Clin Transl Radiat Oncol* 2018;9:35–41.
4. Luhr A, von Neubeck C, Pawelke J, et al. "Radiobiology of proton therapy": Results of an international expert workshop. *Radiother Oncol* 2018;128:56–67.
5. Paganetti H. Relative biological effectiveness (RBE) values for proton beam therapy. Variations as a function of biological endpoint, dose, and linear energy transfer. *Phys Med Biol* 2014;59:R419–R472.
6. Giantsoudi D, Adams J, MacDonald S, Paganetti H. Can differences in linear energy transfer and thus relative biological effectiveness compromise the dosimetric advantage of intensity-modulated proton therapy as compared to passively scattered proton therapy? *Acta Oncol* 2018;57:1259–1264.
7. Bahn E, Bauer J, Harrabi S, Herfarth K, Debus J, Alber M. Late contrast enhancing brain lesions in proton-treated patients with low-grade glioma: Clinical evidence for increased periventricular sensitivity and variable RBE. *Int J Radiat Oncol Biol Phys* 2020;107:571–578.
8. Eulitz J, Lutz B, Wohlfahrt P, et al. A Monte Carlo based radiation response modelling framework to assess variability of clinical RBE in proton therapy. *Phys Med Biol* 2019;64:225020.
9. Peeler CR, Mirkovic D, Titt U, et al. Clinical evidence of variable proton biological effectiveness in pediatric patients treated for ependymoma. *Radiother Oncol* 2016;121:395–401.
10. Niemierko A, Schuemann J, Niyazi M, et al. Brain necrosis in adult patients after proton therapy: Is there evidence for dependency on linear energy transfer? *Int J Radiat Oncol Biol Phys* 2020;109:10.
11. Giantsoudi D, Grassberger C, Craft D, Niemierko A, Trofimov A, Paganetti H. Linear energy transfer-guided optimization in intensity modulated proton therapy: Feasibility study and clinical potential. *Int J Radiat Oncol Biol Phys* 2013;87:216–222.
12. Engeseth GM, Stieb S, Mohamed ASR, et al. Outcomes and patterns of radiation associated brain image changes after proton therapy for head and neck skull base cancers. *Radiother Oncol* 2020;151:119–125.
13. Shah R, Vattoth S, Jacob R, et al. Radiation necrosis in the brain: Imaging features and differentiation from tumor recurrence. *Radiographics* 2012;32:1343–1359.
14. Wang YX, King AD, Zhou H, et al. Evolution of radiation-induced brain injury: MR imaging-based study. *Radiology* 2010;254:210–218.
15. International Commission on Radiation Units and Measurements. *Report 16: Linear Energy Transfer*. Oxford: Oxford University Press; 1970.
16. Grassberger C, Paganetti H. Elevated LET components in clinical proton beams. *Phys Med Biol* 2011;56:6677–6691.

17. Yepes P, Randeniya S, Taddei PJ, Newhauser WD. A Track-Repeating Algorithm for Fast Monte Carlo Dose Calculations of Proton Radiotherapy. *Nuclear technology* 2009;168:736–740.

18. Yepes PP, Eley JG, Liu A, et al. Validation of a track repeating algorithm for intensity modulated proton therapy: clinical cases study. *Phys Med Biol* 2016;61:2633–2645.

19. Yepes PP, Mirkovic D, Taddei PJ. A GPU implementation of a track-repeating algorithm for proton radiotherapy dose calculations. *Phys Med Biol* 2010;55:7107–7120.

20. Cortes-Giraldo MA, Carabe A. A critical study of different Monte Carlo scoring methods of dose average linear-energy-transfer maps calculated in voxelized geometries irradiated with clinical proton beams. *Phys Med Biol* 2015;60:2645–2669.

21. Agostinelli S, Allison J, Amako K, et al. Geant4—a simulation toolkit. *Nucl Instrum Methods Phys Res* 2003;506:250–303.

22. Bolker BM, Brooks ME, Clark CJ, et al. Generalized linear mixed models: A practical guide for ecology and evolution. *Trends Ecol Evol* 2009;24:127–135.

23. Bouwmeester W, Twisk JW, Kappen TH, van Klei WA, Moons KG, Vergouwe Y. Prediction models for clustered data: Comparison of a random intercept and standard regression model. *BMC Med Res Methodol* 2013;13:19.

24. Harrison XA, Donaldson L, Correa-Cano ME, et al. A brief introduction to mixed effects modelling and multi-model inference in ecology. *Peer J* 2018;6:e4794.

25. Saito T, Rehmsmeier M. The precision-recall plot is more informative than the ROC plot when evaluating binary classifiers on imbalanced datasets. *PloS One* 2015;10 e0118432.

26. Bouwmeester W, Moons KG, Kappen TH, et al. Internal validation of risk models in clustered data: A comparison of bootstrap schemes. *Am J Epidemiol* 2013;177:1209–1217.

27. R Core Team. *A language and environment for statistical computing.* Vienna, Austria: R Foundation for Statistical Computing; 2019 Available at: https://www.R-project.org/ Accessed April 26, 2019.

28. Bates D, Mächler M, Bolker B, Walker S. Fitting linear mixed-effects models using lme4. *J Stat Soft* 2015;67:48.

29. Eulitz J, Troost EGC, Raschke F, et al. Predicting late magnetic resonance image changes in glioma patients after proton therapy. *Acta Oncol* 2019;1–4.

30. Paganetti H, Blakely E, Carabe-Fernandez A, et al. Report of the AAPM TG-256 on the relative biological effectiveness of proton beams in radiation therapy. *Med Phys* 2019;46:e53–e78.

31. Lawrence YR, Li XA, el Naqa I, et al. Radiation dose-volume effects in the brain. *Int J Radiat Oncol Biol Phys* 2010;76(3 Suppl):S20–S27.

32. Grassberger C, Trofimov A, Lomax A, Paganetti H. Variations in linear energy transfer within clinical proton therapy fields and the potential for biological treatment planning. *Int J Radiat Oncol Biol Phys* 2011;80:1559–1566.

33. Liu C, Patel SH, Shan J, et al. Robust optimization for intensity modulated proton therapy to redistribute high linear energy transfer from nearby critical organs to tumors in head and neck cancer. *Int J Radiat Oncol Biol Phys* 2020;107:181–193.

34. Unkelbach J, Botas P, Giantsoudi D, Gorissen BL, Paganetti H. Reoptimization of intensity modulated proton therapy plans based on linear energy transfer. *Int J Radiat Oncol Biol Phys* 2016;96:1097–1106.
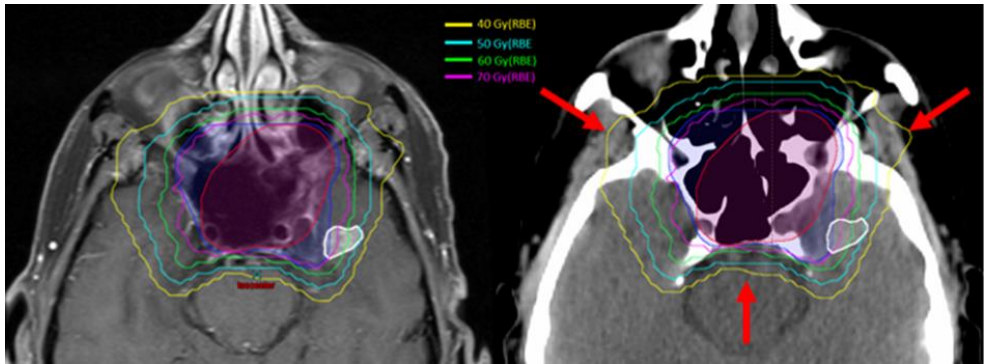
Supplementary material

Figure 1: Dose distributions and typical beam directions (red arrows). White contour is contrast enhanced region from MRI (left) and on planning CT (right). Yellow, cyan , green and magenta isodose lines represents 40 GyRBE, 40, 60 and 70 GyRBE, respectively. Red contour is CTV-70 GyRBE and blue contour is CTV-66 GyRBE.
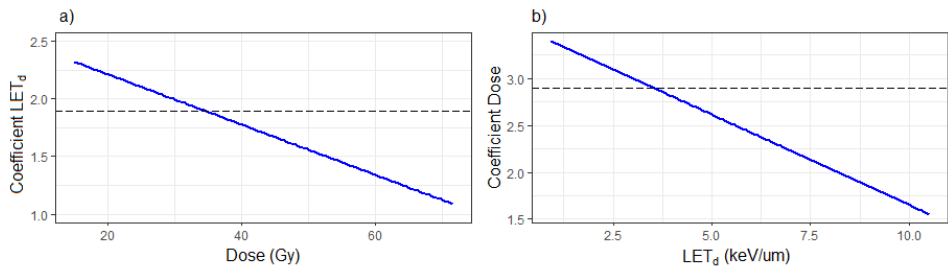

Figure 2: Conditional effects of dose and LET_d for the main model. As dose increases, the effect of LET_d decreases (a) and vice versa (b). Further, the negative interaction between LET_d and dose means that the combined effect of LET_d and dose is less than the sum of the individual effects.
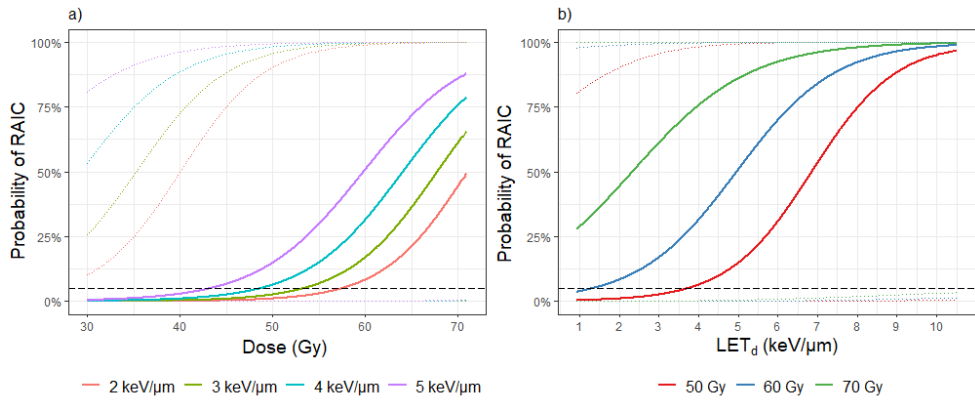
Figure 3: Probability curves (solid lines) including 95% prediction intervals (dotted lines) for four different values of LET$_d$ (a) and three different dose levels (b). In both plots the dashed horizontal line corresponds to 5% probability of RAIC.

Table I: Result from subgroup analysis of mixed effect regression modelling for voxel with dose > 40 Gy

Parameter	Univariate		Multivariate	
	Coefficient	Random effects	Coefficient	Random effects
LET$_d$ (keV/µm)	1.17 (0.15, 2.18)*	1.87 (1.35, 2.82)	1.46 (0.24, 2.69)**	2.26 (1.63, 3.40)
Dose (Gy)	1.10 (0.50, 1.70)***	1.10 (0.80,1.66)	1.14 (0.43, 1.85)***	1.31 (0.95,1.97)
LET$_d$:dose			-0.55 (-0.60,0-0.51)***	

Random effects: standard deviation, p < 0.05, **p < 0.01, ***p < 0.001. LET$_d$: dose: interaction term
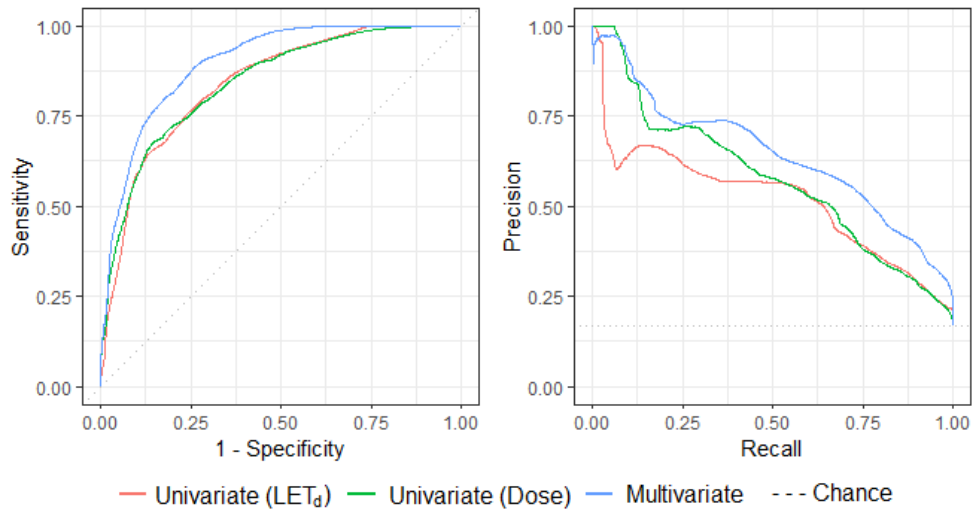
Figure 4: Result from the subgroup analysis. ROC- and PR curves for the univariate and multivariate models displayed at the left and right figure, respectively. The AUC were 0.84 for both the univariate models and 0.90 for the multivariate model. The PR-AUC were 0.52 for univariate model with LET_d as predictor, 0.57 for the model with dose as predictor and 0.63 for the multivariate model. Dotted lines represents a no-skill model.

uib.no